Yingkang Wei

Propagation of Electromagnetic Signal along a Metal Well in an Inhomogeneous Medium

Thesis for the degree of Philosophiae Doctor

Trondheim, Januray 2013

Norwegian University of Science and Technology
Faculty of Information Technology, Mathematics
and Electrical Engineering
Department of Electrical Power Engineering

NTNU – Trondheim
Norwegian University of
Science and Technology

NTNU
Norwegian University of Science and Technology

Thesis for the degree of Philosophiae Doctor

Faculty of Information Technology, Mathematics and Electrical Engineering
Department of Electrical Power Engineering

ISBN 978-82-471-4096-3 (printed ver.)
ISBN 978-82-471-4097-0 (electronic ver.)
ISSN 1503-8181

Doctoral theses at NTNU, 2013:3

Printed by NTNU-trykk

Abstract

In this thesis, the problem of deriving the current distribution along a metal casing surrounded by a conductive earth is studied. The metal casing can be taken as a long and thin metal wire antenna in this case. The current distribution is unknown and can be decomposed into tiny current elements along the wire antenna. The total field from the wire antenna can be achieved by using the principle of linear superposition of the fields generated by each of the current element. The solution of the scalar wave equation for a point source is well known to be the Green's function. For a tiny vector source of current element, the solution of the scalar wave equation can be achieved by a dyadic Green's function. By taking advantage of the boundary conditons at the metal surface, an electric field integral equation can be built up which can be solved by the method of moments.

A real composition of the conductive earth is complicated and usually is modelled as a planarly layered isotropic medium, where the eletromagnetic properties of the medium, μ and ϵ vary only in one direction, e.g. the z direction. The advantage of using such a simple model is that the vector wave equations can be reduced to two scalar wave equations. The electromagnetic wave represented by these two scalar wave equations are two types of waves, namely, the transverse electric (TE) waves and the transverse magnetic (TM) waves, which are decoupled from each other. The electromagentic field at an arbitrary point in the medium can be accurately derived by combining the fields propagating directly from the source with the fields reflected by the interfaces between layers, which has been well developed in the case of plane waves. However, the electromagnetic field generated from a dipole source goes out not in the form of plane wave, but spherical waves. In order to decompose it into a combination of plane waves, the Weyl's identity (in a Cartesian coordinate system) and the Sommerfeld identity (in a cylindrical coordinate system) are applied to the dyadic Green's function mentioned above.

The thesis starts with a short review of different electromagnetic technologies applied in the oil and gas industry today. Then, Chapter 2 considers a particular model where the wire antenna is assumed to be perpendicular to the interfaces between the layers. Due to the inherent geometrical symmetry

of this particular model, the source elements along the antenna are treated as vertical electric dipoles (VEDs). As a result, the wave equations are in this case reduced to one dimensional wave equations. Chapter 3 develops the model further by assuming that the wire antenna is at an offset angle compared to a line normal to each interface. The source elements are in this case modelled as a combination of both a vertical and a horizontal electric dipole (HED). The fields will then propagate in both TM and TE mode, and these are then treated separately.

In a geophysical problem where the medium is highly conductive and the operating frequency is extremely low, it is usually quite difficult to calculate the Sommerfeld identity accurately by traditional methods. Hence, the error in the calculation result of the Sommerfeld identity is shown to have a significant impact on the derived current distribution. Chapter 4 presents a new method to evaluate the Sommerfeld identity by using a combination of numerical and analytical methods. The new method gives much more accurate results with no extra cost in computational complexity. Chapter 5 introduces how to use the new method to enhance previous analysed case studies in Chapter 2 and Chapter 3. In this chapter, the results given by the numerical method are compared to the data achieved from an experiment.

Preface

This dissertation is submitted in partial fulfillment of the requirements for the degree of *doctor engineer* at the Department of Electrical Power Engineering, Norwegian University of Science and Technology (NTNU). My advisors have been Professor Lars Norum at the Department of Electrical Power Engineering, NTNU, Doctor Bengt Holter at the SINTEF ICT and Professor Ingve Simonsen at the Department of Physics, NTNU. The studies have been carried out in the period from September 2008 to September 2011.

The work has been funded by a scholarship from the Research Council of Norway, via the project *Wireless Electromagnetic Data Communication for Downhole Use*(WEDAC), and SINTEF ICT.

Acknowledgements

I am grateful to SINTEF ICT and my supervisor, Doctor Bengt Holter, for financial support and guiding me to this project. I also want to thank him for that he has helped me so much in my studying and researching. I want thank my supervisor, Professor Ingve Simonsen, for he gave me many inspiring theoretical advices and was always willing to discuss with me even when he was outside of Norway. I would like to thank my supervisor, Professor Lars Norum, for the powerful support he offered to me in the past three years.

Before I start my Ph.D studying, I worked for SINTEF for a year. I met Mr. Ole Christian Bendixen, Per Schjølberg-Henriksen, Sverre Knudsen and Magnus Hjelstuen. I want to thank them for the warm help they gave me both on my work and my personal life. I would like to thank Karsten Husby and Jacob Kuhnle from SINTEF ICT Trondheim, who discussed with me a lot on the project and gave me many good comments.

In the last year of my study, I had the opportunity of working with WINS and met Atle Hjertenas, Peter Aronstam and Roger Fincher. I had a good time to work with them in U.S. for a month and was deeply moved by their spirit of enthusiasm, optimism and hard working. I am very happy that I can work with them in the future.

I want to thank my parents for all the support during the last three years. They were so positive and brave in spirit that they overcame the

serious illness of cancer. I hope they will always be healthy and happy in the future.

Trondheim, December 2012
Yingkang Wei

List of Figures

Contents

Part I

Introduction

Introduction

1.1 The fast developing technology for oil and gas industry

The rapid increase in world oil consumption promotes concern about oil reserves and supply capability. Many new methods and technologies have been developed to improve production efficiency, extend the life of old wells, and explore for more new reserves. As an example, horizontal well drilling technology can exploit thin oil-rim reservoirs, avoid problems such as water/gas coning, and extend the life of the wells by means of multiple drain holes [1]. According to data from the National Petroleum Council (NPC) of U.S., many breakthroughs and thousands of incremental advances in exploration and production have increased oil recovery levels from less than 10% (of the initial volume in place) to more than 70% in some cases [2].

Another significant breakthrough in production technologies during recent years is a technology known as smart wells or intelligent well systems. The smart well system allows real-time information from downhole and flow control by using permanently installed sensors and valves. With the help of this real-time information, the operators are able to optimize control to the drilling and production [3]. As an example, it enables operators to actively monitor, remotely choke or shut selected zones with poor performance without costly intervention.

Before the emergence of smart well systems, the only available method to obtain downhole information was through the use of intervention-based logging techniques. Interventions can be conducted periodically to measure a variety of parameters, such as pressure, temperature and flow. Although it provides valuable information, the operation is very expensive to be done frequently, especially in the sub-sea environment. The lack of timely data often compromise the ability of the operator to optimize production [4]. Compared to an intervention based approach, the use of smart well systems has several important advantages. (i), it can improve information and knowledge management, reduce the frequency of intervention and even realize automatic exploration and production. (ii), it can increase net present value by the recovery of hydrocarbons from reservoirs. (iii), it can reduce capital ex-

penditures by decreasing the number of wells drilled and that in turn will reduce the number of surface facilities required. In 2006, some oil and gas fields in Saudi Arabia were equipped with experimental smart well technology and their performance have been compared to conventional vertical and horizontal wells that were deployed in the same field. It was reported that 48 smart wells could achieve the desired production target of 66 conventional horizontal wells or 150 vertical wells [5].

Today it is widely recognized that this technology can not only increase operating efficiency greatly, but also save enormous expenses and risks associated with the execution of those processes. This is accomplished by providing a better understanding of downhole processes and by helping reconcile short-term production optimization approachs with long-term objectives.

Since the first smart well system was installed in August 1997 at Saga's Snorre Tension Leg Platform in the North Sea, over 300 such systems have been installed globally. These installations range from mature land assets to deep water off the coast of Brazil. However, the adoption of smart well systems has not been without challenges. The most challenging problem is the harsh wellbore environment of high temperature, high pressure and the limited space. Since the instruments are permanently-installed downhole and inaccessible once deployed, the value of the system is directly linked to the life of the system devices. Many early systems were rendered inoperable due to their low reliability. For example, high temperature electronic devices, such as the Field-Effect Transistors (FET) and capacitors which are available on the market today can at most work in a range of $175 - 200^0$C. The derated performance of these devices at these temperatures make them barely sufficient for long term downhole operation. New developments in the field of high temperature devices will enable new technologies for oil and gas exploration and production in the future [6, 7, 8].

Another challenging problem is how to transmit data between downhole sensors and surface facilities to obtain real-time data and realize optimized production. Until now, there have been a few different methods developed in data communication for this purpose. For example, BJ Services Company has developed a wired communication system by using coaxial cable or fiber optic cable. Unfortunately, these systems have had limited reliability because of the strong impact of oil or gas fluid on the components deployed. Other wireless methods have also been developed, such as pressure pulses that propagate in the flow of the production fluid, or using an acoustic signal that can propagate through the earth as well as along the well. According to a report by Paul Tubel, the acoustic system they tested could communicate over a length of 500 feet [9, 10].

Another attractive method of realizing wireless communication is to use

electromagnetic (EM) signals. The main challenge of this method is that the earth is highly conductive, which causes the EM signal to attenuate very rapidly with increasing distance. In addition, the transmission power and the size of antenna are all limited in a downhole environment. These challenges limit the effective communication distance and the data rate of the transmitted signals. Compared to the earth, the metal well is much more conductive and can be taken as the core of a coaxial transmission line, on which, the EM wave can propagate much easier. This method has been studied much, especially in the field of measurement while drilling (MWD) system . However this topic still benefit from further study as most of the early research has been based on simple models, such as assuming the earth to be a homogeneous medium. In the following section, a brief review of this earlier research and applications of EM technologies in the oil and gas industry is presented.

1.2 The application of EM technology in oil and gas industry

EM technology has been applied in oil and gas industry in many aspects, such as logging systems, borehole antennas, MWD and controlled source electromagnetic (CSEM) surveying, also known as seabed logging (SBL). The application of EM technology in the oil and gas industry can be traced back to Conrad Schlumberger, who tried to measure the resistivity of the earth by using EM technology in a well logging system in 1927 [11]. The research on high-frequency EM logging technology started in the 1960s [12] and in the 1980s, a borehole radar operating at 1.1GHz appeared [13, 14, 15]. However, the detection depth was too shallow for such a high frequency and a system that worked at lower frequency, 25MHz, was proposed by Blenkinsop and others in 1986 [16, 17]. In the 1990s, multi-frequency electromagnetic logging with an ultra-broadband antenna was developed [18].

For an electronic system, the load determines how much power can be delivered. For example, in a radiation system, the source impedance should be matched to the antenna to minimize reflection signal. In the 1960s, King and others addressed this issue by looking into the input impedance characteristics of a dipole antenna when immersed in a homogeneous isotropic conductive medium [19, 20]. In particular, King studied the relationship between the antenna input admittance and the properties of a conductive medium reflected through the parameter $\sigma/(\omega\epsilon_r\epsilon_0)$, where σ is the conductivity of the medium, ω is the operating frequency (in rad/s), ϵ_r is the relative

permittivity of the medium, and ϵ_0 is the vacuum permittivity. In Fig.1.1 and Fig. 1.2, the input conductance and susceptance of an antenna are plotted as a function of the parameter $\sigma/(\omega\epsilon_r\epsilon_0)$ and the antenna electrical length βh, where h is the physical antenna length. $\beta = 2\pi/\lambda$, and λ is the wavelength of the signal in the surrounding medium. In [19], salt water and a frequency of 114MHz was applied, in which case the medium wavelength was reported to be $\lambda = 29.77$cm. From Fig.1.2, it can be observed that the susceptance of the input admittance becomes negative when the parameter $\sigma/(\omega\epsilon_r\epsilon_0)$ becomes large and $\beta h > 1$. In addition, the susceptance approaches a constant negative value as βh increases. Since the parameter $\sigma/(\omega\epsilon_r\epsilon_0)$ becomes very large at low frequencies and in a highly conductive medium, it can be concluded that the input impedance of an antenna immersed in a conductive medium usually is inductive at low frequencies.

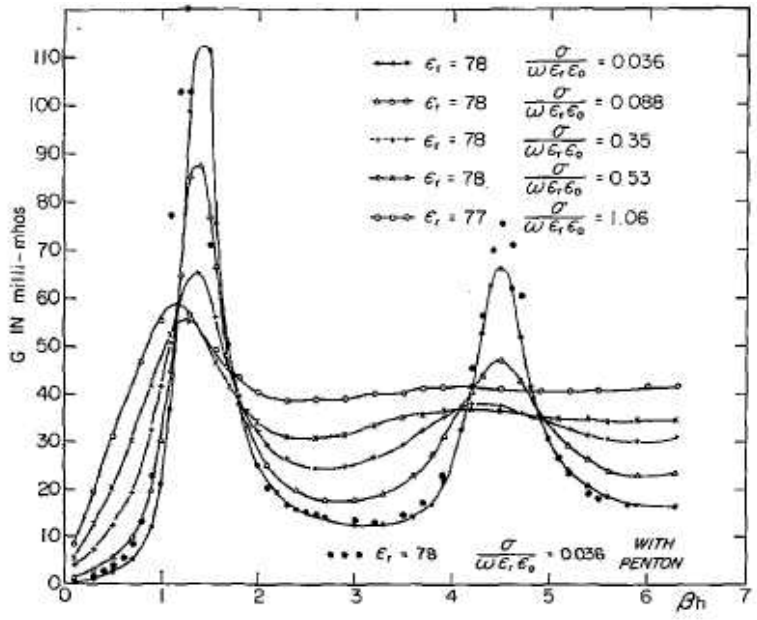

Figure 1.1: Driving point conductance vs antenna length [19, Fig.7].

In the beginning of this century, the application of CSEM technique for oil and gas industry became popular in offshore applications. This application can be traced back to J.R.Wait who studied the EM fields of a phased line current over a layered conducting half-space [21, 22]. In using CSEM, a cable with powerful low frequency current flowing on it is immersed in the sea. The EM field induced by the wire current propagates in the earth and is reflected at the interfaces of discontinuous electrical properties. Since

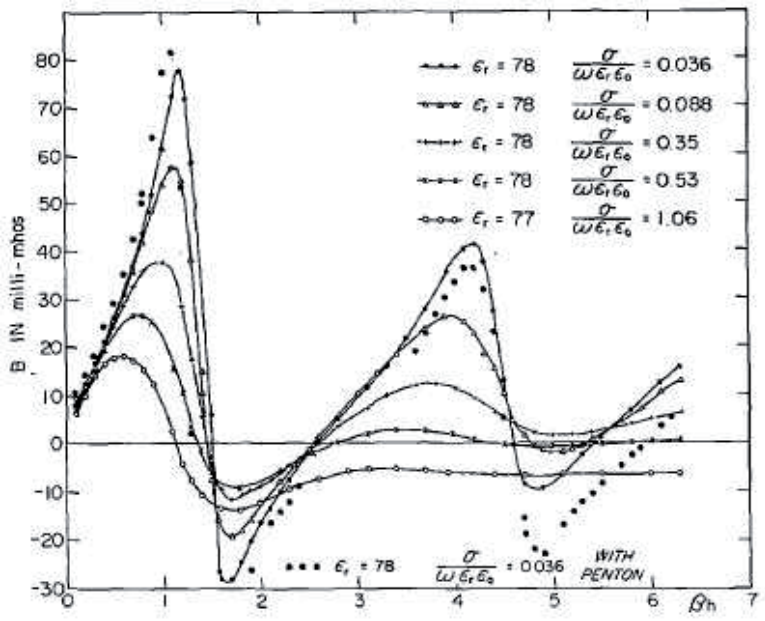

Figure 1.2: Driving point susceptance vs antenna length [19, Fig.8].

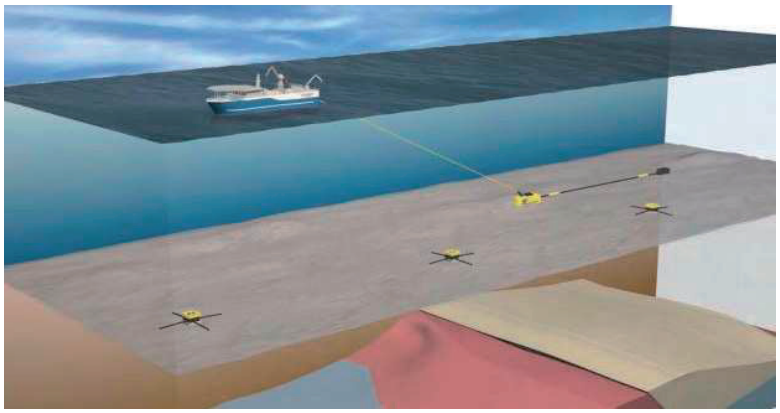

Figure 1.3: The SBL, this figure is from lecture note for mathematical geophysics given by Lasse Amundsen.

hydrocarbons in the subsurface are significantely more resistive than non-hydrocarbon-bearing layers such as shale or sandstone which contain salt water, they provide measureable reflections. Hydrocarbons can therefore be detected by a reflected signal at the seabed in a range of distances from the source [23, 24, 25, 26].

As mentioned above, the propagation of EM waves along the drill rod or metal casing has been a topic of discussion in oil and gas industry for a long time, driven largely by MWD applications. J. R. Wait studied this problem theoretically with a model where a perfectly conductive metal rod was surrounded by a homogeneous earth rock of a very low conductivity, $\sigma = 10^{-6}$S/m, which is shown in Fig.1.5. Using this highly idealized model, he concluded that the current attenuation along the drill rod would be at least as great as plane waves in the surrounding medium [27]. He also pointed out that an optimum frequency could be found for a fixed depth, as shown in Fig.1.4. However, in real earth situations, the conductivity of the earth rock is usually much higher than the value he adopted and thus his optimum frequency could be too low to be observed.

In 1987, DeGauque and Grudzinski studied a more advanced model where the drill rod was assumed to have a finite conductivity and the surrounding medium was assumed to be sea water with a much higher conductivity of $\sigma = 0.5$S/m. Their model is shown in Fig.1.5. In their research, the metal drill rod was taken as a long thin wire antenna and the current distribution along it was solved by applying the well known Pocklington's integral equation. The influence of the finite conductivity of the drill rod was characterized by assigning an internal impedance and then accounting for it with boundary conditions. The Pocklington's integral equation was discretized and solved by the method of moments. The authors found that the drill rod internal impedance played a major role in attenuating the signal and for the operating frequencies below a few Hertz, the attenuation did not vary much yielding an optimum frequency for maximum data rate around 3Hz [29].

In 1993, Xia and Chen developed a model where the drill rod could not only be vertical, but could be in an arbitrary direction in a homogeneous medium [30]. They built up an electric field integral equation (EFIE) for this model, which could handle more complicated geometries than Pocklington's integral equation. Not surprisingly, their results matched those previously published by DeGauque and Grudzinski. The authors claimed (without proof) that a layered earth consideration might be estimated by using the most conductive case for the computation, and they also pointed out that detections should be carried out near the well head.

More recently (2009), Yang and others studied a model where a metal well was assumed to be vertically placed in a horizontally stratified earth [31]. At

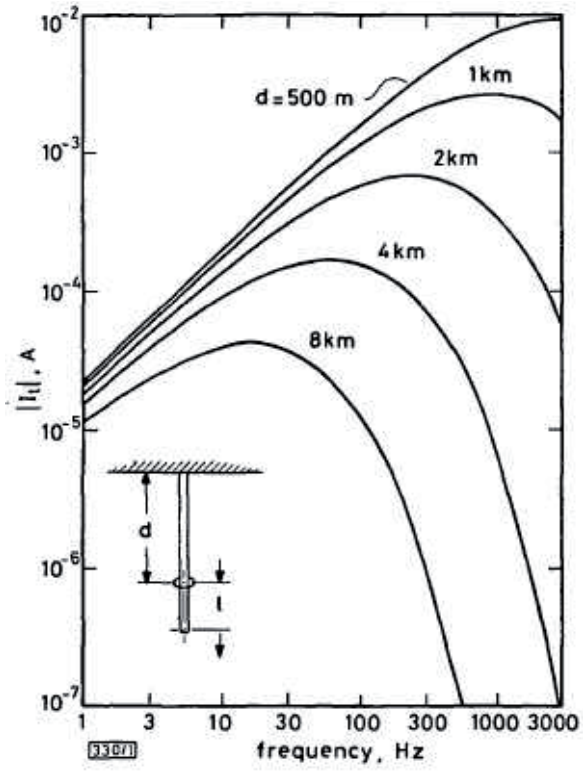

Figure 1.4: The total current on the drill rod at the surface for a source toroid at depth d, when $\sigma = 10^{-3}$S/m [28, Fig.1].

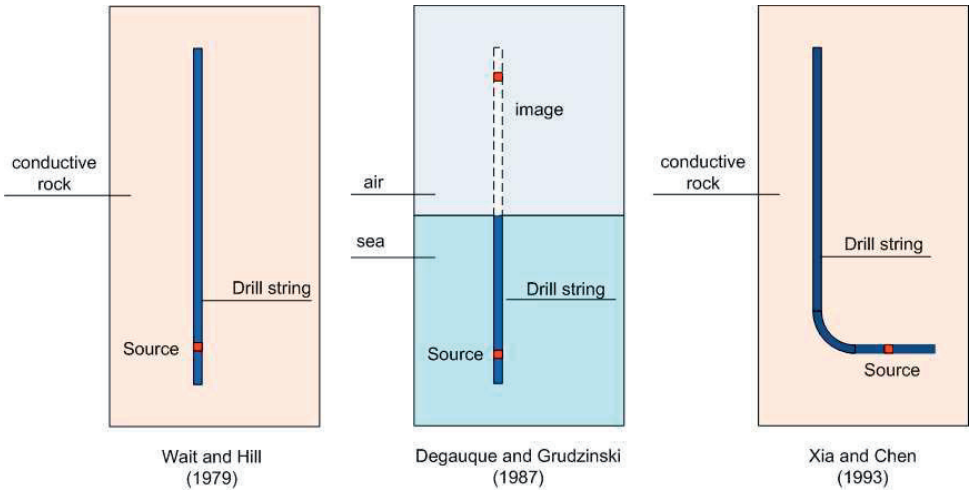

Figure 1.5: The models studied by Wait, Degauque and Xia.

the same time, the author of this thesis also studied a similar model and submitted a paper to the Applied Computational Electromagnetics Society (ACES) 2010 conference. Both of these two studies considered the reflections of the EM field from the interfaces of the layers and accounted for them in the EFIE developed for the model. To do this, a Sommerfeld identity was applied to transform the spherical wave due to a point source into a summation of plane waves, which was in the form of Fourier transform. For the plane waves, the field in a horizontally layered medium can be evaulated accurately by summing up the direct propagation from the source and the reflections at the interfaces between the layers. Yang claimed in his work that the discretization step didn't influence the final results. However, the numerical results given in this thesis show that the discretization step influences the accuracy of the Sommerfeld integration, so a special mathematical method has been developed to solve this problem.

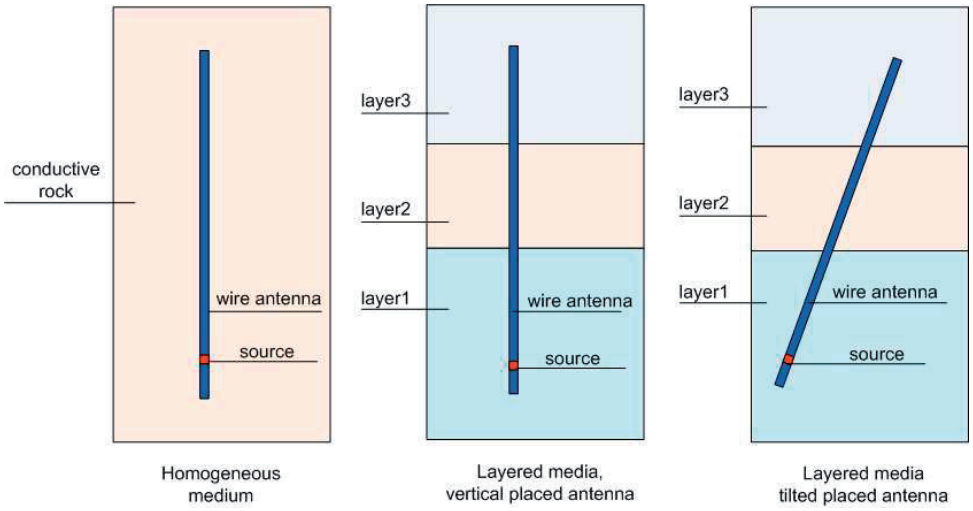

Figure 1.6: The models studied in this thesis.

There are other ways to approach this interesting problem other than the application of the EFIE method. For example, in 2000, Trofimenkoff and others developed a method which used an electric circuit network model to study the current distribution along the metal well casing. They discretized the metal well and the surrounding medium into small elements which was then modeled into circuit elements of resistors, inductors and capacitors [32]. The advantage of this method is speed, as the computation is much faster than using the EFIE method. Their results compare favorably with those published before by DeGauque and Grudzinski, and those by Xia and Chen.

Today, with the development of smart well systems, the communication between surface and downhole instruments becomes an urgent need. Using an EM signal that propagates along the metal well casing is one of the more promising solutions. In this case, it is necessary to study the attenuation of the signal along the surface of the metal casing. This then will provide a theoretical basis for the assessment of the channel capacity. This problem is closely related to the studies of the current distribution along the drill rod in an MWD system. Until now, most of the models applied to solve this problem have assumed that the earth is a homogeneous medium. However, in the most recent paper published by Yang, a layered medium was considered and a metal well was assumed to be placed along a line normal to the interfaces. In reality, the well can penetrate the layers at an arbitrary angle and how this will influence the current distribution is an interesting problem that (to our knowledge) has never been studied. This thesis presents new models and special mathematical methods to provide a solution to this problem. In the following, a brief introduction to methods used to solve EM problems is presented.

1.3 Methods in solving EM problems

Maxwell equations are a set of coupled first-order differential equations, which are almost always too complicated to be solved exactly in practical problems. The methods for solving Maxwell equations can be classified into experimental, analytical and numerical approaches. Experimental methods are very important and often play a key roll in practical problems. However, they are often very expensive and almost all experiments can only approximate the real situation. What's more, the experiment should be done based on a theoretical model and the experiment data needs to be studied and compared to the theoretical analysis for interpretation.

The analytical solutions are always based on highly idealized models and can only be applied to some very simple problems. The most commonly used analytical methods are image method and the separation of variables [33, Ch.2,3]. Under special conditions, asymptotic methods could be applied and approximate solutions are available, which can also be classified as analytical methods [34, Ch.2],[35]. With the development of computer technology, more and more problems can be solved by numerical methods. The most commonly used numerical methods are the finite difference time domain method (FDTD) [36], the finite element method (FEM) and the methods of moments (MOM).

The FDTD algorithm can be traced back to Yee's paper in 1966 and the

acronym was given by Taflove in 1980 [37, 38]. Application of FDTD usually involves three steps: (i), divide the solution region into a grid of nodes. (ii), the given differential equations can be discretized into finite difference equations by using Taylor's theorem, in which case, the derivatives can be approximated by the following equations:

$$f'(x_0) \approx \frac{f(x_0 + \Delta x) - f(x_0)}{\Delta x}, \tag{1.3.1a}$$

$$f''(x_0) \approx \frac{f(x_0 + \Delta x) - 2f(x_0) + f(x_0 - \Delta x)}{(\Delta x)^2}. \tag{1.3.1b}$$

(iii), solve the difference equations subject to the prescribed boundary conditions [39, Ch.3]. FDTD usually works in time domain and it can present transient responses accurately. Similar to FDTD, the integral form of Maxwell equations can also be discretized into finite difference equations, which was developed by Weiland independently and is called the finite integration technique (FIT) [40, 41, 42].

FEM methods are based on the theory of variational method, in which a functional is first derived and trial functions are then used to find the solution in order to minimize or maximize the functional. For example, for the differential equation

$$\frac{\partial F}{\partial u} - \frac{\partial}{\partial x}(\frac{\partial F}{\partial u_x}) - \frac{\partial}{\partial y}(\frac{\partial F}{\partial u_y}) = 0, \tag{1.3.2}$$

a functional integral equation $I(u)$ can be constructed as

$$I(u(x,y)) = \int dxdyF\Big(x, y, u(x,y), u_x, u_y\Big). \tag{1.3.3}$$

The function $u(x,y)$ which minimize $I(u)$ will also be a valid solution to the differential equation in (1.3.2). It can be approximated by a series of trial functions

$$u = \sum_{m=1}^{N} a_m g_m, \tag{1.3.4}$$

for which the Rayleigh-Ritz procedure is applied to find the coefficients,

$$\frac{\partial I}{\partial a_m} = 0, \quad m = 1, 2, \cdots, N \tag{1.3.5}$$

If the basis functions g_m are global over the solution region, it is classified as a Rayleigh-Ritz method. If they are piecewise for each local region, the

method is considered a FEM. The FEM is usually more powerful and versatile compared to the Rayleigh-Ritz method.

MOM is a sub-method of the weighted residual method. For a linear operation

$$Lu = f, \tag{1.3.6}$$

the unknown function can be expanded by a series of trial functions (basis functions) g_m as shown in (1.3.4). For a limited number of basis functions, the expanded function usually can not provide an exact solution for u, but only an approximation to it. There will be an error (residual) between them:

$$R = \sum_m L \langle u, g_m \rangle \langle g_m - f, \tag{1.3.7}$$

where $<>$ is inner product, $f >$ denotes a vector and $< f$ is its transpose. Weight funtions w are orthogonal to the residual

$$\langle w, R \rangle = 0. \tag{1.3.8}$$

For different weight functions, there are (at least) five sub methods

1. Collocation method
2. Subdomain method
3. Least square method
4. Galerkin method
5. Method of moments

Highlighting the differences in these five methods, the collocation method use Dirac delta function δ as weight function, which forces the residual to be zero at specific points. The response to the Dirac delta source is the Green's function, as shown in the following equation

$$LG(\mathbf{r}, \mathbf{r}') = \delta(\mathbf{r} - \mathbf{r}'). \tag{1.3.9}$$

By using convolution theory, the equation can be transformed into the following equation

$$L \langle G(\mathbf{r}, \mathbf{r}'), f(\mathbf{r}') \rangle = \langle \delta(\mathbf{r} - \mathbf{r}'), f(\mathbf{r}') \rangle = f(\mathbf{r}), \tag{1.3.10}$$

which indicates the unknown function u is equal to

$$u(\mathbf{r}) =< G(\mathbf{r}, \mathbf{r}'), f(\mathbf{r}') > \tag{1.3.11}$$

The subdomain method can be considered as a modification of the collocation method, which forces the weighted residual to be zero not only at fixed

points, but over various subsections. The least square method uses the residual function R as the weight function. In this case, to find the zero points of (1.3.7), the minimum of the equation by the derivatives with respect to the unknown parameters is computed. The Galerkin method uses the basis functions as the weight functions and can be viewed as a modification of the least square method. By contrast, the last method, the method of moments, weight functions are chosen from the family of polynomials:

$$W_i = x^i. \tag{1.3.12}$$

If the basis functions for the approximation are the same polynomials, then the method of moments is identical to the Galerkin method. Sometimes, the meaning of MOM is equivalent to the meaning of weighted residual method and the other four sub methods may also be referred to as MOM.

Comparing these three methods, FDTD and FEM are partial differential equations (PDE) methods while one is in time domain and the other is in frequency domain. Usually, both of them use volume meshing so that the number of unknowns increases with the cube of the linear meshing density. For these two methods, memory and solution time scale proportionally with the number of unknowns. MOM is an integral equation method which uses surface mesh. It imposes certain boundary conditions to the structure in its solution technique and is not good for complex 3D volumes and non-metallic surfaces. However, for solving surface current problems of 1D and 2D, MOM is a good choice.

Today, there are dozens of software packages developed for solving EM problems based on the three methods introduced above. However, most of them are not appropriate for solving geophysical problems, where the operating frequencies are usually very low and the earth composition is very complicated. In addition to that, the model shown in Fig.1.6 is very difficult to mesh since it is extremely large in one dimension but extremely small in the other dimension. For this kind of problem, the best method is to build a special EFIE, which is then solved by the MOM.

1.4 Contributions of the included papers

This thesis consists of four papers, which are numbered with the capital letters A, B, C and D. In the following, a summary of the included papers is presented.

1.4.1 Paper A

Y. Wei, B. Holter, I. Simonsen and L. Norum, "Current Distribution Along a Long Thin Wire Antenna Vertically Placed in a Horizontally Layered Medium", in Proc. Applied Computational Electromagnetic Symposium Conference, Tampere, Finland, April 2010.

To use the metal well casing to transmit EM signal between downhole and surface has been an interesting topic in oil and gas industry, especially for MWD application. Many people have contributed to this topic as introduced above. However, most of them modelled the earth to be a homogeneous medium (to the author's knowledge in 2009). This paper tries to make an improvement by modelling the earth to be a horizontally layered medium and each layer can be characterized by its conductivity independently. The metal well is then treated as a long thin wire antenna and is assumed to be perpendicular to the interfaces between different layers. Geometrically, xy-plane is defined to be parallel to the interfaces and the wire antenna is on z-axis.

The EM field induced by a delta gap source will cause an incident current in the wire antenna and this incident current will induce a scattered field again. The electric field at a point $\mathbf{r} = (x, y, z)$ in space induced by the current element $I(z')dz'\hat{z}$ at point $\mathbf{r}' = (0, 0, z')$ is equal to

$$\mathbf{E}(\mathbf{r}) = i\omega\mu(\bar{\mathbf{I}} + \frac{\nabla\nabla}{k^2}) \cdot I(z')dz'\hat{z}\frac{e^{ik|\mathbf{r}-\mathbf{r}'|}}{4\pi|\mathbf{r}-\mathbf{r}'|}, \tag{1.4.1}$$

where k is the wavenumber in the vicinity of the source point and ∇ is the vector differential operator. The electric field at point $\mathbf{r}$ induced by the total wire antenna can be evaluated by doing integration

$$\mathbf{E}(\mathbf{r}) = i\omega\mu \int_\ell dz'(\bar{\mathbf{I}} + \frac{\nabla\nabla}{k^2}) \cdot I(z')\hat{z}\frac{e^{ik|\mathbf{r}-\mathbf{r}'|}}{4\pi|\mathbf{r}-\mathbf{r}'|}. \tag{1.4.2}$$

By taking advantage of the boundary condition at the surface of the wire antenna, an EFIE is built for the unknown current $I(z')$. For a model of homogeneous medium, the EFIE can be transformed into the well known Pocklington's integral equation, which can be solved by MOM [43, Ch.8].

When a horizontally layered medium is considered, the scalar Green's function in (1.4.2) needs to be expanded into an integration of plane waves first, which can be done by applying the Sommerfeld identity [34, Eq.2.2.30]

$$\frac{e^{ik|\mathbf{r}-\mathbf{r}'|}}{|\mathbf{r}-\mathbf{r}'|} = i\int_0^\infty dk_\rho \frac{k_\rho}{k_z} J_0(k_\rho\rho)e^{ik_z|z-z'|}, \tag{1.4.3}$$

in which k_ρ is the wavenumber in the radial direction and $k_z = \sqrt{k^2 - k_\rho^2}$. $J_0()$ is the 0th order Bessel function of the first kind.

The propagation of plane waves in a horizontally layered medium can be evaluated accurately by calculating the reflections at the interfaces between different layeres. When there are multiple layers, the multi-reflections from different layeres can be calculated by a recursive equation, which is defined as the generalized reflection coefficient [34, Ch.2.1]. The propagation element $e^{ik_z|z-z'|}$ in (1.4.3) will be changed into the following form

$$A[e^{ik_z(z-z')} + \tilde{R}e^{-ik_z(z-z')}] \tag{1.4.4}$$

where $\tilde{R}$ is the generalized reflection coefficient.

In the paper, this method is applied for the homogeneous models published by others and also compared to a FIT program by using a simple homogeneous model. These tests show that the method works quite well for the homogeneous models which are special cases of the layered medium model. Finally, a horizontally layered medium model is used and the numerical results show that the attenuation of EM field in different layers depends on the conductivities of the independent layers. The distribution of the current can not be estimated by only using the most conductive case as claimed by Xia and Chen [30].

1.4.2 Paper B

Y. Wei, B. Holter, I. Simonsen and L. Norum, "Current Distribution Along a Long Thin Wire Antenna Placed in a Horizontally Layered Medium", in Proc. Conference on Electromagnetic Field Computation, Houston, U.S., May 2010.

In the first paper, the metal well casing is assumed to be vertically placed in the layered earth. With the development of drilling techniques, such as horizontal well tochnology, the metal well can penetrate the earth layer at an arbitrary angle. In this case, a question is how much the tilt angle between the well and the medium will influence the current distribution. To the author's knowledge, a solution to this problem has never been published.

This paper tries to improve the model presented in Paper A by allowing an arbitrary tilt angle between the wire antenna and the interface surface. In this case, xy-plane is still assumed to be parallel to the interfaces and the wire antenna is assumed to lie in xz-plane. The angle between the wire antenna and z-axis is θ, $0 \leq \theta < \pi/2$. The model is not symmetric with respect to the z-axis and therefore can not be simplified to a 1-D model.

However, it is symmetric to the xz-plane and therefore can be treated as a 2-D model.

As presented in (1.4.2), an EFIE can be constructed for the unknown current along the wire antenna. In this case, the current element is $I(z')d\ell\hat{\ell}$ in stead of $I(z')dz'\hat{z}$. Since there is a tilt angle θ between the wire antenna and the z-axis, the current element $I(z')d\ell\hat{\ell}$ can be decoupled into a vertical current element $I(z')d\ell\cos\theta\hat{z}$ and a horizontal current element $I(z')d\ell\sin\theta\hat{x}$, which can be treated as a vertical electric dipole (VED) and a horizontal electric dipole (HED), respectively. The electric field due to the current element $I(z')d\ell\hat{\ell}$ can be evaluated by the superposition of the fields generated by the VED and the HED.

According to the geometry used in this paper, the EM field due to a VED is only in the transverse magnetic (TM) mode in z direction, which can be decoupled into two components pointing in z direction and x direction, denoted as $E^{\mathrm{TM}}_{z,\mathrm{VED}}$ and $E^{\mathrm{TM}}_{x,\mathrm{VED}}$ respectively. The EM field due to a HED is also decoupled into components in z and x direction but they are different in mode. The component in z direction is only in TM mode, denoted as $E^{\mathrm{TM}}_{z,\mathrm{HED}}$. The components in x direction are in both TM and transverse electric (TE) mode, denoted by $E^{\mathrm{TM}}_{x,\mathrm{HED}}$ and $E^{\mathrm{TE}}_{x,\mathrm{HED}}$. In this way, the integrand of the EFIE includes five electric field components which should be calculated independently.

For a homogeneous medium model, the tilt angle will not influence the result and so it can be taken as a reference for validation. This method is then applied to the homogeneous models published and compared to other method such as FIT. The results presented by this method agrees to the published results quite well. Then a layered model is applied and the results show that the stability of calculation depends on the discretization size of the wire antenna, which is studied in paper C of this thesis.

1.4.3 Paper C

Y. Wei, B. Holter, I. Simonsen and L. Norum, "Calculation of Sommerfeld Integrals for Conductive Media at Low Frequencies", IEEE International Workshop on Electromagnetics, Taipei, Taiwan, 2011.

In Paper A and B, an EFIE is constructed for the unknown current distribution which is then calculated by MOM. Since for a homogeneous case, the EFIE can be simplified into the well known Pocklington's integral equation, which has an analytical equation in the integral, the Pocklington's integral equation can be used as a reference to validate the calculation of the EFIE. In using MOM, the current along the wire antenna is discretized into small

evenly distributed elements, $I(z')d\ell$. When the size of the elements is small, the current in each element can be assumed to be a constant. The EFIE is then transformed into a series of linear equations

$$\mathbf{G}(z, z')\mathbf{I}(z') = \mathbf{b}(z), \tag{1.4.5}$$

Theoretically, the smaller the size of the elements, the more accurate the result will be. However, comparison to the results of the Pocklington's integral equation shows that there is a big error when the size is small. This paper addresses the reason of this error and presents a mathematical method for solving it.

By carefully comparing the calculations of the two methods, small differences are found in the two coefficient matrixes, especially the sub-diagonal elements. Numerical tests prove that even though the differences are tiny, they will introduce a significant difference in the calculation of the EFIE. In other words, the coefficient matrix is ill conditioned. Further study shows that the difference comes from the calculation error of the Sommerfeld identity, which is an integral of an oscillating function. To evaluate such an integral, traditionally, one can use asymptotic methods or numerical methods. The asymptotic methods include method of stationary phase and method of steepest descent [34, Ch2]. The claimed best numerical method for the integration of an oscillating function is the Integration-Summation-Extrapolation (ISE) method [44]. However, for geophysical problems, which often operates in a highly conductive medium and at very low frequency, all of these methods present difficulties. The asymptotic method does not work for the near field and the numerical method is computationally intense with large convergence ranges.

To overcome these difficulties, a new asymptotic split method is developed to calculate the Sommerfeld identity for the special geophysical condition. The concept is that if an asymptotic equation is subtracted from the integral kernel, the new equation will converge much faster than the original function, which makes it much easier to be calculated numerically. The integral of the additional asymptotic equation can be evaluated by a Laplace transform, which yields an analytical solution. This method reduces the error compared to previous methods at least 50 times for the example presented in the paper without increasing computational difficulties for the calculations.

1.4.4 Paper D

Y. Wei, B. Holter, I. Simonsen and L. Norum, "Efficient and Accurate Numerical Evaluation of Sommerfeld Integrals for Conductive Media at Low

Frequencies", proc. Geophysics, submitted.

Based on the study in Paper A, B and C, this paper presents a complete dissertation of applying the metal well casing as a medium to transmit EM signals between downhole and surface. Theoretically, by using Maxwell equations, the scattered electric field $\mathbf{E}^{(s)}$ related to a current density can be represented by a Helmholtz equation,

$$\nabla \times \nabla \times \mathbf{E}^{(s)}(\mathbf{r},\omega) - k^2\mathbf{E}^{(s)}(\mathbf{r},\omega) = i\omega\mu\mathbf{J}(\mathbf{r},\omega), \tag{1.4.6}$$

the solution to (1.4.6) can be expressed as

$$\mathbf{E}^{(s)}(\mathbf{r},\omega) = i\omega\mu \int dr^3 G(\mathbf{r},\mathbf{r}')\mathbf{J}(\mathbf{r}',\omega), \tag{1.4.7}$$

where $G(\mathbf{r},\mathbf{r}')$ is the dyadic Green's function in (1.4.1). For the longitudinal component of the electric field on the surface of the well casing, $\mathbf{E}^{(i)}(\mathbf{r},\omega) + \mathbf{E}^{(s)}(\mathbf{r},\omega) = 0$, if the metal of the well casing is considered a perfect electric conductor. With this result, an EFIE for the unknown current $I(\mathbf{r})$ can be built,

$$\int_0^\ell dz' G(\mathbf{r},\mathbf{r}')I(\mathbf{r}') = i4\pi\epsilon\omega E^{(i)}(\mathbf{r}). \tag{1.4.8}$$

For a homogeneous medium, the EFIE can be simplified to the wellknown Pocklington's integral equation, which has an analytic equation in the integral and can be calculated by MOM directly. When the surrouding medium is a horizontally layered medium, the fields induced from each of the point sources must first be expanded into an integral of plane waves by the Sommerfeld identity. The field in the surrounding medium can be evaluated by carefully considering the transmission and reflection of the plane waves at interfaces between layers.

It is obvious that the Pocklington's integral equation is a special case of the latter and both of them should achieve the same results for a homogeneous earth. Therefore, the Pocklington's integral equation can be used as a reference to the calculation of the latter. By comparing the calculation of the two methods, the difficulty in calculating the Sommerfeld identity in the latter is found and a new asymptotic split method is introduced for low operating frequencies and highly conductive medium case. This method is applied to a homogenous model and proved that it can improve the calculation accuracy greatly without adding extra calculation complexity. It is also applied to a model where the wire antenna is assumed to be vertically placed in a horizontally layered medium. The numerical results are compared to

those achieved by using electric network method and show that they agree to each other quite well.

The asymptotic split method is applied to models where the wire antenna is assumed to be arbitrarily placed in a horizontally layered model, as studied in Paper B. Numerical results for this model are presented in Appendix in this thesis. In particular, the effects of different tilt angles between the wire antenna and the z-axis are studied and compared.

In 2010, an experiment was carried out by WINS [1] and SINTEF [2] to test signal transmission along a metal well casing. With the permission authorized by them, the experiment data can be applied to test the numerical results given by the method presented in this paper. The comparison of the numerical results to the experiment data shows that they agree to each other quite well.

1.4.5 Supplement

Just as I was about to finish my thesis, I was informed through a review process that a mathematical method similar to that introduced in Paper D had been published by others. In the following, a brief review on the published papers and a comparison to my work are presented.

In 1986, D. R. Jackson and N. G. Alexopoulos published a paper in which they introduced a method for the evaluation of the electric field from a Hertzian dipole in a layered geometry [45]. They started from the calculation of the Hertzian potential

$$\Pi = \int_0^\infty f(\lambda) J_0(\lambda r) d\lambda, \tag{1.4.9}$$

in which the integrand is equal to

$$f(\lambda) = \frac{2}{D_e(\lambda)} \frac{\lambda}{u_1} \left[\frac{1}{\mu_r} u_1 \cosh u_1(B - z') + u \sinh u_1(B - z') \right] \sinh u_1 z, \tag{1.4.10}$$

where λ is denoted as k_ρ and u_1 is denoted as k_z in this thesis. B is the coordinate of the interface. The author pointed out that the integral was nonconvergent when the observation point $z = z'$. To overcome this problem,

[1] WINS is the abbreviation of a norwegian company, Wireless Instrumentation Systems AS. This company develops technology and solutions for down-hole energy generation, instrumentation and wireless communication.

[2] SINTEF is the largest independent research organisation in Scandinavia, which develops technology solutions that are brought into practical use.

the hyperbolic functions could be approximated by [45, (11)]

$$\sinh(u_1 a) \approx \frac{1}{2} e^{+\lambda a}. \tag{1.4.11}$$

as $\lambda \to \infty$. Then an asymptotic function $f_0(\lambda)$ could be composed for the integrand,

$$f_0(\lambda) = \sum_{n=1}^{N} \frac{a_n}{k_0} e^{-\lambda \xi_n}, \tag{1.4.12}$$

where N depended on the number of layers. This asymptotic function was then subtracted and added from the original integrand $f(\lambda)$. The integration on the added term could be calculated in a closed form and the integration on the term $f(\lambda) - f_0(\lambda)$ could be evaluated numerically.

Compared to [45], we developed the method in a similar way by adding and subtracting an asymptotic function to the original integrands. The integration of the asymptotic function can then be calculated analytically and the integration of the tail term can be evaluated numerically. When we developed this method, we were focusing on a special low frequency and high conductive problem, based on which the asymptotic equation was deduced. Unlike their work, we started from dyadic Green's function, not from Hertzian potential ant when we apply this method, we only use it on the points near the source point. For the point $z = z'$, the field is evaluated directly by Pocklington's integral equation.

In 2006, Ergun Simsek, QingHuo Liu and BaoJun Wei published a paper in which they presented a method to evaluate mulitlayered medium Green's functions for general electric and magnetic sources [46]. In their method, a special subtraction procedure was applied to each term of the Sommerfeld integrands to make them rapidly decreasing and the contribution of the subtracted terms are calculated analytically.

I think the main difference between their work and our work is the project and procedure of finding the method. In our case, we are studying the current distribution along a metal casing in a multilayered medium and find that the results are not stable by using ordinary integral method. Then we find the reason of the big calculation error by comparing the EFIE method to the Pocklington's integral method in a homogeneous case. In addition to this, there is a small difference in finding the asymptotic equation. In this thesis, the asymptotic equation is found by studying the each term of the Green's function at a condition $\sigma/\omega >> \epsilon$ for a homogeneous model. In their paper, they considered a point source in a layered medium, in particular, they studied the source point near an interface between different layers and deduced asymptotic equations for different cases of receiver points.

In 2006, M. P. Spowart and E. F. Kuester published a paper in which they introdued a method for the studying of microstrip antennas [47]. Similar to [45], the integral equation was developed from the Hertzian potential and an asymptotic equation was added and subtracted from the original integrand in the following way

$$I = \int_0^N f(\lambda)d\lambda + \int_N^\infty f(\lambda)d\lambda \tag{1.4.13}$$

$$= \int_0^N f(\lambda)d\lambda + \int_N^\infty (f - f_{AET})d\lambda + \int_N^\infty f_{AET}d\lambda. \tag{1.4.14}$$

The integration of the asymptotic equation can be found by

$$\int_N^\infty f_{AET}d\lambda = (\texttt{explicit closed form expression}) + \int_0^N g(\lambda)d\lambda, \tag{1.4.15}$$

and finally the original integral can be evaluated by

$$I \approx \int_0^N (f + g)d\lambda + (\texttt{explicit closed form expression}) \tag{1.4.16}$$

Compared to [45], the author went one step further by studying the pole problem and applied steepest-descent path evaluation method for calculating the integral for the pole.

Compared to their idea, the method introduced in this thesis was developed in a slightly different way,

$$I = \int_0^N f(\lambda)d\lambda + \int_N^\infty f(\lambda)d\lambda \tag{1.4.17}$$

$$= \int_0^N (f(\lambda) - f_{AET}(\lambda))d\lambda + \int_N^\infty (f(\lambda) - f_{AET}(\lambda))d\lambda + \int_0^\infty f_{AET}(\lambda)d\lambda. \tag{1.4.18}$$

Since $(f(\lambda) - f_{AET}(\lambda)) \to 0$ when $\lambda \to \infty$, the second integral can be neglected and the total integral is approximately equal to

$$I = \int_0^N (f(\lambda) - f_{AET}(\lambda))d\lambda + \int_0^\infty f_{AET}(\lambda)d\lambda. \tag{1.4.19}$$

where the first part can be calculated numerically and the second part gives an explicit closed form. In addition to the difference of development, we

develop this method for problem of using low frequency and highly conductive medium, which ensures that there is no difficulty in pole problems.

In 2010, Shaun D. Walker, Deb Chatterjee and Michael S. Kluskens submitted a paper to Antennas and Propagation Society International Symposium [48], in which they also mentioned to use analytical method for closed-form evalution of the Sommerfeld integral tail. They deduce their method for the z-component electric field from a HED. In 2012, Deb Chatterjee, Sadasiva M. Rao and Michael S. Kluskens published a paper in 2012 IEEE International Symposium on Antennas and Propagation and USNC-URSI National Radio Science Meeting [49]. In this paper, they developed a method a little difference to that in [48] by keeping the Bessel function intact. In their method, the Sommerfeld integral is divided into two parts

$$I = \int_0^{k_p} k_\rho^2 J_1(k_\rho \rho) W^p(k_\rho) dk_\rho + \int_{k_p}^{\infty} k_\rho^2 J_1(k_\rho \rho) W^p(k_\rho) dk_\rho. \tag{1.4.20}$$

The second term in the equation is the Sommerfeld tail. To calculate it, W^p is replaced by an asymptotic equation but the Bessel function is not replaced by asymptotic equation, which leads to

$$I = \int_0^{k_p} k_\rho^2 J_1(k_\rho \rho) [W^p(k_\rho) - W^p_{asy}(k_r ho)] dk_\rho + \mathcal{G}^p_{tail} \tag{1.4.21}$$

Bibliography

[1] Rober F. King. Drilling sideways – a review of horizontal well technology and its domestic application. *Energy Information Administration*, Apr. 1993.

[2] NPC working group. Working document of the NPC global oil & gas study, oil and gas technology development. 18(Topic paper # 26), Jul. 2007.

[3] Ingebenose Aitokhuehi. Real-time optimization of smart wells. *Report of Stanford University*, Jun. 2004.

[4] Changhong Gao and T. Rajeswaran. A literature review on smart well technology. *SPE, Production and Operations Symposium, Oklahoma, U.S.A.*, Mar. 2007.

[5] S. M. Mubarak, S. S. Shamrani, and M. Shafiq. Case study: Using down-hole control valves to sustain oil production from the first maximum reservoir contact, multilateral and smart well in ghawar field. *International Petroleum Technology Conference*, 2007.

[6] J. J. den Boer. The use of high temperature electronics in downhole applications. *Hiten'99 Conference in Berlin*, Jul. 1999.

[7] Ognjen Krkac, Vedran Bilas, and Davorin Ambrus. Thermal uprating of a mixed signal microcontroller. *IEEE ISIE 2005*, Jun. 2005.

[8] J. A. Henfling, Jeff Greving, Frank Maldonado, David Chavira, and Jim Uhl. Development of a ht seismic monitoring tool for downhole. *IEEE CITRES 2010*, Sep. 2010.

[9] Benjamin Jeffryes. Downhole communication method and system. *SCHLUMBERGER Patent*, (IPC8 Class : AE21B4714F1).

[10] Paul Tubel. Downhole power generation and wireless communications for intelligent completions applications. *Work Report*, Dec. 2005.

[11] Hamilton M. Johnson. A history of well logging. *Geophysics*, pages 507–527, Aug. 1962.

[12] D. C. Daev. High-frequency electromagnetic logging method. *Beijing: Petroleum Industry Press, translated into Chinese from Russian*, 1973.

[13] Weng Cho Chew. Modelling of the dielectric logging tool at high frequencies: theory. *IEEE Transactions on Geoscience and Remote Sensing*, 26 (4):382–387, Jul. 1988.

[14] Weng Cho Chew. Modelling of the dielectric logging tool at high frequencies: applications and results. *IEEE Transactions on Geoscience and Remote Sensing*, 26(4):388–398, Jul. 1988.

[15] Satoshi Ebihara and Weng Cho Chew. Calculation of sommerfeld integrals for modeling vertical dipole array antenna for borehole radar. *IEICE Trans. Electron.*, E86-C(10):2085–2096, Oct. 2003.

[16] C. Besson, M. Blenkinsop, and J. C. Trouiller. Environmental effect on deep propagation tools. *Society of Petrophysicists & Well Log Analysts*, 1986.

[17] M. Blenkinsop, P. Baker, C. Clavier, W. Kenyon, and S. D. Ligneris. Deep electromagnetic propagation tool interpretation. *Society of Petrophysicists & Well Log Analysts*, 1986.

[18] B. R. De and M. A. Nalson. Ultrabroadband electromagnetic well logging: a potential future technology. *Society of Petrophysicists & Well Log Analysts*, 1992.

[19] K. Iizuka and R. W. P. King. The dipole antenna immersed in a homogeneous conducting medium. *IRE Transactions on Antennas and Propagation*, 10:384–392, Jul. 1962.

[20] K. Iizuka and R. W. P. King. An experimental study of the half-wave dipole antenna immersed in a stratified conducting medium. *IRE Transactions on Antennas and Propagation*, 10:393–399, Jul. 1962.

[21] James R. Wait and W.C.G.Fraser. Radiation from a vertical dipole over a stratified ground. *IRE Trascations-Antennas and Propagation*, 14:144–146, Oct. 1954.

[22] James R. Wait. Em fields of a phased line current over a conducting half-space. *IEEE Transactions on Electromagnetic Compatibility*, 38(4): 608–611, Nov. 1996.

[23] A. D. Chave and C. S. Cox. Controlled electromagnetic sources for measuring electrical conductivity beneath the oceans 1. forward problem and model study. *J. Geophys. Res.*, 87(B7):5327–5338, Jul. 1982.

[24] S. Ellingsrud, T. Eidesmo, T. Schaug-Pettersen, and H. M. Pedersen. Method and apparatus for determining the nature of subterranean reservoirs. *European Patent Office EP 1-309-887-B1*, Mar. 2004.

[25] S. Ellingsrud, T. Eidesmo, M. C. Shinha, L. M. MacGregor, and S. C. Constable. Remote sensing of hydrocarbon layers by seabed logging(sbl): Results from a cruise offshore angola. *The Leading Edge*, 21(10), Oct. 2002.

[26] Steven Constable. Ten years of marine csem for hydrocarbon exploration. *Geophysics*, 75, 2010.

[27] James R. Wait and David A. Hill. Theory of transmission of electromagnetic waves along a drill rod in conducting rock. *IEEE Transactions on Geoscience Electronics*, GE-17(2):21–24, Apr. 1979.

[28] David A. Hill and James R. Wait. Electromagnetic basis of drill-rod telemetry. *Electronics Letters*, 14:532–533, Aug. 1978.

[29] P. DeGauque and R. Grudzinski. Propagation of electromagnetic waves along a drillstring of finit conductivity. *SPE Drilling Engineering*, pages 127–134, Jun. 1987.

[30] M. Y. Xia and Z. Y. Chen. Attenuation predictions at extremely low frequencies for measurement-while-drilling electromagnetic telemetry system. *IEEE Transactions on Geoscience and Remote Sensing*, 31(6): 1222–1228, Nov. 1993.

[31] Wei Yang, Carlos Torres-Verdin, Junsheng Hou, and Zhiyi Zhang. 1d subsurface electromagnetic fields excited by energized steel casing. *Geophysics*, 74(4):E159–E180, July 2009.

[32] F. N. Trofimenkoff, Michael Segal, Allan Klassen, and J. W. Haslett. Characterization of EM downhole-to-surface communication links. *IEEE Transactions on Geoscience and Remote Sensing*, 38(6):2539–2548, Nov. 2000.

[33] J. D. Jackson. *Classical Electrodynamics*. New York, Wiley, 3rd edition, 1998.

[34] Weng Cho Chew. *Waves and Fields in Inhomogeneous Media*. IEEE Press, 1st edition, 1995.

[35] Carl M. Bender and Steven A. Orszag. *Advanced Mathematical Methods for Scientists and Engineers*. Springer. Inc., 1st edition, 1999.

[36] Allen Taflove and Susan C. Hagness. *Computational Electrodynamics: The Finite-Difference Time-Domain Method*. Artech House, 2nd edition, 2000.

[37] Kane S. Yee. Numerical solution of initial boundary value problems involving maxwell's equations in isotropic media. *IEEE Transactions on Antennas and Propagation*, 14(3):302–307, May. 1966.

[38] Allen Taflove. Application of the finite-difference time-domain method to sinusoidal steady-state electromagnetic penetration problems. *IEEE Transactions on Electromagnetic Compatibility*, 22:191–202, Aug. 1980.

[39] Matthew N. O. Sadiku. *Numerical Techniques in Electromagnetics*. CRC, 2nd edition, 2000.

[40] T. Weiland. A discretization model for the solution of maxwell's equations for six-component fields. *Archiv fuer Elektronik und Uebertragungstechnik*, 31:116–120, Mar. 1977.

[41] T. Weiland. Time domain electromagnetic field computation with finite difference methods. *International Journal of Numerical Modelling*, 9: 295–319, 1996.

[42] T. Weiland. Discrete electromagnetism with the finite integral technique. *Progress in Electromagnetics Research*, 32:65–87, 2001.

[43] Constantine A. Balanis. *Antenna Theory*. John Wiley & Sons, Inc., 2nd edition, 1997.

[44] S. K. Lucas and H. A. Stone. Evaluating infinite integrals involving bessel functions of arbitrary order. *J. Comput. Appl. Math.*, 64:217–231, Dec. 1995.

[45] D. R. Jackson and N. G. Alexopoulos. An asymptotic extraction technique for evaluating sommerfeld-type integrals. *IEEE Trans. Antennas Propag.*, 34:1467–1470, Dec. 1986.

[46] Ergun Simsek, QingHuo Liu, and BaoJun Wei. Singularity subtraction for evaluation of green's functions for multilayer media. *IEEE Transactions on Microwave Theory and Techniques*, 54:216–225, Jan. 2006.

[47] M. P. Spowart and E. F. Kuester. A novel asymptotic extraction technique for the efficient evaulation of a class of double sommerfeld integrals. *Journal of Computational and Applied Mathematics*, 197:597–611, Dec. 2006.

[48] Shaun D. Walker, Deb Chatterjee, and Michael S. Kluskens. A new approach for improved evaluation of sommerfeld integral tails for pec-terminated single layered media. *Antennas and Propagation Society International Symposium (APSURSI), 2010, IEEE*, July.

[49] D. Chatterjee, S. M. Rao, and M. S. Kluskens. Numerical comparison of exact and asymptotic methods for sommerfeld integral evaluation with applications to microstrip antennas. *2012 IEEE International Symposium on Antennas and Propagation and USNC-URSI National Radio Science Meeting*, Jul. 2012.

Part II

Included papers

A Wave Propagation Along a Thin Vertical Wire Antenna Placed in a Horizontally Layered Medium

Yingkang Wei, Bengt Holter, Ingve Simenson, Karsten Husby, Jacob Kuhnle, Lars Norum

The 2010 annual conference of the Applied Computational Electromagnetics Society (ACES2010)

Abstract

A theoretical and numerical analysis of the wave propagation along a long thin wire antenna is presented. The wire is assumed to be placed vertically in a conductive inhomogeneous medium, represented by a finite set of horizontal plane layers each of which is characterized by an individual conductivity. The current distribution along the wire antenna is obtained as the solution of the electric field integral equation that is solved by the method of moments. Numerical results are presented and compared to similar work for homogeneous media.

A.1 introduction

Wave propagation along a wire antenna placed in a conductive medium is an interesting topic in low frequency communications. In 1979, J. R. Wait and D. A. Hill [1] calculated the current distribution along a drill rod surrounded by conducting host rock. They assumed an infinite long perfect conducting rod located in a homogeneous lossy medium. The source was assumed to be a toroidal coil emitting a 5KHz electromagnetic wave riding on the rod. They found that the attenuation would be at least as great as that of plane waves in the conductive medium surrounding the rod. In 1989, P. DeGauque

and R. Grudzinski [2] studied the current distribution along a drillstring of finite conductivity embedded in a homogeneous conductive medium using Pocklington's integral equation[3, Ch.8]. The source was assumed to be an electric delta gap which could be viewed as a simple electric dipole. The frequency range of the emitted sigmal was 0.1 – 10Hz. They found that the surface impedance played a major role in attenuating the signal. However, for frequencies below a few hertz, the attenuation did not vary much and the optimum frequency for maximum data rate was argued to be about 3Hz.

To the author's knowledge, an analytical solution of the current distribution along a long metal wire antenna in a conductive inhomogeneous medium is not known. To address this issue, a theoretical and numerical analysis of the wave propagation along a long thin wire antenna is presented. The wire is assumed to be placed vertically in a conductive inhomogeneous medium, represented by a finite set of horizontal plane layers (orthogonal to the antenna), each of which is characterized by an individual conductivity. The current distribution along the wire antenna is obtained as the solution of the electric field integral equation that is solved by the method of moments.

A.2 Theoretical Approach

A.2.1 The field from a wire current in a homogeneous medium

A long straight wire antenna of length ℓ and radius a is assumed to be placed vertically in a homogeneous medium and oriented along the positive z-axis. The electric field $\mathbf{E}(\mathbf{r})$ at an observation point $\mathbf{r} = (x, y, z)$ is related to the current density $\mathbf{J}(\mathbf{r}')$ on the wire antenna by the integral [4, Eq. (7.1.2)]

$$\mathbf{E}(\mathbf{r}) = i\omega\mu \int_{V'} d^3\mathbf{r}' \overline{\mathbf{G}}(\mathbf{r}, \mathbf{r}') \cdot \mathbf{J}(\mathbf{r}'). \tag{A.2.1}$$

The dyadic Green's function $\overline{\mathbf{G}}(\mathbf{r}, \mathbf{r}')$ is defined as [4, Eq. (7.1.19)]

$$\overline{\mathbf{G}}(\mathbf{r}, \mathbf{r}') = \left[\overline{\mathbf{I}} + \frac{\nabla\nabla}{k^2}\right] g(\mathbf{r}, \mathbf{r}'), \tag{A.2.2}$$

where $\overline{\mathbf{I}}$ denotes the unit dyad and $g(\mathbf{r}, \mathbf{r}')$ is the scalar Green's function. In an unbounded homogeneous medium $g(\mathbf{r}, \mathbf{r}') = \frac{e^{ik|\mathbf{r}-\mathbf{r}'|}}{4\pi|\mathbf{r}-\mathbf{r}'|}$ and $k = \omega\sqrt{\mu(\epsilon + i(\sigma/\omega))}$ ($\mathrm{Im}(k) > 0$) is the complex wave number. In the following, the antenna is assumed to be very thin compared to its length, i.e. $\ell \gg a$. Under this

assumption, the current density along the wire can be approximately written as:

$$\mathbf{J}(\mathbf{r}') = I(z')\delta(x')\delta(y')\hat{\mathbf{z}}, \tag{A.2.3}$$

where $I(z')$ is assumed to be an equivalent line-source current [3, Ch8]. Inserting (A.2.2) and (A.2.3) into (A.2.1), the z-component of the electric field directed along the antenna can be written as

$$E_z(\mathbf{r}) = \frac{i\omega\mu}{4\pi k^2}\int_0^\ell dz' I(z')\left[k^2 + \frac{\partial^2}{\partial z^2}\right]\frac{e^{ikR}}{R}, \tag{A.2.4}$$

where $R = \sqrt{\rho^2 + (z-z')^2}$, and $\rho = \sqrt{x^2+y^2}$.

A.2.2 The field from a wire current in a layered medium

The wire antenna is now assumed to be placed vertically in a conductive inhomogeneous medium represented by a finite set of horizontal plane layers, where each layer is characterized by an individual conductivity. In [4, Ch. 2], a method to obtain a solution for the electromagnetic fields generated by a point or line source embedded in such a multilayered profile is presented. The heart of the approach in [4, Ch. 2] is based on the fact that nonplanar waves generated by finite sources can be expanded into an integral summation of plane waves. The mathematical identity is known as Weyl's identity [4, Eq. (2.2.27)], and it represents a plane-wave expansion of a spherical wave. Once this is done, the general theory of reflection and transmission of plane waves can be used to find the electromagnetic fields within any of the layers in response to a source within one of the layers. In this section, this method is used to find an expression for the z-component of the electric field generated by the antenna. Due to limited space available, a detailed explanation of the method and a presentation of all the involved symbols and expressions are not included. The interested reader is rather referred to [4, Ch.2] for further details. Note that in this paper the z-axis points upwards, whereas in [4, Fig. 2.4.1], it points downwards. As a result, there are some differences in the subindexes of the expressions in this paper and the similar ones in [4].

Since the antenna is assumed to be placed along the z-axis of a cylindrical coordinate system, the electric field component in question is the z-component which is directed along the antenna. To derive an expression for this field, the Sommerfeld identity is used as a starting point. The Sommerfeld identity [4, Eq. (2.2.30)] can be developed from the Weyl's identity and is equal to

$$\frac{e^{ikR}}{R} = i\int_0^\infty dk_\rho \frac{k_\rho}{k_z} J_0(k_\rho\rho)e^{ik_z|z|}, \tag{A.2.5}$$

which shows that a spherical wave can be expanded into an integral summation of cylindrical waves in the ρ direction times a plane wave in the z-direction over all wave numbers k_ρ. In (A.2.5), $J_0(\cdot)$ denotes a Bessel function of the first kind and zeroth order, and $k_z = \sqrt{k^2 - k_\rho^2}$ ($\mathrm{Im}(k_z) > 0$) denotes the z-component of the wave vector $\mathbf{k}$. In the following, it is assumed that a source at $z = z'$ is embedded in layer m of a multilayered profile (see [4, Fig. 2.4.1] or [5, Fig. 1] as a reference). Since the positive z-axis in this case points upwards, layer m is mathematically constrained to be within the limits $d_{m-1} < z' < d_m$. According to [4], the z variation an upgoing and downgoing wave can be expressed as $F(z, z')$. The field inside layer m due to a source in layer m can be divided into two parts, representing an upgoing wave (F_+) and a downgoing wave (F_-), which can be expressed as

$$F_+(z, z') = A_m^+ \left[e^{ik_{mz}(z-z')} + \tilde{R}_{m,m+1} e^{ik_{mz}(2d_m - z - z')} \right] \quad z > z', \tag{A.2.6}$$

$$F_-(z, z') = A_m^- \left[e^{-ik_{mz}(z-z')} + \tilde{R}_{m,m-1} e^{ik_{mz}(z + z' - 2d_{m-1})} \right] \quad z < z', \tag{A.2.7}$$

where $\tilde{R}_{m,m+1}$ and $\tilde{R}_{m,m-1}$ represent generalized reflection coefficients for waves emanating from layer m into layer $m+1$ and $m-1$, respectively, d_m denotes the z-coordinate of the interface separating medium m and $m+1$, and k_{mz} is used to indicate the z-component of the wave vector $\mathbf{k}_m$ of layer m. In addition to the adjacent layers $m+1$ and $m-1$, they also include the effect of the subsurface reflections caused by the layers above $m+1$ and below $m-1$. The amplitudes in (A.2.6) and (A.2.7) are equal to

$$A_m^+ = \tilde{M}_m \left[1 + \tilde{R}_{m,m-1} e^{2ik_{mz}(z' - d_{m-1})} \right] \tag{A.2.8}$$

$$A_m^- = \tilde{M}_m \left[1 + \tilde{R}_{m,m+1} e^{2ik_{mz}(d_m - z')} \right], \tag{A.2.9}$$

in which

$$\tilde{M}_m = [1 - \tilde{R}_{m,m-1} \tilde{R}_{m,m+1} e^{2ik_{mz}(d_m - d_{m-1})}]^{-1}. \tag{A.2.10}$$

In a similar fashion, the field variation in layer $m+1$ and $m-1$ can be written as

$$F_{m+1}(z, z') = A_{m+1}^+ \left[e^{ik_{(m+1)z}(z - d_m)} + \tilde{R}_{m+1,m+2} e^{ik_{(m+1)z}(2d_{m+1} - z - d_m)} \right] \tag{A.2.11}$$

$$F_{m-1}(z, z') = A_{m-1}^- \left[e^{ik_{(m-1)z}(d_{m-1} - z)} + \tilde{R}_{m-1,m-2} e^{ik_{(m-1)z}(z + d_{m-1} - 2d_{m-2})} \right], \tag{A.2.12}$$

where

$$A^+_{m+1} = \frac{T_{m,m+1}A^+_m e^{ik_{mz}(d_m - z')}}{1 - R_{m+1,m}\tilde{R}_{m+1,m+2}e^{2ik_{(m+1)z}(d_{m+1}-d_m)}} \quad (A.2.13)$$

$$A^-_{m-1} = \frac{T_{m,m-1}A^-_m e^{ik_{mz}(z'-d_{m-1})}}{1 - R_{m-1,m}\tilde{R}_{m-1,m-2}e^{2ik_{(m-1)z}(d_{m-1}-d_{m-2})}}. \quad (A.2.14)$$

The expressions $T_{m,m+1}$ and $R_{m+1,m}$ as well as $T_{m,m-1}$ and $R_{m-1,m}$ represent transmission and reflection coefficients between layer m and the adjacent layers $m+1$ and $m-1$ only. The field variations within the layers above $m+1$ or below $m-1$ are obtained through a recursive approach. The above expressions for $F(z,z')$ may be introduced into (A.2.5), and when combined with (A.2.4), the z-component of the electric field directed along the antenna can be expressed as

$$E_z(a,z) = \frac{-\omega\mu}{4\pi k^2}\int_0^\ell dz' I(z')(k^2 + \frac{\partial^2}{\partial z^2})\int_0^\infty dk_\rho \frac{k_\rho}{k_{z'}} J_0(k_\rho a)F(z,z'). \quad (A.2.15)$$

A thing to notice is that when $z = 0$,

$$(k^2 + \frac{\partial^2}{\partial z^2})\int_0^\infty dk_\rho \frac{k_\rho}{k_{z'}} J_0(k_\rho a)F(z,z') = \int_0^\infty dk_\rho \frac{k_\rho^3}{k_{z'}} J_0(k_\rho a)F(z,z') \quad (A.2.16)$$

goes to infinity. The reason for this is that when $z = 0$, it indicates wave propogating in ρ direction and $k_z = 0$. In this case, the integrand in (A.2.4) has the following closed form solution [4, pp. 118]

$$(k^2 + \frac{\partial^2}{\partial z^2})\frac{e^{ikR}}{R} = \frac{e^{ikR}}{R^5}[(1 - ikR)(2R^2 - 3a^2) + (kaR)^2]. \quad (A.2.17)$$

The right hand side of (A.2.17) represents the core of Pocklington's integral equation [3].

A.2.3 Calculating the current by the method of moments

Equation (A.2.4) is the electric field integral equation with $I(z')$ as the unknown current distribution and the electric field as the known excitation function. The current may be determined by the application of boundary conditions on the surface of the antenna. For a perfect conductor, the electric field along the antenna is equal to zero $E_z(a,z) = 0$ at all points except at the source. The integral in (A.2.4) can then be solved with respect to $I(z')$ by using the method of moments [6, 3]. The length of the wire antenna is discretized into N equidistant points $z_i = (i - 1/2)\Delta z$, each of length

$\Delta z = \ell/N$. Under the assumption that the unknown current $I(z)$ varies slowly over the length Δz, and therefore can be approximated to be constant and equal to $I(z_i)$, the following set of linear equation is obtained

$$\mathbf{G}(z, z')\mathbf{I}(z') = \mathbf{b}(z), \tag{A.2.18}$$

where the vector $\mathbf{I}(z')$ represents the current at the points $(z'_1, z'_2, \cdots, z'_N)$ along the wire antenna. The matrix $\mathbf{G}(z, z')$ is defined as

$$\mathbf{G}(z, z') = \begin{bmatrix} g(z_1, z'_1) & g(z_1, z'_2) & \cdots & g(z_1, z'_N) \\ g(z_2, z'_1) & g(z_2, z'_2) & \cdots & g(z_2, z'_N) \\ \cdots & \cdots & & \\ g(z_N, z'_1) & g(z_N, z'_2) & \cdots & g(z_N, z'_N) \end{bmatrix}, \tag{A.2.19}$$

in which the individual matrix elements are equal to

$$g(z_i, z_j) = \frac{-\omega\mu\Delta z}{4\pi} \int_0^\infty dk_\rho \left\{ \frac{k_\rho^3}{k_m^2 k_{nz}} J_0(k_\rho \rho) F(z, z_j) \right\}_{z=z_i}. \tag{A.2.20}$$

Where z_i is in layer m. From the boundary conditions, the vector $\mathbf{b}(z)$ is equal to $\mathbf{b}(z) = [0, 0, \cdots, 0, 1, 0, \cdots, 0]^T$. If the wire is not a perfect conductor, the matrix equation in (A.2.18) changes into [2]

$$(\mathbf{G}(z, z') - Z_i\mathbf{I})\mathbf{I}(z') = \mathbf{b}(z), \tag{A.2.21}$$

where $\mathbf{I}$ is an identity matrix, and Z_i is the internal impedance of the wire antenna equal to

$$Z_i = \frac{ik_s J_0(ik_s a)}{2\pi a \sigma_s J_1(ik_s a)}. \tag{A.2.22}$$

The symbols σ_s and k_s represent the wavenumber and conductivity of the antenna respectively.

A.3 Implementation and numerical results

The numerical results in this paper are obtained using MATLAB. To solve the double integral in (A.2.15), the inner integral with respect to k_ρ needs to be solved first. However, since $1/k_z = 1/\sqrt{k^2 - k_\rho^2}$, there is a pole at $k_\rho = k$ for $k_\rho \in (0, \infty)$. This means that k_ρ should be selected more finely near the pole. For the integration with respect to z', both the built-in MATLAB function *quad* and a direct integration technique have been used. The *quad* function runs faster and is more stable than a direct integration approach. In Fig. A.1, the result of the direct integration approach is depicted for a

perfect conductive wire antenna in a homogeneous medium with conductivity $\sigma_1 = 4\text{S/m}$, operating at a frequency of 100Hz. It shows that the results vary with the number of selected points. In Fig. A.2, similar results are depicted when using the *quad* function. It is observed that the *quad* function achieves the same result as the direct integration approach but with less points involved.

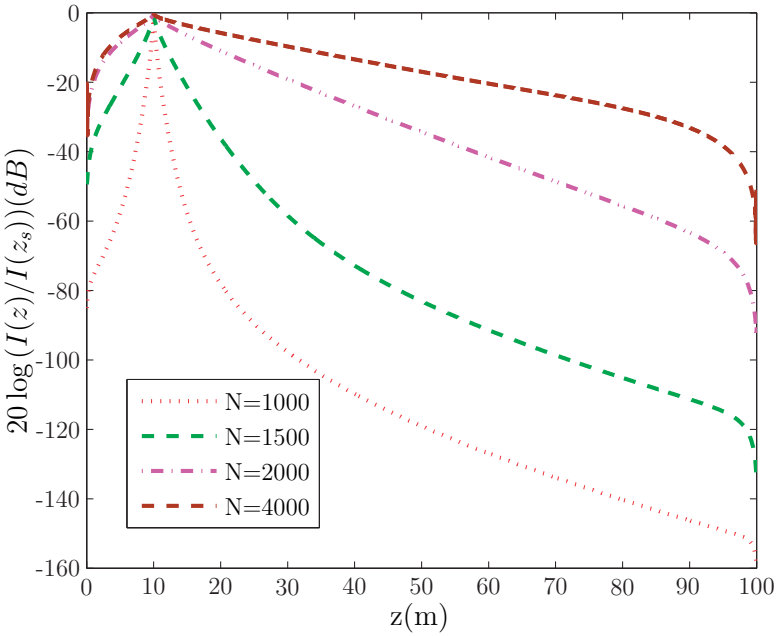

Figure A.1: Current distribution along a perfect conductive wire antenna of length $\ell = 100\text{m}$ and radius $a = 0.1\text{m}$. The source is located at 0.1ℓ. The operating frequency $f = 100\text{Hz}$ and conductivity of the medium is $\sigma_1 = 4\text{S/m}$. Brute integration method is applied.

To verify that the numerical results in this paper are consistent with previously reported results in homogeneous media, the results from [2, Fig. 6] and [2, Fig. 4] have been reproduced and are presented in Fig. A.3 and Fig. A.4, respectively. By inspection, the results obtained in this paper are in good agreement with the previously published results. However, despite a similar shape of the curves, the attenuation of the current distribution in this paper is larger than the those presented in [2, Fig. 4]. As a check, the results using *quad* was compared to a similar model evaluated by finite integral technique (FIT) method. Fig. A.5 shows they are in good agreement with each other.

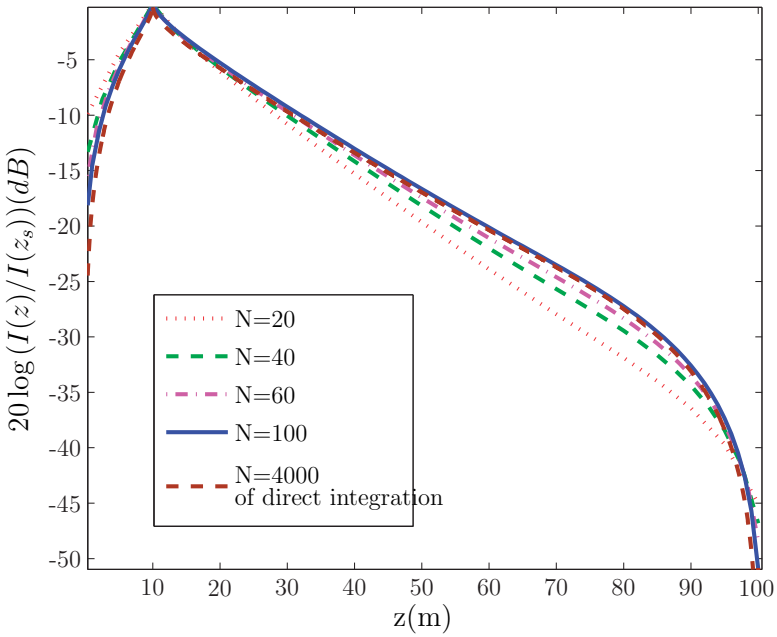

Figure A.2: Numerical results obtained by using the built-in function *quad* to integrate for the same model in figure A.1.

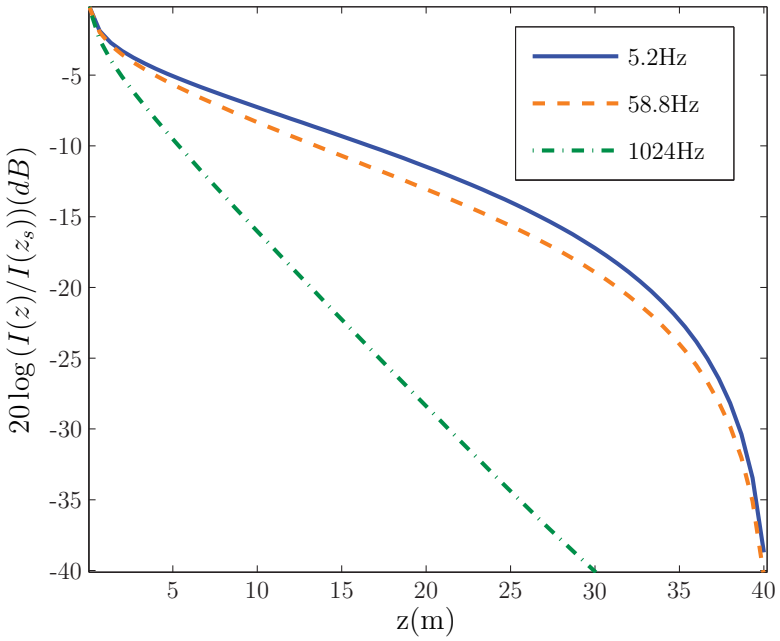

Figure A.3: A replica of [2, Fig. 6], representing the theoretical current distribution at different frequencies for a metallic pipe of 40m immersed in seawater with conductivity $\sigma_1 = 4\text{S/m}$. The conductivity of the pipe is $\sigma_s = 4.2 \cdot 10^6\text{S/m}$.

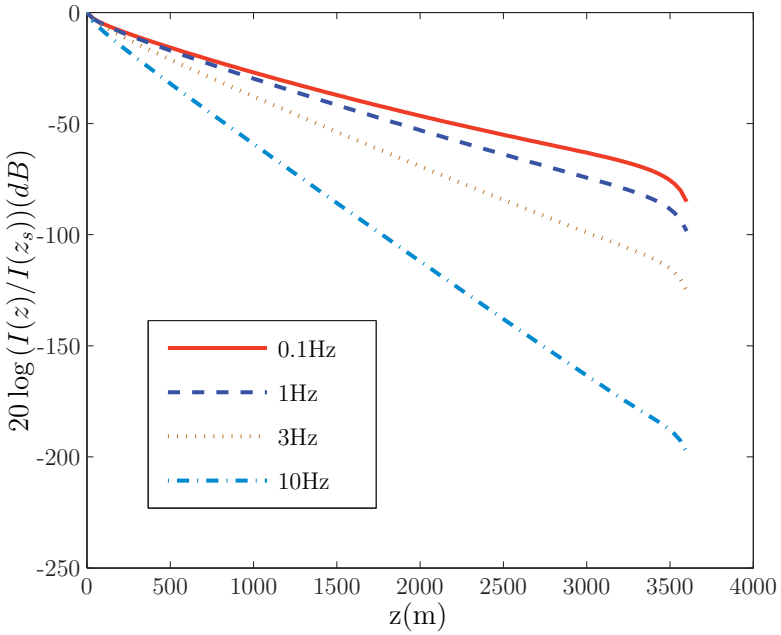

Figure A.4: A replica of [2, Fig. 4], representing the theoretical current distribution along a drillstring of 3600m (radius 10cm) through a homogeneous medium with conductivity $\sigma_1 = 0.5\text{S/m}$. The conductivity of the drillstring is $\sigma_s = 2 \cdot 10^6\text{S/m}$.

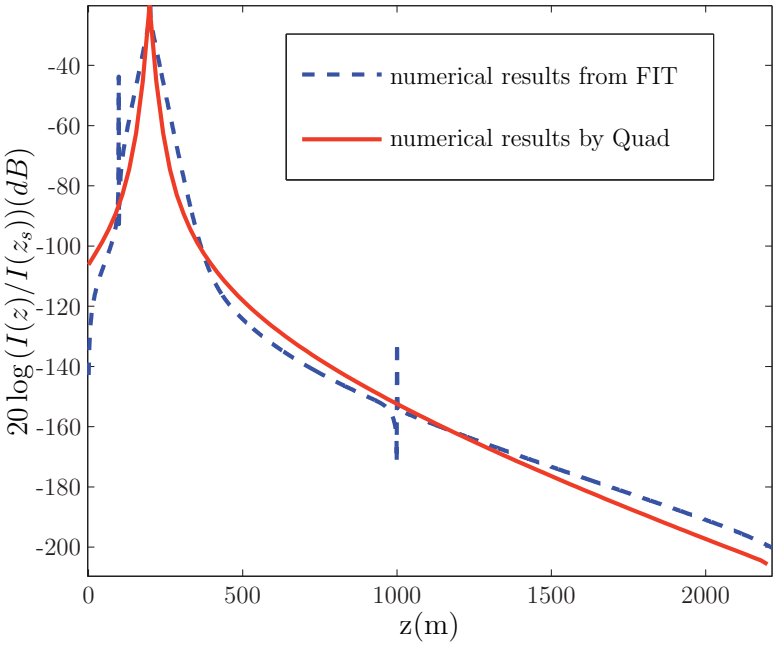

Figure A.5: Comparison with FIT simulation

For the simulations in an inhomogeneous medium, the simple model of Fig. A.6 is considered. In this model, the wire antenna was assumed to have a length $l = 1000m$, the conductivities of layer 1 and layer 3 are identical and equal to $\sigma_1 = \sigma_3 = 1\text{S/m}$, whereas the conductivity of layer 2 is equal to $\sigma_2 = 4\text{S/m}$. The source is located at $z_s = 0.1\ell$ and the interfaces $d_1 = 0.7\ell$ and $d_2 = 0.8\ell$, and the antenna is assumed to be a perfect conductor.

The theoretical current distribution using the *quad* function is presented in Fig. A.7. It is observed that attenuation increases both when the frequency is increased and when the conductivity increases in layer 2. In Fig. A.8, $d_1 = 0.6l$ and $d_2 = 0.8l$, the result at 10Hz is compared to the attenuation of a TEM wave in a similar environment. It is observed that the current along the wire antenna attenuates faster than the TEM wave, which proves the conclusion of J. R. Wait in [1] that a signal along the antenna will attenuate at least as great as that of plane waves in a conductive medium.

A.4 Conclusion and Outlook

A theoretical approach to obtain the current distribution along a wire antenna placed in an inhomogeneous layered medium is presented. The numer-

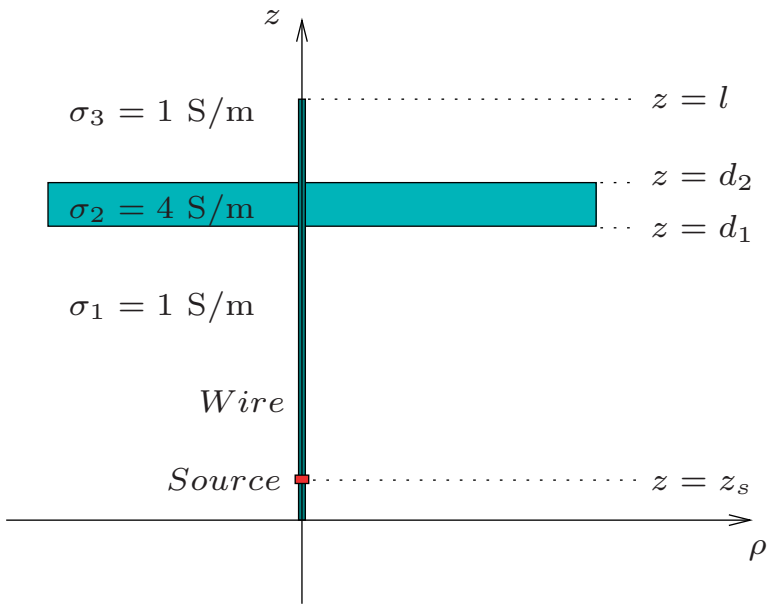

Figure A.6: Inhomogeneous layered profile used in the simulations

ical results show that the attenuation will vary according to the conductivity of the environment and at least as fast as a plane wave propagating in a similar environment.

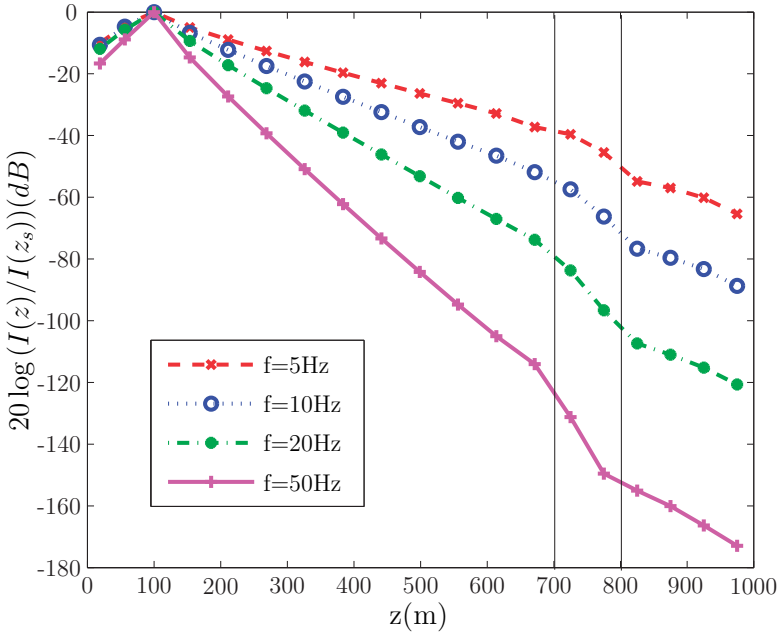

Figure A.7: Theoretical current distribution along the wire antenna as a function of frequency when placed in the inhomogeneous medium profile depicted in Fig. A.6. The source is located at $z_s = 100m$ and the interfaces are $d_1 = 700m$ and $d_2 = 800m$.

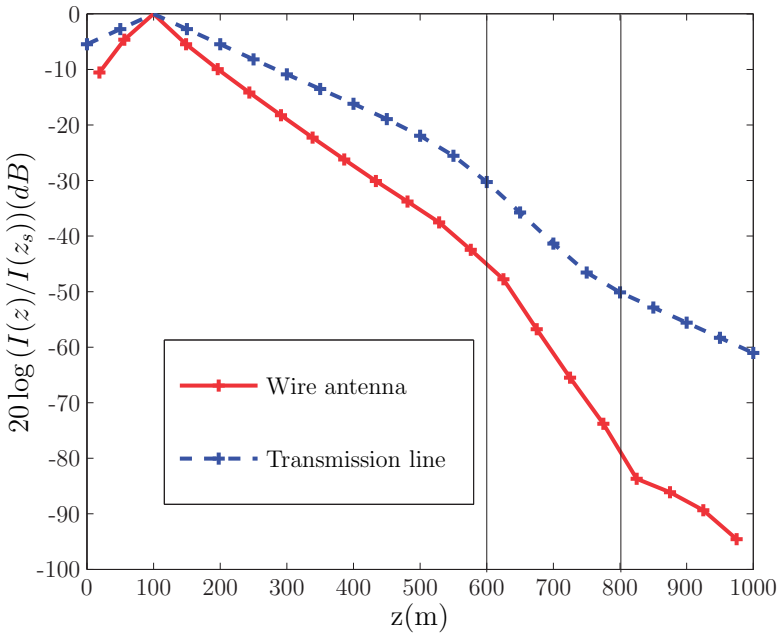

Figure A.8: Comparison of the attenuation of the current distribution along the antenna and that of a TEM wave at 10Hz. The source is located at $z_s = 100m$ and the interfaces are $d_1 = 600m$ and $d_2 = 800m$.

Bibliography

[1] James R. Wait and David A. Hill. Theory of transmission of electromagnetic waves along a drill rod in conducting rock. *IEEE Transactions on Geoscience Electronics*, GE-17(2):21–24, Apr. 1979.

[2] P. DeGauque and R. Grudzinski. Propagation of electromagnetic waves along a drillstring of finit conductivity. *SPE Drilling Engineering*, pages 127–134, Jun. 1987.

[3] Constantine A. Balanis. *Antenna Theory*. John Wiley & Sons, Inc., 2nd edition, 1997.

[4] Weng Cho Chew. *Waves and Fields in Inhomogeneous Media*. IEEE Press, 1st edition, 1995.

[5] Satoshi Ebihara and Weng Cho Chew. Calculation of sommerfeld integrals for modeling vertical dipole array antenna for borehole radar. *IEICE Trans. Electron.*, E86-C(10):2085–2096, Oct. 2003.

[6] R. F. Harrington. *Field Computation by Moment Methods*. IEEE Press, 2nd edition, 1993.

B Current Distribution Along a Long Thin Wire Antenna Placed in a Horizontally Layered Medium

Yingkang Wei, Bengt Holter, Ingve Simenson, Karsten Husby, Jacob Kuhnle, Lars Norum

IEEE Conference on Electromagnetic Field Computation (CEFC2010)

Abstract

A method is presented for obtaining the current distribution along a thin, arbitrarily oriented wire antenna embedded in a conductive inhomogeneous medium. The inhomogeneous medium is modeled as a finite set of horizontal layers, where each layer is assumed to be homogeneous and characterized by an individual conductivity. The current distribution along the wire antenna is obtained by dividing the antenna into a set of small current elements, each of which can be considered as a linear combination of a vertical and horizontal electric dipole. The electric field generated by each dipole is derived using the dyadic Green's function approach. An electric field integral equation is obtained after imposing the boundary conditions satisfied on the surface of the wire antenna, and it is solved by the method of moments in order to obtain the current distribution along the antenna. Numerical results for the current attenuation along the antenna are presented and discussed for cases where the embedding conducting medium is either homogeneous or inhomogeneous.

B.1 Introduction

Wireless downhole communication using electromagnetic (EM) signals at low frequencies have for a long time been exploited by the oil and gas industry in

measurement-while-drilling (MWD) systems. In such systems, information is conveyed by EM signals excited as longitudinal currents along the drillstring. Since the attenuation increases with frequency, low frequency signaling is necessary in order to increase the communication range. As such, research into the current distribution along an electric conductor embedded in a conductive medium is an interesting topic, and there are several papers in the literature which have studied this particular subject.

In 1979, J. R. Wait and D. A. Hill [1] studied the current distribution along a drill rod surrounded by conducting host rock. They found that the attenuation would be at least as great as that of plane waves in the conductive medium surrounding the rod. In 1989, P. DeGauque and R. Grudzinski [2] derived the current distribution at low frequencies (0.1–10Hz) along a drillstring of finite conductivity in a conductive medium by using Pocklington's integral equation. These authors found that the surface impedance played a major role in attenuating the signal. However, for frequencies below a few Hertz, the attenuation did not vary much and the optimum frequency for maximum data rate was argued to be about 3Hz. In 1993, Xia and Chen [3] presented a paper on the receivability of EM signals in a MWD system by studying the propagation of EM waves along a drillstring placed in a conductive homogeneous medium. They examined the attenuation properties of such a system for various parameters such as the earth's conductivity, operating frequency, and the length of the drill string. A subsequently study [4] treated a downhole to surface communication channel that consisted of a long vertical cylinder embedded in a homogeneous earth and a line current technique was used to model the system. Moreover, the results reported in [4] were found to be in good agreement with those by Xia and Chen [3] obtained under the assumption of zero metal resistivity as well as those of DeGauque and Grudzinski [2] that considered an uncoated steel pipe submerged in sea water (homogeneous medium).

The three studies [4, 2, 3] all have in common that the surrounding medium of the well is assumed to be homogeneous. In the present study, however, the medium surrounding the well is allowed to be an *inhomogeneous* medium and the orientation of the drillstring is arbitrary, *i.e.* it may have a non-zero tilt-angle with respect to the vertical direction. For such a rather general geometry, we introduce a simple, yet effective, numerical method for obtaining the current distribution along the drillstring.

B.2 Geometry

The geometry that we consider consists of a layered earth, *i.e.* a horizontal stack of layers each characterized by their thickness, h_m, and dielectric properties, $\epsilon_m(\omega)$, where ω denotes the angular frequency and the subscript refers to layer m. For low frequencies, that will be considered here, one has to a good approximation that $\epsilon_m(\omega) \approx i\sigma_m(\omega)/\omega$ where the conductivity of layer m is $\sigma_m(\omega)$. Without loss of generality, we take the interfaces between the various layers to be parallel to the xy-plane with the z-axis pointing upward (Fig.B.1). The origin of the coordinate system is chosen to coincide with the lower point of the antenna. With this coordinate system, the top interface of layer m is $z = z_m$. In such a stratified medium, one can place a long thin wire antenna of length ℓ and radius a (with $\ell \gg a$) in the xz-plane so that it makes an arbitrarily tilt angle, θ, with the positive z-axis.

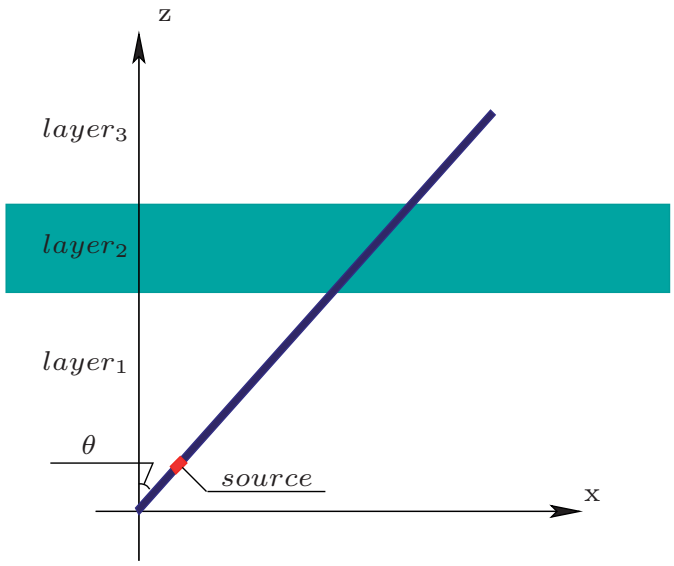

Figure B.1: A model of a long wire antenna in a 3-layer media

B.3 Theoretical Approach

To obtain the EM fields generated by the antenna, it is divided into a finite set of small current moments, where each is assumed to be a linear combination of a vertical electric dipole (VED) and a horizontal electric dipole (HED). Each VED is assumed to be parallel to the z-axis, whereas each HED is

assumed to be parallel to the x-axis:

$$I(z')\Delta\ell\hat{\ell} = I(z')(\Delta x\hat{\mathbf{x}} + \Delta z\hat{\mathbf{z}}). \tag{B.3.1}$$

With the given geometry, the EM wave generated by a VED will not have a magnetic component in the z-direction, *i.e.* it is a TM wave. Hence, the wave from a VED is characterized by the electric field components $E^{\mathrm{TM}}_{\mathrm{VED},z}$ and $E^{\mathrm{TM}}_{\mathrm{VED},x}$. Similarly, the wave from a HED propagating in z-direction is also only in TM mode, which can be represented by $E^{\mathrm{TM}}_{\mathrm{HED},z}$. In the x-direction, however, the electric field from the HED will have both TM and TE components, which we denote $E^{\mathrm{TM}}_{\mathrm{HED},x}$ and $E^{\mathrm{TE}}_{\mathrm{HED},x}$.

By the dyadic Green's function [5, Eq. (2.3.1)], the electric field components $E^{\mathrm{TM}}_{\mathrm{VED},z}$, $E^{\mathrm{TM}}_{\mathrm{VED},x}$, $E^{\mathrm{TM}}_{\mathrm{HED},z}$ and the electric field in $\hat{x}$ direction from a HED source, $E_{\mathrm{HED},x}$, can be found from

$$\mathbf{E}(\mathbf{r},\mathbf{r}') = \frac{i\omega\mu}{4\pi}\left(\bar{\mathbf{I}} + \frac{\nabla\nabla}{k^2}\right)\cdot I(z')(\Delta x\hat{\mathbf{x}} + \Delta z\hat{\mathbf{z}})\frac{e^{ikR}}{R}, \tag{B.3.2}$$

where $\mathbf{r} = (x, y, z)$ (with similar definition for $\mathbf{r}'$), $R = |\mathbf{r} - \mathbf{r}'|$, and wavenumber $k = \omega\sqrt{\mu\epsilon}$.

The component $E^{\mathrm{TE}}_{\mathrm{HED},x}$ can be derived from the general relation

$$E_x = \frac{i}{k^2 - k_z^2}\left[k_z\frac{\partial E_z}{\partial x} + \omega\mu\frac{\partial H_z}{\partial y}\right], \tag{B.3.3}$$

where $E_z = 0$ in TE mode and H_z can be obtained from:

$$\mathbf{H}(\mathbf{r},\mathbf{r}') = \nabla \times I(z')(\Delta x\hat{\mathbf{x}} + \Delta z\hat{\mathbf{z}})\frac{e^{ikR}}{4\pi R}. \tag{B.3.4}$$

Finally, we have that $E^{\mathrm{TM}}_{\mathrm{HED},x} = E_{\mathrm{HED},x} - E^{\mathrm{TE}}_{\mathrm{HED},x}$.

The term $\exp(ikR)/R$ contained in (B.3.2) can be expanded into an integral over plane waves by the Weyl identity [5, Eq. (2.2.26)]. This identity can further be used to derive the so-called Sommerfeld identity [5, Eq. (2.2.30)] where $\exp(ikR)/R$ is represented as an integral with respect to wave numbers k_ρ over cylindrical waves in the ρ direction times a plane wave in the z direction. The electric field from the antenna can then be expressed as

$$E(r, r') = \frac{i\omega\mu I\Delta z}{4\pi}\int_0^\infty dk_\rho\Phi\cdot e^{ik_z|z-z'|}, \tag{B.3.5}$$

where

$$\Phi = \begin{cases} \Phi^{\mathrm{TM}}_{\mathrm{VED},x} = \frac{z-z'}{|z-z'|}\frac{k_\rho^2}{k^2}J_1(k_\rho\rho) \\ \Phi^{\mathrm{TM}}_{\mathrm{VED},z} = \frac{ik_\rho^3}{k^2k_z}J_0(k_\rho\rho) \\ \Phi^{\mathrm{TM}}_{\mathrm{HED},z} = \frac{z-z'}{|z-z'|}\frac{k_\rho^2}{k^2}J_1(k_\rho\rho) \\ \Phi^{\mathrm{TE}}_{\mathrm{HED},x} = \frac{i}{k_z\rho}J_1(k_\rho\rho) \\ \Phi^{\mathrm{TM}}_{\mathrm{HED},x} = \frac{ik_\rho k_z}{k^2}\Big[J_0(k_\rho\rho) - \frac{1}{k_\rho\rho}J_1(k_\rho\rho)\Big] \end{cases}, \tag{B.3.6}$$

$k_\rho = \sqrt{k^2 - k_z^2}$, and $J_0(\cdot)$ and $J_1(\cdot)$ are Bessel functions of the first kind.

However, at the position of the source ($z = z'$), $\exp(ikR)/R$ can not be expanded by the Weyl identity [5, Ch. 2.7.3], but analytical solutions called Pocklington's integral can be found (Appendix 3.3).

When the electric dipole is placed in a horizontally layered medium, instead of the factor $\exp(ik_z|z - z'|)$, the z variation should include reflections from the interfaces of the layers, which can be represented by $F(z, z')$, see [5, Ch.2.4]. Since in our model, the z direction is opposite to that in [5], the explicit form of the needed equations are given in Appendix 3.11. Put $F(z, z')$ into (B.3.5) and it will be the analytical solution of the fields from an electric dipole placed in a layered medium.

The total field from the wire antenna is given in terms of the geometric integral of the electric field along the wire antenna. At the surface of the wire antenna, by using the boundary condition for the tangential component of the electric field, the electric field integral equation (EFIE) is equal to:

$$\frac{i\omega\mu}{4\pi}\int_\ell I(z')d\ell\int_0^\infty dk_\rho\Phi F(z, z') = g, \tag{B.3.7}$$

where g is a source term that is non-zero only for points not on the source that we here will model as a delta gap source. The finite conductivity of the wire antenna is taken into account *via* the impedance $Z_i = \sqrt{\mu_i/\epsilon_i}$ [2, Eq. (A-22)] that appears as a diagonal matrix in the equation.

B.4 Numerical results

The numerical simulations for the current distribution that we perform are based on solving the integral equation in (B.3.7), for a given source type, and this is done by applying the method of moments [6].

In particular note that for the k_ρ-integration appearing in (B.3.7) care has to be taken in order to produce accurate results. Since the media are conductive, there will be no singularity for k_ρ values on the (positive) real

axis (0 to ∞). Still, however, the integrand will vary rapidly in the region around $k_\rho = Re\,(k)$, and for this reason, a smaller discretization interval will be needed in this region.

For the ℓ-integration, a point match method has been applied. The wire antenna has been divided into equal small elements and there is a finite number of equally-sized elements within each layer. The mid-points of each element are selected to be the value points. By this method the EFIE of (B.3.7) is converted into series of linear equations which can be written in matrix form as $\mathbf{LI} = \mathbf{g}$. The current distribution along the wire antenna is then obtained as the solution $\mathbf{I} = \mathbf{L}^{-1}\mathbf{g}$.

The accuracy of the numerical results depends on the length of the elements, the size of the group of k_ρ and the radius of the wire antenna. Normally, the smaller the element, the more accurate the result will be. However, consider the radius of the wire antenna, an element can not be too small, especially when the antenna is tilted at an angle. In the program, with the point match method, the optimal size of the element is about 100 times of the radius. The running speed will also depend on the size of the group of elements and k_ρ.

To verify that this procedure produce reliable results, several homogeneous media geometries are considered and the prediction of the code for these cases have been compared to previously reported results from the literature and to those obtained by alternative numerical techniques. In Fig. B.2, the current attenuation along a wire antenna placed in a conductive homogeneous medium with $\sigma = 4$ S/m is compared to the results obtained by a Finite Integration Technique (FIT) program. The results are shown to be in good agreement.

In Fig. B.3, a replica of the results originally presented in [2, Fig. 6] are presented, but using the method of this paper. The results represent the theoretical current distribution at different frequencies for a metallic pipe of 40m immersed in seawater with $\sigma = 4$S/m. By inspection, the reproduced results are in good agreement with the original results presented.

A simple 3 layer model will now be considered (Fig. B.1) where the conductivities equal $\sigma = [1, 4, 1]$S/m (from down up). The length of the antenna is $\ell = 1000m$ and the radius is $r_a = 0.05$m. The source is located at $z_s = 50 \times \cos\theta$m and the interfaces of the second layer are $d_1 = 500 \times \cos\theta$m and $d_2 = 700 \times \cos\theta$m. Three tilt angles that will be considered are $\theta = [0, \pi/6, \pi/3]$ and the source operates at 5Hz and 50Hz. The numerical results are shown in Fig. B.4. For each case, a homogeneous model was first simulated in order to compare the results for different tilt angles. The simulation time in Matlab (in elapsed CPU seconds) for such a model when $k_\rho = 250$ and the length of each current element is $10m$ is 324s (5minutes)

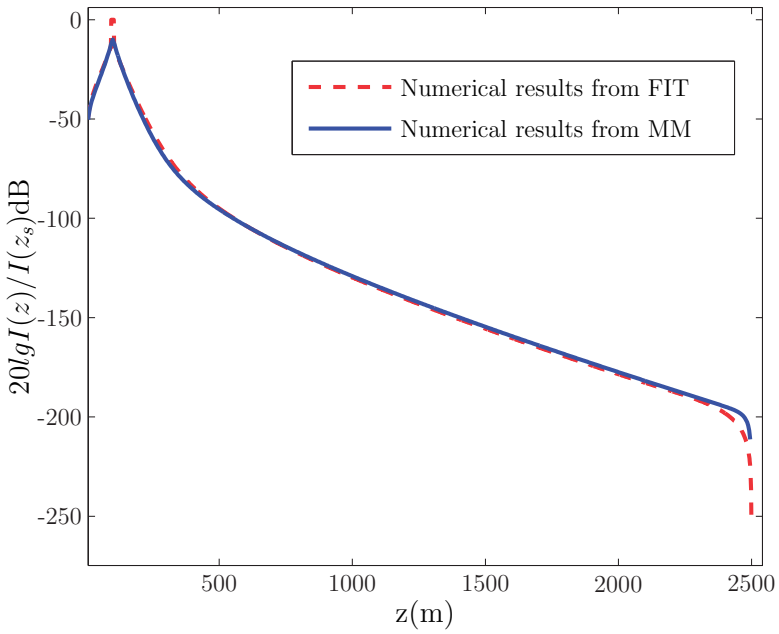

Figure B.2: Current attenuation along a wire antenna in a conductive homogeneous medium as a function of depth. The result of this paper is compared to the a similar setup in FIT. The conductivity of the wire antenna is $\sigma_s = 1 \cdot 10^5$S/m and the conductivity of the homogeneous medium is equal to $\sigma = 4$S/m, The radius of the wire is $r_a = 0.1$m and the frequency $f = 1$Hz.

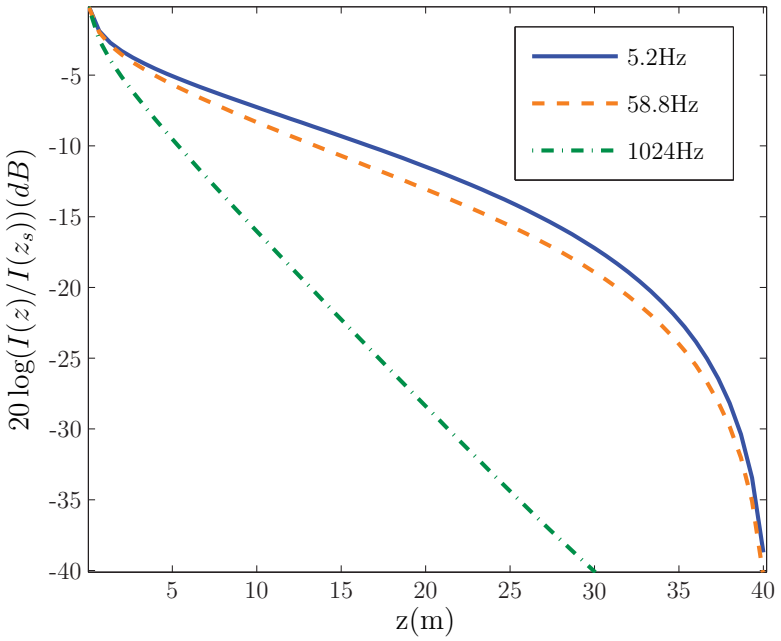

Figure B.3: A replica of [2, Fig. 6], representing the theoretical current distribution at different frequencies for a metallic pipe of 40m immersed in seawater with conductivity $\sigma = 4$S/m. The conductivity of the metal pipe is $\sigma_s = 4.2 \cdot 10^6$S/m.

using a desktop computer with a 2.66GHz processor and 2.5GB of memory.

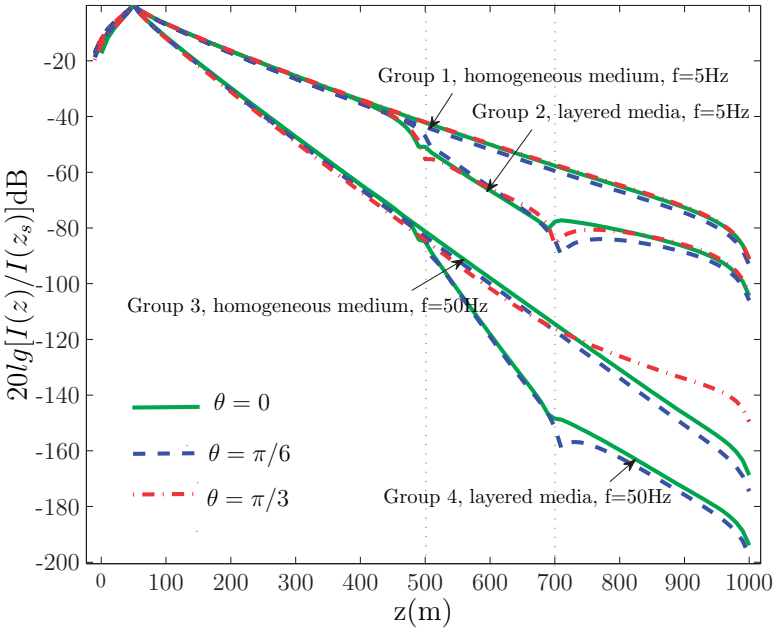

Figure B.4: Simulation results of a 3 layer model, where the conductivities of the media are (1,4,1)S/m and the conductivity of the antenna is $\sigma_s = 1 \cdot 10^6$S/m. The length of each current element is 10m and $k_\rho = 250$.

It shows that the current will attenuate faster when the medium around is more conductive. In addition, it is observed that the angle θ does not have a big impact on the attenuation. However, at 50Hz, there seems to be less attenuation at the far end for a highly tilted antenna. To analyze this behavior, results have been obtained when an antenna is placed in a homogeneous medium where the attenuation should be independent of the angle. In Fig. B.5, the results show that for higher frequencies and angles, a higher population of k_ρ is needed to give a correct result. This approach is not very efficient and asymptotic method can be applied, especially for higher frequencies.

B.5 Conclusion

A method for obtaining the current distribution along a thin arbitrarily oriented wire antenna embedded in a conductive inhomogeneous medium is presented. The simulation results show that the current attenuation along

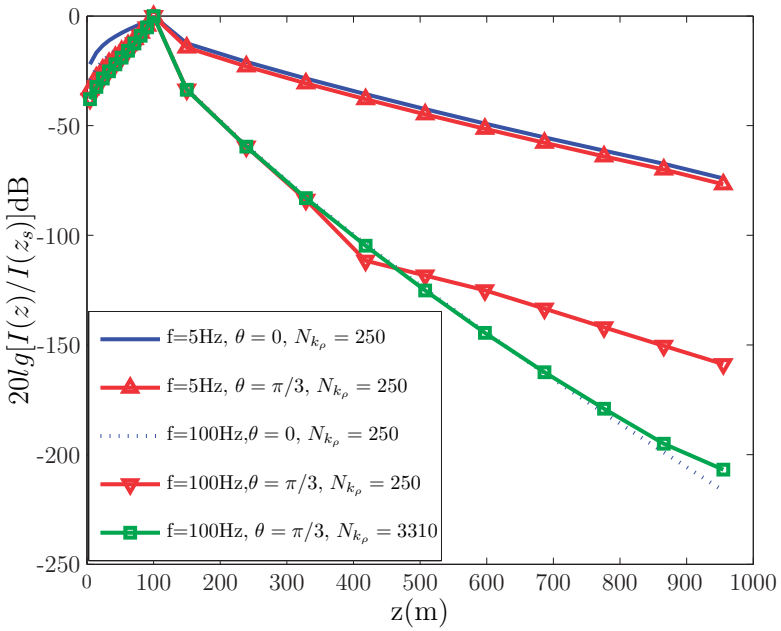

Figure B.5: The influence of the frequency and angle to the results

the antenna varies as a function of depth according to the conductivity value within each layer. Moreover, it is observed that at low frequencies the orientation of the antenna does not significantly influence the attenuation. At higher frequencies, however, asymptotic methods are needed to improve the accuracy of the proposed method.

Bibliography

[1] James R. Wait and David A. Hill. Theory of transmission of electromagnetic waves along a drill rod in conducting rock. *IEEE Transactions on Geoscience Electronics*, GE-17(2):21–24, Apr. 1979.

[2] P. DeGauque and R. Grudzinski. Propagation of electromagnetic waves along a drillstring of finit conductivity. *SPE Drilling Engineering*, pages 127–134, Jun. 1987.

[3] M. Y. Xia and Z. Y. Chen. Attenuation predictions at extremely low frequencies for measurement-while-drilling electromagnetic telemetry system. *IEEE Transactions on Geoscience and Remote Sensing*, 31(6):1222–1228, Nov. 1993.

[4] F. N. Trofimenkoff, Michael Segal, Allan Klassen, and J. W. Haslett. Characterization of EM downhole-to-surface communication links. *IEEE Transactions on Geoscience and Remote Sensing*, 38(6):2539–2548, Nov. 2000.

[5] Weng Cho Chew. *Waves and Fields in Inhomogeneous Media*. IEEE Press, 1st edition, 1995.

[6] R. F. Harrington. *Field Computation by Moment Methods*. IEEE Press, 2nd edition, 1993.

C Calculation of Sommerfeld Integrals for Conductive Media at Low Frequencies

Yingkang Wei, Bengt Holter, Ingve Simonsen, Karsten Husby, Jacob Kuhnle, Lars Norum

IEEE International Workshop on Electromagnetics; Applications and Student Innovation (iWEM2011)

Abstract

A method for accurately evaluating the Sommerfeld integral for conductive media at low frequencies that is commonly encountered in geophysics is presented. The motivation is that when we subtract an asymptotic function to the integrand, the new integral will converge much faster than the original Sommerfeld integral, which can be computed numerically while the asymptotic function can be integrated analytically by a Laplace transform. Numerical results that quantify the performance of the proposed method are presented.

C.1 Introduction

To quantify the performance of a downhole wireless communication system based on transmission of low frequency electromagnetic signals along a metal pipe used in oil and gas production, it is of interest to establish the current distribution along the pipe as a function of its length. To simplify the exposition, we have assumed that the metal pipe is placed in a homogeneous medium in this paper and the current distribution can then be achieved by solving the following electric field integral equation (EFIE)

$$\frac{-\omega\mu}{4\pi}\int_{z'} dz' I(z') \int_0^\infty dk_\rho \frac{k_\rho^3}{k_z} J_0(k_\rho \rho) e^{ik_z|z-z'|} = E_z(z) \tag{C.1.1}$$

in which $I(z')$ is the unknown current distribution along the pipe. $J_0()$ is the Bessel function of the first kind, $k_z = \sqrt{k^2 - k_\rho^2}$, and k is the wave number. $E(z)$ is the electric field at the surface of the pipe, and z and ρ are pipe length and radius coordinate variables. The inside integral of (C.1.1) is a Sommerfeld integral, which expands the spherical wave into plane waves in order to study the more complicated cases of layered media [1, Ch2]. The focus of this paper is the evaluation of the inner integral (with respect to k_ρ) in a conductive medium at low frequencies that is commonly encountered in geophysics. It has an oscillatory function in its kernel and basically there are two kinds of methods in evaluating such an integral: numerical and asymptotic methods.

The best numerical method for solving an integral containing an oscillatory function is to apply a technique denoted ISE (integration, summation and extrapolation), which can be found in popular textbooks on numerical integration, such as [2]. With the ISE approach, the zeros of $J_0(k_\rho\rho)$ are found first, then the integral is divided at these zeros and an alternating sequence is summed. Finally, to accelerate convergence, extrapolation is applied, such as Euler transformation [3], ϵ-algorithm of Wynn [4] and w-transform of Sidi [5, 6]. Lucas et.al [7] have compared the efficiency of the different algorithms and a good review are presented in [8] by Michalski.

Asymptotic methods can be applied when $|z - z'| \to \infty$, [1, 9], and different methods are applied based on whether $ik_z|z - z'|$ in (C.1.1) is a real, imaginary or complex function. If it is real and negative, (C.1.1) can be evaluated by Laplace integral [9, Ch.6.4]. If it is pure imaginary, (C.1.1) can be evaluated by the method of stationary phase [1, Ch.2.5.1]. If it is complex and $Re(ik_z|z - z'|) < 0$, (C.1.1) can be evaluated by the method of steepest descent [1, Ch.2.5.2].

However, if $|z-z'|$ becomes small, both the numerical and the asymptotic methods face difficulties. The numerical approach will converge slowly and a large integral range is required. The asymptotic approach is only valid in the far field (when $|z-z'| \to \infty$). To overcome these shortcomings, we find that in conductive media at low frequencies, the Sommerfeld integral will converge much faster if we subtract an asymptotic equation to the integrand. The new integral can be calculated numerically while the asymptotic equation can be integrated analytically by a Laplace transform.

C.2 The Error Analysis on the Calculation of the EFIE

In a homogeneous medium, (C.1.1) can be simplified into the Pocklington's integral equation[10, Ch. 8.3.1]:

$$\frac{i\omega\mu}{4\pi k^2}\int_{z'} dz' I(z')\frac{e^{ikR}}{R^5}[(1-ikR)(2R^2-3\rho^2)+(k\rho R)^2] = E_z(z) \qquad \text{(C.2.1)}$$

where$R = \sqrt{\rho^2+(z-z')^2}$. Both (C.1.1) and (C.2.1) can be evaluated numerically by the method of moments, which can be represented by a set of linear equations:

$$\mathbf{A}(z-z')I(z') = E(z). \qquad \text{(C.2.2)}$$

However, (C.1.1) can not be applied to obtain a solution at the source $z = z'$, where (C.2.1) has to be applied [1, Ch. 2.7.3]. In this paper, Pocklington's method is used as a reference for the evaluation of (C.1.1) since it can produce stable numerical results as illustrated in Fig.C.1, where a pipe of length 1000m and radius 0.1m is assumed to be enclosed in a homogeneous medium. The conductivities of the pipe and the surrounding are assumed to be $\sigma_a = 1\times10^6$S/m and $\sigma_m = 1$S/m respectively. An electric delta gap source operating at a frequency $f = 5$Hz is located 100m from the end of the pipe.

As $|z-z'|$ becomes smaller, (C.1.1) and (C.2.1) should provide more accurate results. However, by using the normal quadrature method for the inside integral, the evaluation of (C.1.1) is not stable as illustrated in Fig.C.2. A study of the coefficient matrices $\mathbf{A}(z,z')$ in (C.2.2) of the two methods shows that they have a Toeplitz structure and the biggest difference occurs in the elements on the first subdiagonal. In our simulation example, a tiny difference of $4.5\times10^{-2}\%$ is observed but it is enough to generate a significant error in the final result. In the following, the properties of the integral are examined and a method to evaluate it accurately is presented.

C.3 Derivation of the Method

In the following, the kernel of the inner integral in (C.1.1) is examined.

$$\Phi(k_\rho, z, z') = \frac{k_\rho^3}{k_z}J_0(k_\rho\rho)e^{ik_z|z-z'|}, \qquad \text{(C.3.1)}$$

The real part is small and can be neglected. The imaginary part of this term increases as $|z-z'|$ decreases and ultimately, it will oscillate due to the

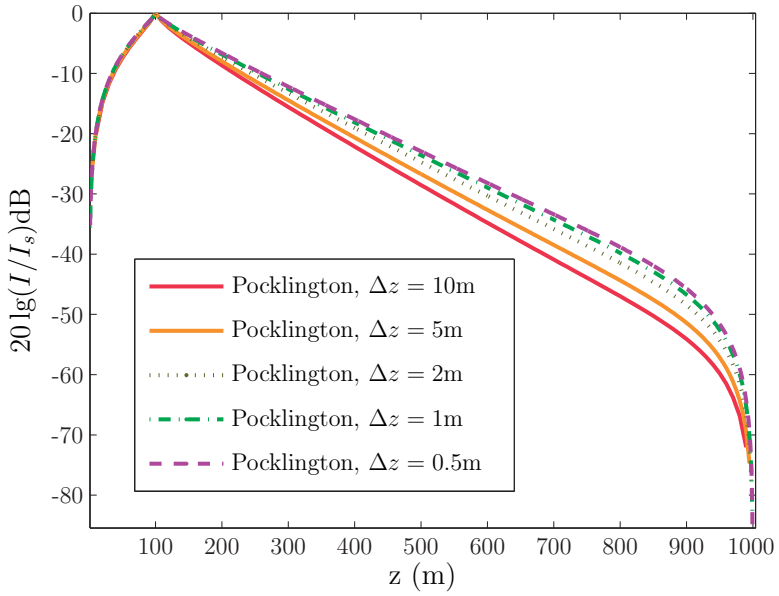

Figure C.1: Numerical results of $I(z')$ along the metal pipe relative to the source $I(z'_s)$ with different integral step Δz . The results are obtained by using Pocklington's integral (C.2.1).

presence of the Bessel function $J_0()$. When $|z - z'| = 0$, $Im(\Phi(k_\rho, z, z'))$ will be an ever increasing oscillating function which makes the Sommerfeld integral unsolvable. This is illustrated in Fig.C.3 and C.4.

In the geophysics, the operating frequency is usually very low, less than 100Hz. The conductivities are usually in the range $(0, 10)$S/m, Under these conditions, $\frac{\sigma}{\omega} >> \epsilon$ and the wave number can be approximated as $k \approx (1+i)/\delta$ where δ is the skin depth of the medium. Furthermore, k_z can be approximated by $k_z = \sqrt{k^2 - k_\rho^2} \approx ik_\rho$ when $k_\rho >> 1/\delta$. Moreover, with the asymptotic expansion of the Bessel function in the large argument limit [1, Ch.1.2.4], $\Phi(k_\rho, z, z')$ asymptotically equals

$$\Psi(k_\rho, z, z') = -i\sqrt{\frac{2}{\pi\rho}} k_\rho^{\frac{3}{2}} \cos(k_\rho\rho - \frac{\pi}{4}) e^{-k_\rho|z-z'|}. \tag{C.3.2}$$

Add and subtract (C.3.2) to the integrand, the Sommerfeld integral equals

$$\begin{aligned} \int_0^\infty dk_\rho \Phi(k_\rho, z, z') &= \int_0^\infty dk_\rho [\Phi(k_\rho, z, z') - \Psi(k_\rho, z, z') + \Psi(k_\rho, z, z')] \\ &= \int_0^\infty dk_\rho \mathcal{E}(k_\rho, z, z') + \int_0^\infty dk_\rho \Psi(k_\rho, z, z'). \end{aligned} \tag{C.3.3}$$

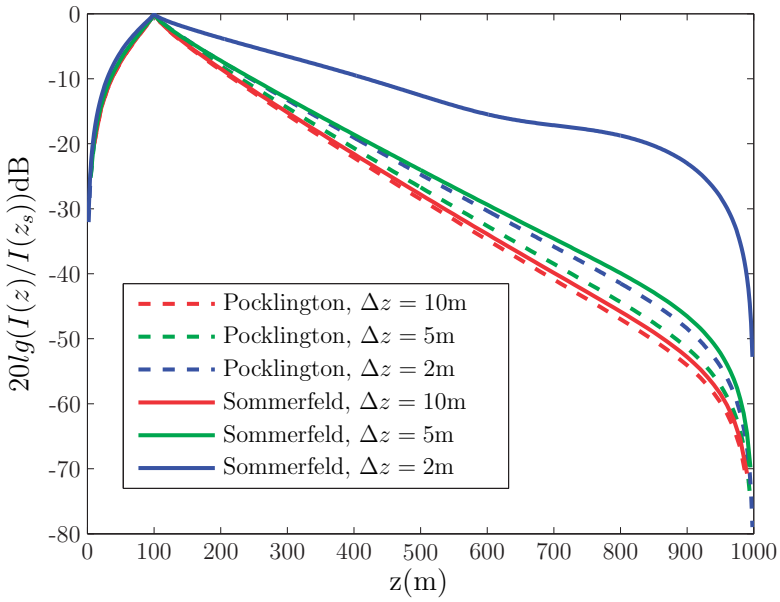

Figure C.2: Numerical results of $I(z')$ along the metal pipe relative to the source $I(z'_s)$ with different integral step Δz . The results compare the evaluation of (C.1.1) and (C.2.1).

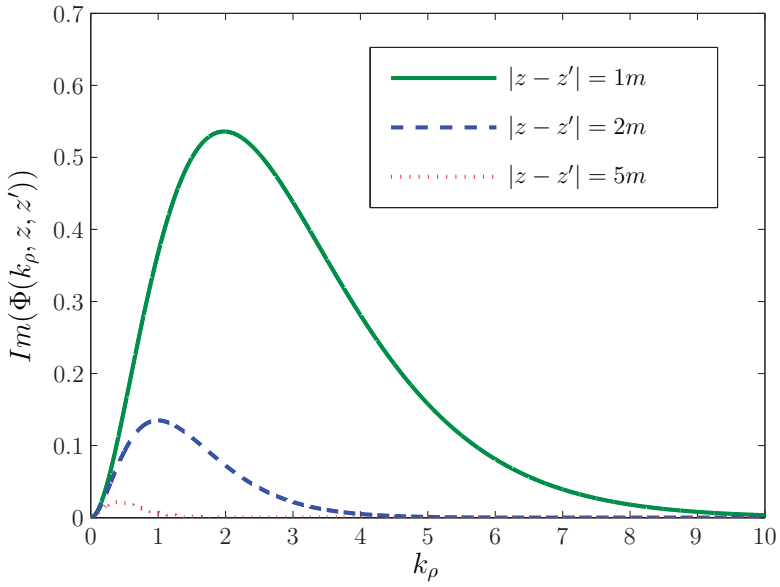

Figure C.3: The imaginary part of $\Phi(k_\rho, z, z')$ as a function of k_ρ for $|z-z'| = 5, 2$m.

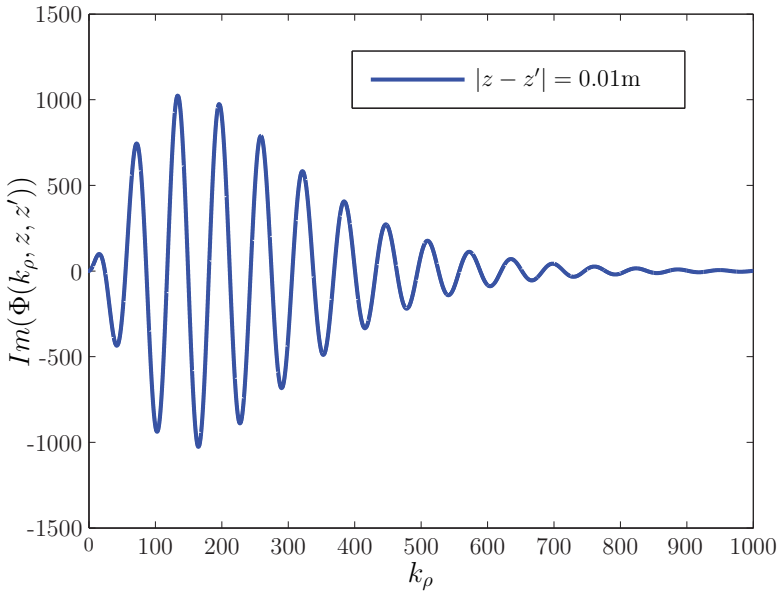

Figure C.4: The imaginary part of $\Phi(k_\rho, z, z')$ as a function of k_ρ for $|z-z'| = 0.01$m.

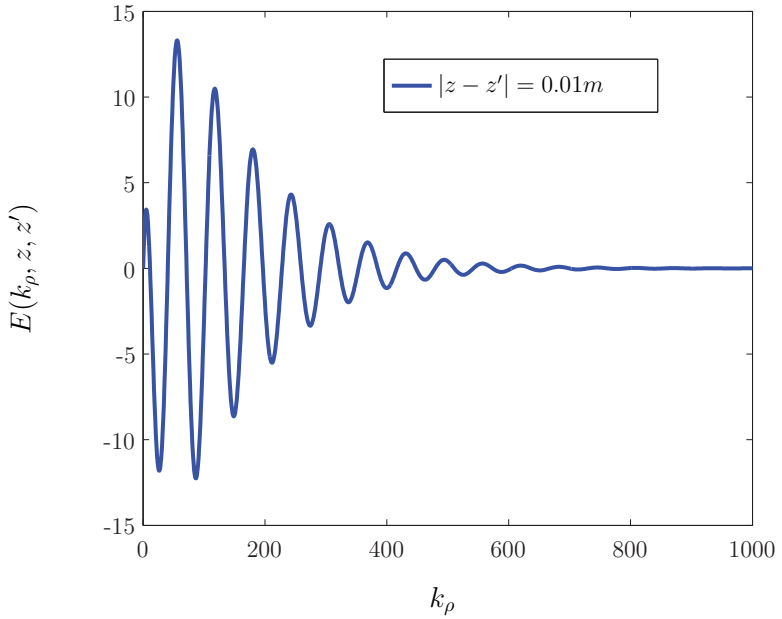

Figure C.5: The difference $\mathcal{E}(k_\rho, z, z')$ between $Im(\Phi(k_\rho, z, z'))$ and $\Psi(k_\rho, z, z')$ for $\Delta z = 0.01$m.

The difference $\mathcal{E}(k_\rho, z, z')$ between (C.3.1) and (C.3.2) is depicted in Fig.C.5, which shows that it converges much faster than $\Phi(k_\rho, z, z')$. Therefore, it will be much easier to obtain an accurate integration numerically over $\mathcal{E}(k_\rho, z, z')$. As for the second term on the right hand side in (C.3.3), it can be evaluated analytically by a Laplace transform:

$$\int_0^\infty dk_\rho k_\rho^{\frac{3}{2}} \cos(k_\rho \rho - \frac{\pi}{4}) e^{-k_\rho |z-z'|} = \frac{e^{-i\frac{\pi}{4}}}{2} \frac{3\sqrt{\pi}}{4} s_1^{-\frac{5}{2}} + \frac{e^{i\frac{\pi}{4}}}{2} \frac{3\sqrt{\pi}}{4} s_2^{-\frac{5}{2}} \quad \text{(C.3.4)}$$

where $s_1 = -|z - z'| + i\rho$ and $s_1 = -|z - z'| - i\rho$.

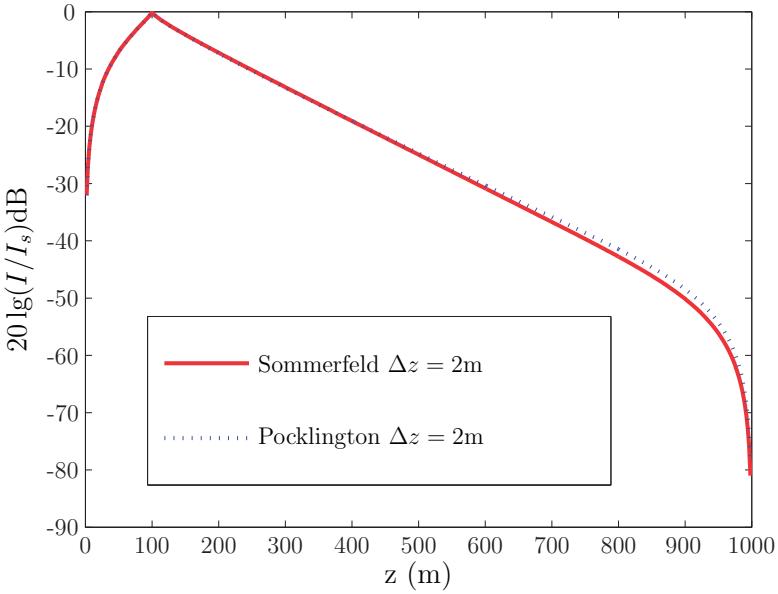

Figure C.6: Numerical results of $I(z')$ relative to the source with integral step $\Delta z = 2$m by using the Laplace transform method.

In Fig.C.6 the new approach is applied to similar data as in Fig.C.2 for $\Delta z = 2$m, with the same quadrature method. An examination on the coefficient matrix shows that the difference of the elements on the first subdiagonal has decreases from $4.5 \times 10^{-2}\%$ to $8.5 \times 10^{-4}\%$.

C.4 Conclusion

A method for evaluating Sommerfeld integral for conductive media at low frequency has been presented. The method is valid for $\frac{\sigma}{\omega} >> \epsilon$, which is commonly encountered in geophysics. The Sommerfeld integral is transformed

into a sum of two parts, where part one can be calculated numerically and part two can be evaluated analytically by a Laplace transform. The method has been presented and applied in a homogeneous medium, but it can also be applied in inhomogeneous cases.

Bibliography

[1] Weng Cho Chew. *Waves and Fields in Inhomogeneous Media*. IEEE Press, 1st edition, 1995.

[2] P. J. Davis and P. Rabinowitz. *Methods of Numerical Integration*. Academic Press. Inc. Orlando, 2nd edition, 1984.

[3] J. N. Lyness. Integrating some infinite oscillating tails. *J. Comput. Appl. Math.*, 12-13:109–117, May 1985.

[4] P. Wynn. On a device for computing the $e_m(s_n)$ transformation. *MTAC*, 10:91–96, 1956.

[5] A. Sidi. The numerical evaluation of very oscillatory infinite integrals by extrapolation. *Math. Comput.*, 38(158):517–529, Apr. 1982.

[6] A. Sidi. Extrapolation methods for divergent oscillatory infinite integrals that are defined in the sense of summability. *J. Comput. Appl. Math.*, 17:105–114, Feb. 1987.

[7] S. K. Lucas and H. A. Stone. Evaluating infinite integrals involving bessel functions of arbitrary order. *J. Comput. Appl. Math.*, 64:217–231, Dec. 1995.

[8] Krzysztof A. Michalski. Extrapolation methods for sommerfeld integral tails. *IEEE Trans on Antennas and Propagation*, 46:1405–1418, Oct. 1998.

[9] Carl M. Bender and Steven A. Orszag. *Advanced Mathematical Methods for Scientists and Engineers*. Springer. Inc., 1st edition, 1999.

[10] Constantine A. Balanis. *Antenna Theory*. John Wiley & Sons, Inc., 2nd edition, 1997.

D Efficient and Accurate Numerical Evaluation of Sommerfeld Integrals for Conductive Media at Low Frequencies

Yingkang Wei, Bengt Holter, Ingve Simenson, Karsten Husby, Jacob Kuhnle, Lars Norum

IEEE Geophysics (submitted)

Abstract

An efficient method for evaluating Sommerfeld integrals with oscillating kernels is presented. The method is based on subtracting and adding an asymptotic and analytically integrable function to the oscillating kernel, which transforms the original integral into a sum of two integrals. For the purpose of numerical calculations, the first integral, now containing a slowly oscillating kernel, is calculated quickly and accurately numerically, while the second integral, the strongly oscillating kernel, can be treated analytically. In this way the original Sommerfeld integral can be calculated numerically. In this paper, the method is outlined and applied to the geophysical problem of finding the current distribution along a thin metallic conductor immersed in a conductive medium. To this end, the metallic conductors represent wells immersed in conductive earth, where the earth is modeled both as a homogeneous and a horizontally layered medium. As such, the findings are relevant and applicable for evaluating the feasibility of using low frequency electromagnetic signals to convey information along metal casings. The method is targeted and applicable for high loss materials, traditionally characterized by the material intrinsic impedance having a phase angle at approximately 45 degrees. Under these conditions, it is demonstrated that the new approach converges at least

50 times faster and produces more reliable results compared to a traditional brute force approach.

D.1 Introduction

Propagation of electromagnetic waves through a planarly layered medium is a topic of interest within the field of optics, geophysics, remote sensing, and microwaves [1, 2]. In geophysics, the interest of this topic is mainly linked to the application of measuring physical properties of the subsurface earth, since the manner in which the formation responds to the field excited by an electromagnetic source can be used to determine the resistivity and dielectric constant of a particular rock formation. The application is known as exploration geophysics, also referred to as the applied branch of geophysics. Exploration geophysics is used by the oil and gas industry to infer or detect the presence of hydrocarbons, since oil-impregnated rocks have higher resistivity than water-saturated rocks. The data are typically derived using a dedicated well logging tool which is lowered vertically into the earth through a borehole. By inducing an electromagnetic signal and measuring an increase or decrease in electric potential between two electrodes, resistivity data related to vertical changes in the geological formations can be collected. Electromagnetic signaling may however also be applied in measurement-while-drilling (MWD) systems, where it is used as a communication technique to guide the drill-bit trajectory toward the oil producing strata in the earth formation. The electromagnetic signals then propagate through the formation adjacent to the wellbore, but the electric properties of the formation and the mud that encircles the wellbore will greatly influence the attenuation of the signal [3]. As a result, the reliable communication distance achieved in one well may not be equaled in another well unless the rock formations are almost identical.

From the literature, it can be deduced that communication based on electromagnetic signaling is quite ineffective in deep wells, since electromagnetic signals lose their strength rapidly in certain types of rock formations. To be able to predict the expected amount of attenuation in advance, a mathematical model which can be used to simulate the propagation of electromagnetic waves through a particular rock formation is needed. For simplicity and mathematical tractability, it is often then assumed that the earth is homogeneous. However, geologic scenarios are extremely varied, and few actual cases can be described accurately in terms of simple geometric forms like plane horizontal layers. However, despite this fact, it is quite common to model an inhomogeneous earth by dividing it into separate plane layers, where each individual layer is modeled as a homogeneous layer [4]. Such a model may

then be applied to predict whether or not a particular rock formation may support a successful deployment of an electromagnetic telemetry system.

In an electromagnetic telemetry system such as MWD, the signal travels along a metal pipe from the transmitter to the receiver by using the pipe as a transmission line. However, there is wireless transmission of data as well, since some of the current will divert from the pipe and leak into the surroundings. As a result, the signal may either be picked up by a receiver by detecting the current flow in close proximity to the well, or it can be picked up by electromagnetic sensors placed a certain distance from the well. The latter case resembles the act of picking up signals from a Controlled Source Electromagnetic (CSEM) system [5, 6], which is a relatively new technique used in exploration geophysics. However, in contrast to a traditional CSEM system which uses a high powered signal from a towed antenna in the sea to record a reflected signal, the received signal from a MWD telemetry system is a direct signal which is in essence guided by a metal pipe as it propagates from the transmitter to the receiver[7]. In order to predict the communication range of such a system, an estimate of the current distribution along the pipe as a function of its geophysical surroundings is needed. As shown in this paper, this requires, under reasonable assumptions, the evaluation of the so-called Sommerfeld integrals [8]. For a long time, a reliable numerical evaluation of Sommerfeld integrals has been a challenge [9]. However, this paper presents an efficient and accurate numerical evaluation technique which is needed to obtain reliable results for the current distribution along a metal pipe in conductive media.

This paper is organized as follows: we start by presenting the geometry considered in this study. Then we introduce the theoretical formulation of the problem and sketch the derivation of the two central integral equations — the Pocklington's and Sommerfeld's integral equations — that our numerical calculations based on. We then present the numerical calculations for the current distribution along the well casing due to a source located somewhere along it, assuming either a homogeneous or layered earth model. To this end, we introduce an algorithm for accurate and efficient numerical evaluation for the so-called Sommerfeld integrals for conductive media at low frequencies and apply it to both homogeneous and layered model.

D.2 Geophysical System

The geophysical system that we consider in this study is depicted in Figure D.1. It consists of a horizontally layered earth model in which a straight vertical well of length ℓ is located. The metal casing of the well has a circular

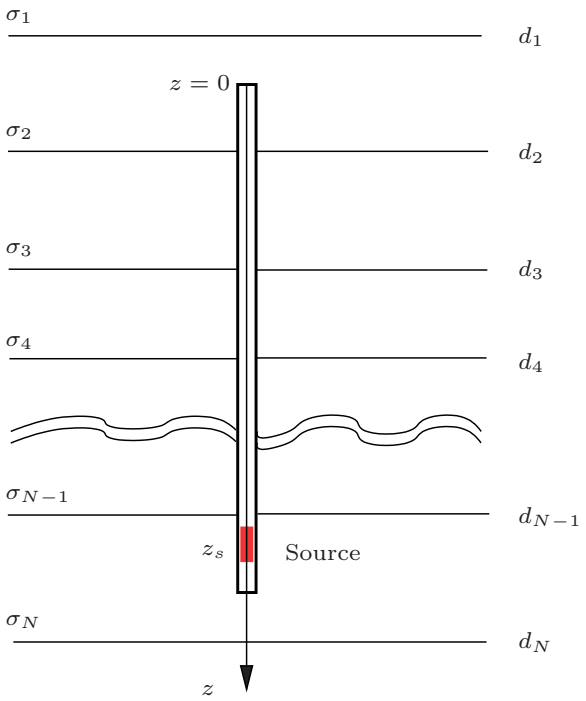

Figure D.1: A sketch of the geometry considered in this work.

cross section of radius a. The origin of the coordinate system is chosen to coincide with the top point of the well, and the z-axis, located at the center of the well, is positive downwards. With this definition, the top (bottom) of the well is located at $z = 0$ ($z = \ell$), and the interface separating medium m from medium $m + 1$ is located at depth $z = d_m$.

An electromagnetic source, of angular frequency ω, is located in the well at depth z_s ($0 \leq z_s \leq \ell$). Medium in layer m ($m \geq 1$) is characterized by its frequency dependent permittivity and permeability, $\varepsilon_m(\omega)$ and $\mu_m(\omega)$, respectively, and the wavenumber k_m is equal to $k_m = \sqrt{\varepsilon_m \mu_m}\omega$.

We will mostly be concerned with low frequency signals, $f = \omega/(2\pi) \leq 10\,\mathrm{Hz}$, for which the permittivity of the media of interest to a good approximation can be written as $\varepsilon_m(\omega) \approx \mathrm{i}\sigma_m(\omega)/\omega$ [10, Eq.8.5]. For simplicity, we will assume that the $\mu_m(\omega)$ of the media is real and positive. Under these assumptions, the wavenumber reads

$$k_m(\omega) \approx \frac{1+\mathrm{i}}{\delta_m}, \tag{D.2.1a}$$

where the skin depth is equal to

$$\delta_m(\omega) = \sqrt{\frac{2}{\sigma_m \mu_m \omega}}. \tag{D.2.1b}$$

D.3 Theory

In the application that we consider in this work, a delta-gap source [11, Ch.8] is placed somewhere along the length of the well. The source corresponds to an incident electric field, $\boldsymbol{E}^{(i)}(\boldsymbol{r}, \omega)$, that will induce a current density, $\boldsymbol{J}(\boldsymbol{r}, \omega)$, in the metal casing of the well. This current density will give rise to a scattered electric field, $\boldsymbol{E}^{(s)}(\boldsymbol{r}, \omega)$, in and around the well. Hence, the well casing acts as a linear wire-antenna. Moreover, if the radius (a) of the cylindrical casing is tiny compared to its length, $a \ll \ell$, the current density will have an azimuthal symmetry, and we can write it as

$$\boldsymbol{J}(\boldsymbol{r}, \omega) = \hat{\boldsymbol{z}} \frac{I(z)}{2\pi a} \delta(\rho - a). \tag{D.3.1}$$

The corresponding scattered electric field is related to this current density *via* the Helmholtz equation, well-known from electromagnetic theory and readily derived from Maxwell equations [10, Ch.9]

$$\boldsymbol{\nabla} \times \boldsymbol{\nabla} \times \boldsymbol{E}^{(s)}(\boldsymbol{r}, \omega) - k^2 \boldsymbol{E}^{(s)}(\boldsymbol{r}, \omega) = \mathrm{i}\omega\mu \boldsymbol{J}(\boldsymbol{r}, \omega), \tag{D.3.2}$$

where the wave number is defined as $k = \sqrt{\varepsilon\mu}\omega$. The general solution to Eq. (D.3.2) can be expressed as

$$\boldsymbol{E}^{(s)}(\boldsymbol{r},\omega) = \mathrm{i}\omega\mu \int \mathrm{d}^3\boldsymbol{r}'\, \mathbb{G}(\boldsymbol{r},\boldsymbol{r}') \cdot \boldsymbol{J}(\boldsymbol{r}',\omega). \tag{D.3.3}$$

In writing Eq. (D.3.3), we have introduced the (electric) dyadic Green's tensor [2, Ch.6]

$$\mathbb{G}(\boldsymbol{r},\boldsymbol{r}') = \left[\mathbb{I} + \frac{\nabla\nabla}{k^2}\right] g(\boldsymbol{r},\boldsymbol{r}'), \tag{D.3.4a}$$

with the free-space Green's function defined as

$$g(\boldsymbol{r},\boldsymbol{r}') = \frac{e^{\mathrm{i}\boldsymbol{k}\cdot(\boldsymbol{r}-\boldsymbol{r}')}}{4\pi\,|\boldsymbol{r}-\boldsymbol{r}'|}. \tag{D.3.4b}$$

In what follows, our main concern will be the z-component of the electric field on the surface of the well casing. If the metal of the well casing is considered a perfect electric conductor, at the casing surface ($\boldsymbol{r} = (\rho = a, \phi, z)$) , $E_z^{(i)}(\boldsymbol{r},\omega) + E_z^{(s)}(\boldsymbol{r},\omega) = 0$. With this result and the substitution of Eq. (D.3.1) into Eq. (D.3.3) it follows that the (unknown) current $I(z)$ along the well satisfies the following integral equation [12, Ch.12]

$$\int_0^\ell \mathrm{d}z'\; K(z,z')I(z') = \mathrm{i}4\pi\varepsilon\omega E_z^{(i)}(z,a;\omega), \tag{D.3.5a}$$

where the kernel reads

$$K(z,z') = \left[k^2 + \partial_z^2\right] \frac{e^{\mathrm{i}kR}}{R}, \tag{D.3.5b}$$

with $R = \sqrt{(z-z')^2 + a^2}$ and $\partial_z = \partial/\partial z$. Furthermore, in writing Eq. (D.3.5b), it has been assumed that $a^2 \ll |z-z'|^2$, an approximation known in antenna theory as the thin wire antenna approximation [11, Ch.8]. If the metal of the well casing is considered as a non perfect electric conductor, then at the casing surface, the boundary conditon should be $E_z^{(i)}(\boldsymbol{r},\omega) + E_z^{(s)}(\boldsymbol{r},\omega) = ZI(z)$, where Z is a parameter of internal impedance of the well [13, A-22].

If the surroundings of the well is a homogeneous medium, then the kernel can be readily evaluated so that the resulting integral equation reads

$$\begin{aligned}\int_0^\ell \mathrm{d}z'\; \frac{e^{\mathrm{i}kR}}{R^5} \left[(1-\mathrm{i}kR)(2R^2-3a^2) + (kaR)^2\right] I(z') \\ = \mathrm{i}4\pi\varepsilon\omega\; E_z^{(i)}(z,a;\omega).\end{aligned} \tag{D.3.6}$$

Equation (D.3.6), known as *Pocklington's integral equation* [11, Ch.8], can be solved numerically by the method of moments [14] to produce reliable results (see examples below).

However, if the surroundings of the well constitute a plane layered medium, then the field generated by the current in the antenna is partly reflected by the surrounding media back to the antenna region, thus affecting the overall current in the antenna. This effect can only be taken into account by properly describing how the field is scattered and transmitted by the surrounding layered media. The scattering and transmission amplitudes between two adjacent media bounded by a planar interface is known for plane waves only. Hence, to handle the plane layered earth model, a plane wave expansion of the kernel $K(z, z')$ is required. This is achieved by taking advantage of the Sommerfeld identity [8] which reads

$$\frac{e^{\mathrm{i}kr}}{r} = \mathrm{i}\int_0^\infty \mathrm{d}k_\rho \, \frac{k_\rho}{k_z} J_0(k_\rho \rho) e^{\mathrm{i}k_z|z|}, \tag{D.3.7}$$

where $J_0(k_\rho\rho)$ denotes the Bessel function of the first kind and order zero [15, Ch.6], $k_\rho = \sqrt{k_x^2 + k_y^2}$ and $k_z = \sqrt{k^2 - k_\rho^2}$ ($\mathrm{Re}\, k_z > 0$, $\mathrm{Im}\, k_z > 0$) are radial and perpendicular wave numbers, respectively. Introducing Eq. (D.3.7) into Eq. (D.3.5) results in an alternative integral equation for the current

$$\int_0^\ell \mathrm{d}z' \; S(z, z') I(z') = 4\pi\varepsilon\omega \, E_z^{(i)}(z, a; \omega), \tag{D.3.8a}$$

where

$$S(z, z') = \int_0^\infty \mathrm{d}k_\rho \frac{k_\rho^3}{k_z} J_0(k_\rho a) e^{\mathrm{i}k_z|z-z'|}, \tag{D.3.8b}$$

is a Sommerfeld integral. Equation (D.3.8) has been derived under the assumption that the medium surrounding the well is homogeneous. If the medium surrounding the well instead is a plane layered medium, the field reflected from the layers will have to be taken into account. This amounts to replacing the exponential factor $\exp(\mathrm{i}k_z|z - z'|)$ appearing in Eq. (D.3.8) with a function, $F(z, z')$, that in addition to the original exponential factor also contains the generalized reflection coefficients for the stack of layers located above and below the source. The mathematical form of the function $F(z, z')$ is given by 3.11.

Since the derivation of Eq. (D.3.8) relies on the Sommerfeld identity, we will below refer to it, and its generalization to layered media, as the *Sommerfeld's intergral equations* (even if this is a not commonly used nomenclature).

D.4 Numerical Study

D.4.1 Homogeneous Earth Model

The first case we will study is the situation when the well is placed in a homogeneous medium. The current along the well that is due to a delta-gap source located at depth $z = z_s$ can then be obtained by solving numerically either Eq. (D.3.6) or (D.3.8) since these two equations are equivalent under the conditions considered here.

Numerical solution of the integral equations (D.3.6) and (D.3.8) can be obtained by the method of moments [14]. This amounts to discretizing the length of the wire antenna into N elements each of length $\Delta z = \ell/N$ and centered at depth $z_n = (n - 1/2)\Delta z$ $(n = 1, \ldots, N)$. Under the assumption that the unknown current varies slowly over each of the elements, and therefore is well approximated by its value at the center of the element $I(z_n)$, one obtains

$$\sum_{n=1}^{N} \mathcal{K}(z, z_n) I(z_n) \simeq \mathrm{i}4\pi\varepsilon\omega \; E_z^{(i)}(z, a; \omega), \tag{D.4.1a}$$

where

$$\mathcal{K}(z, z_n) = \int_{z_n - \Delta z/2}^{z_n + \Delta z/2} \mathrm{d}z' \; K(z, z'), \tag{D.4.1b}$$

and $K(z, z')$ is some integral kernel. Equation (D.4.1) represents a relation among the N unknown currents $I(z_n)$, and to determine them, we will need a closed set of equations for these currents. To this end, we evaluate Eq. (D.3.5) at discrete depth $z = z_m$ $(m = 1, \ldots, N)$ with the result that Eq. (D.4.1) is converted into a linear system of equations for the currents $I(z_n)$, that can be solved efficiently by standard linear algebra packages.

In passing we note that on the assumption that the kernel $K(z, z')$ also being a smooth function of z', the matrix elements obtained from Eq. (D.4.1b) can be approximated as

$$\mathcal{K}_{mn} \equiv \mathcal{K}(z_m, z_n) \approx \Delta z \, K(z_m, z_n). \tag{D.4.2}$$

On the other hand, if $K(z, z')$ is not a smooth function of z', care must be taken to evaluate more accurately the integral present in Eq. (D.4.1b).

By the method just described, we have solved numerically both the Pocklington's and Sommerfeld's integral equations, Eqs. (D.3.6) and (D.3.8), for a homogeneous medium. The numerical results for the current along the well

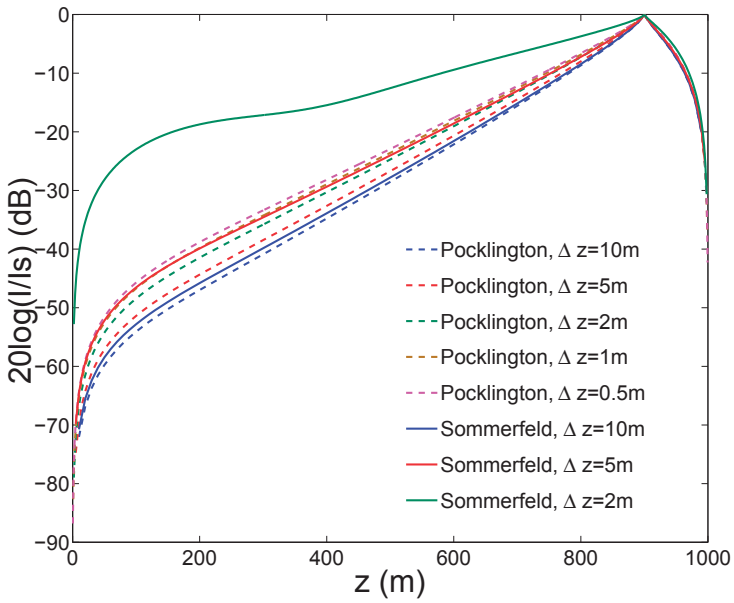

Figure D.2: Figure 2. The current distribution (relative that of the source I_s) along the well casing, $I(z)/I_s$, obtained by numerically solving either the Pocklington's integral Eq. (D.3.6) or Eq. (D.3.8) for various vertical discretization intervals Δz. The length of the well is assumed to be $\ell = 1\,000\,\mathrm{m}$, and its metal casing has radius $a = 0.1\mathrm{m}$ and conductivity $\sigma = 10^6\,\mathrm{S/m}$. The source, operating at frequency $f = \omega/(2\pi) = 5\,\mathrm{Hz}$, is located a distance $100\,\mathrm{m}$ from the lower end of the well ($z_s = 900\,\mathrm{m}$). The medium surrounding the well is assumed to be homogeneous and characterized by a conductivity of $\sigma_0 = 1\,\mathrm{S/m}$. The numerical calculation of the integrals appearing in Eqs. (D.3.6) and (D.3.8) are both performed with standard quadrature schemes.

are presented in Figure D.2 assuming various values for the discretization interval Δz. Figure D.2 demonstrate that the Pocklington's integral equation produces stable numerical results in the sense that as Δz becomes small, the current along the well, $I(z)$, converges towards a well defined function that seems to be independent of Δz. On the other hand, basing the simulations on the Sommerfeld's integral equation, that for a homogeneous medium is equivalent to the integral equation of Pocklington, Figure D.2 shows that a convergent result for the current is not obtained, at least not with the numerical implementation that was described above and used to obtain the results presented in Figure D.2.

In passing, we note that in a recent study, a similar geometry was considered by [16]. These authors, basing their numerical study on a similar integral equation, reported good agreement between their numerical results for a small current element (*i.e.* a vertical electric dipole) placed in a homogeneous medium and corresponding predictions made from analytic formula (see Figure 2(a) of [16]), and these numerical results were found to be little sensitive to the length, $\ell = \Delta z$, of the current element. Using the parameters from [16] we can reproduce their results. Moreover, when a long well is placed in a homogeneous medium we can also reproduce the results obtained by Yang *et al.* and presented in their Figure 4(a), when we used similar parameters and assumed a casing radius of $a = 0.02\,\mathrm{m}$ (a parameter we from their paper could not find the value used). In particular, a discretization interval of $\Delta z = 12.5\,\mathrm{m}$ was assumed by these authors and us. However, if the value assumed for Δz is decreased when studying this latter geometry, we find a strong influence in the predicted current distribution along the casing of the well. The difference between the results obtained when using $\Delta z = 12.5\,\mathrm{m}$, that we can reproduce after [16], and those results that we obtain when $\Delta z = 2\,\mathrm{m}$, say, is of the order 10 dB at 2500m. Hence, we note that for the parameters assumed by [16] we get strong dependence on Δz similar to that presented in our Figure D.2. Therefore, we speculate that also the study of [16] face the numerical issue addressed in the current study.

So why do we not get convergent results when solving the Sommerfeld's integral equation numerically. To see the cause of the problem, let us start by introducing $\mathcal{S}(k_\rho; z, z')$ as the integrand of the integral defining $S(z, z')$. Figure D.3 shows that the convergence range of the imaginary part of $\mathcal{S}(k_\rho; z, z')$ becomes large as $|z - z'|$ is small, while the real part of $\mathcal{S}(k_\rho; z, z')$ is tiny compared to the imaginary part and doesn't change much with $|z - z'|$. When the integrand function $\mathcal{S}(k_\rho; z, z')$ converges slowly, it is hard to evaluate the integral $S(z, z')$ accurately. In the extreme case, when $|z - z'| = 0$, $\mathcal{S}(k_\rho; z, z')$ becomes an ever increasing oscillating function, whose integral can not be evaluated numerically. In the example presented in Figure D.2, the maxi-

mum difference appears at the subdiagonal of the coefficient matrix, which is only $4.5 \times 10^{-2}\%$ when $|z - z'| = 2\text{m}$, but it is big enough to generate a significant error in the final result.

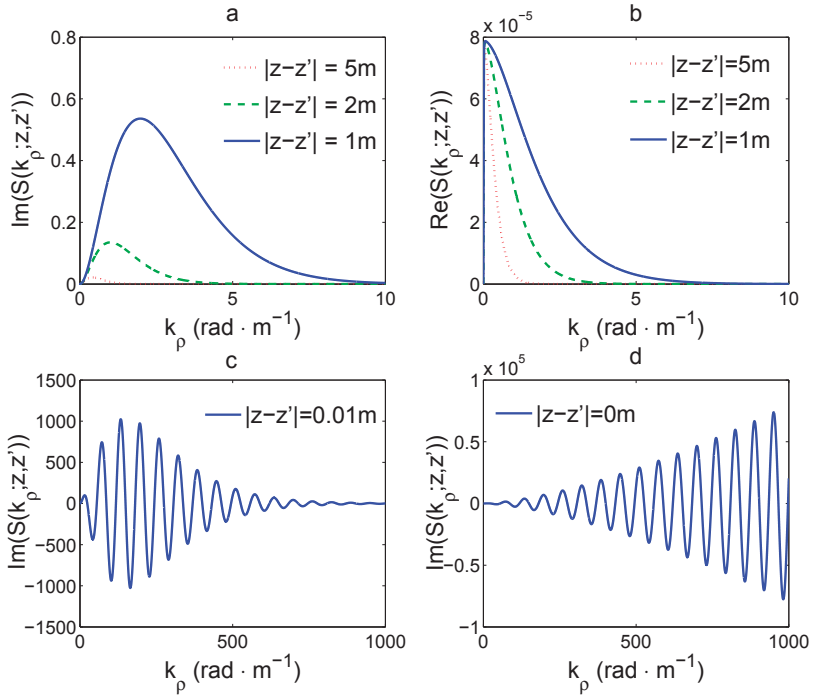

Figure D.3: $\text{Im}(\mathcal{S}(k_\rho; z, z'))$ and $\text{Re}(\mathcal{S}(k_\rho; z, z'))$ vs. k_ρ for various choices of $|z - z'|$. The radius is assumed to be $a = 0.1\,\text{m}$ and the conductivity is assumed to be $\sigma = 4\,\text{S/m}$. The operating frequency $f = 5\,\text{Hz}$.

The root of the problem comes from the strongly oscillating integrand which causes standard numerical integration schemes to fail miserably. Currently there are essentially two classes of methods used for the numerical evaluation of Sommerfeld integrals; numerical and asymptotic methods.

One of the best numerical method for evaluating integrals of oscillating integrands is the integration, summation and extrapolation(ISE) method (see *e.g.* Davis and Rabinowitz[17]). To use the ISE method, the zeros of the Bessel function are found first, then the integral is divided at these zeros and an alternating sequence is summed. Finally, to accelerate convergence, extrapolation methods are applied such as Euler transformation [18], ϵ-algorithm of Wynn [19] and W-transform of Sidi [20, 21]. Lucas and Stone [22] have compared the efficiency of the different algorithms and a good

review is presented by Michalski [23].

Asymptotic methods can be applied when $|z - z'| \to \infty$ and different methods are applied based on whether $\mathrm{i}k_z|z - z'|$ is a real, imaginary or complex function. If it is real and negative, the Sommerfeld integral can be evaluated as a Laplace integral [24, Ch.6.4]. If it is pure imaginary, the Sommerfeld integral can be evaluated by the method of stationary phase [2, Ch.2.5.1]. If it is complex and $\mathrm{Re}(\mathrm{i}k_z|z - z'|) < 0$, the Sommerfeld integral can be evaluated by the method of steepest descent [2, Ch.2.5.2].

However, when $(|z - z'|)$ becomes small, both the numerical and the asymptotic methods face difficulties. The numerical approach will converge slowly so that a large integral range is required. The asymptotic approach, on the other hand, is only valid in the far field region where $|z - z'| \to \infty$. In conclusion, existing techniques for evaluating Sommerfeld integrals numerically are not sufficient for geophysical applications.

D.4.2 Asymptotic Splitting Method

We have seen that the main challenge for obtaining a reliable and efficient evaluation of Sommerfeld integrals (assuming relevant geophysical parameters), is the huge amplitude, oscillating and slowly decaying behavior with k_ρ of the integrand

$$\mathcal{S}(k_\rho; z, z') = \frac{k_\rho^3}{k_z} J_0(k_\rho a) e^{\mathrm{i}k_z|z-z'|}, \tag{D.4.3}$$

for small values of $|z - z'|$.

With the aim of making the integrand more suited for accurate numerical integration, we will subtract and add to it, a function $\mathcal{A}(k_\rho; z, z')$ that has the same asymptotic form as $\mathcal{S}(k_\rho; z, z')$, but which also can be integrated analytically. If such a function can be found, one has that

$$\begin{aligned} S(z, z') = &\int_0^\infty \mathrm{d}k_\rho \ [\mathcal{S}(k_\rho; z, z') - \mathcal{A}(k_\rho; z, z')] \\ &+ \int_0^\infty \mathrm{d}k_\rho \, \mathcal{A}(k_\rho; z, z') \end{aligned} \tag{D.4.4}$$

where the second integral is evaluated analytically, while the first is evaluated numerically. Since, the two integrands $\mathcal{S}(k_\rho; z, z')$ and $\mathcal{A}(k_\rho; z, z')$ have the same asymptotic form, the difference between them, is expected to decay much quicker, so that its integral can be calculated quicker and much more reliably. To illustrate this technique, we start by noting that the asymptotic

form of $\mathcal{S}(k_\rho; z, z')$, as given by Eq. (D.4.3), is

$$\mathcal{A}(k_\rho; z, z') = -\mathrm{i}\sqrt{\frac{2}{\pi a}} k_\rho^{\frac{3}{2}} \cos\left(k_\rho a - \frac{\pi}{4}\right) e^{-k_\rho |z-z'|}, \tag{D.4.5}$$

where we have used Eq. (D.2.1), $k_z = \sqrt{k^2 - k_\rho^2} \approx ik_\rho$ when $k_\rho \gg 1/\delta$, and the asymptotic expansion of the Bessel function $J_0(k_\rho a)$ [2, Eq.(1.2.32)]. The integral of the function in Eq. (D.4.5) can be evaluated analytically by the Laplace transform to produce

$$\int_0^\infty \mathrm{d}k_\rho \, \mathcal{A}(k_\rho; z, z') = -\mathrm{i}\frac{3}{4}\sqrt{\frac{1}{2a}} \left[e^{-\mathrm{i}\frac{\pi}{4}} s_+^{-\frac{5}{2}} + e^{\mathrm{i}\frac{\pi}{4}} s_-^{-\frac{5}{2}} \right] \tag{D.4.6}$$

where $s_\pm = -|z - z'| \pm \mathrm{i}a$.

To investigate how well the asymptotic splitting method works in practice, we in Figure D.4 present the dependence of the imaginary part of $\mathcal{S}(k_\rho; z, z') - \mathcal{A}(k_\rho; z, z')$ *vs.* k_ρ for given value of $|z - z'|$. By comparing the results of Figure D.3(c) and D.4, it is observed that the asymptotic separation method reduces the integrand by about two orders of magnitude, at least for the parameters considered here.

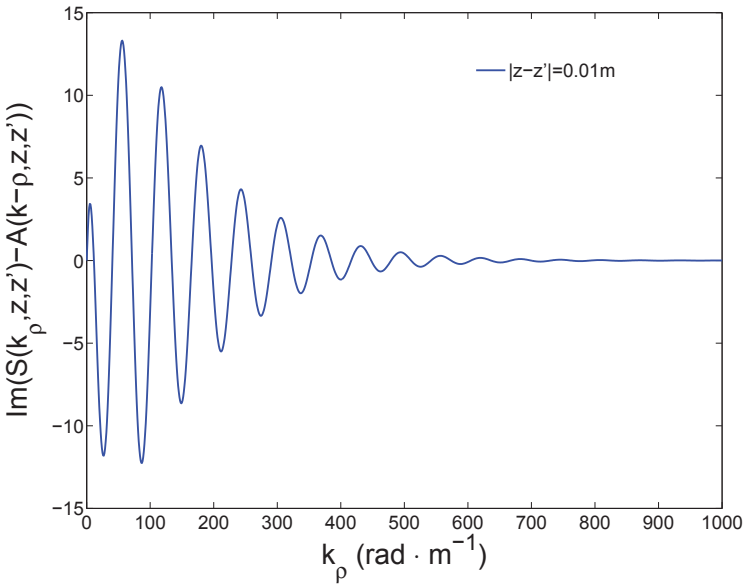

Figure D.4: $\mathrm{Im}(\mathcal{S}(k_\rho; z, z') - \mathcal{A}(k_\rho; z, z'))$ vs. k_ρ for $|z - z'| = 0.01\,\mathrm{m}$. The assumed parameters in these calculations are equal to those of Figure D.3.

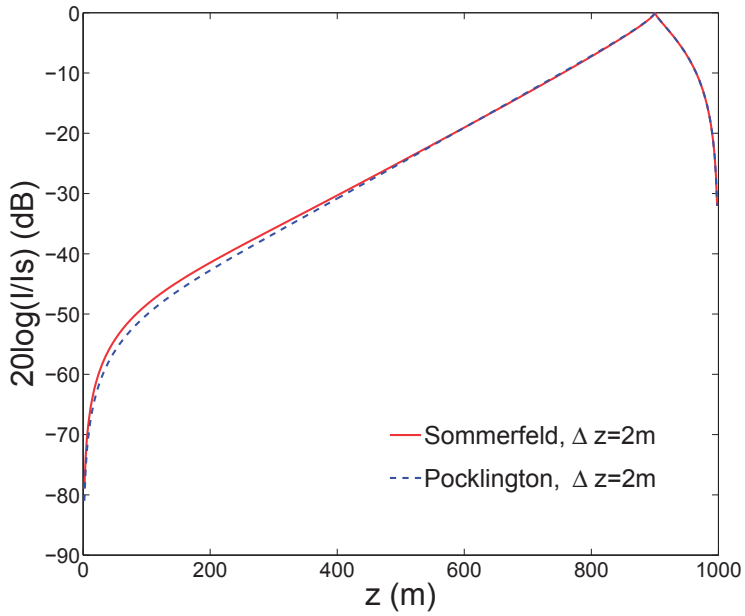

Figure D.5: Numerical results obtained by applying the new method to Eq. (D.3.8) and compared to that given by Eq. (D.3.6) for the integral step $\Delta z = 2\,\mathrm{m}$. The length of the well $\ell = 1000\mathrm{m}$ and the radius $a = 0.1\mathrm{m}$. The source is located at 100m from the lower end of the well. The conductivity of the well is assumed to be $\sigma_a = 1 \times 10^6$ S/m and the conductivity of the surroundings is assumed to be $\sigma_m = 1\,\mathrm{S/m}$. The system operates at $f = 5\,\mathrm{Hz}$.

By performing the calculation of the Sommerfeld kernel $S(z, z')$ as outlined above, it is hoped that better numerical accuracy can be obtained. This is indeed the case, as demonstrated in Figure D.5. An examination on the coefficient matrix shows that the difference of the elements on the first sub-diagonal decreases from $4.5 \times 10^{-2}\%$ to $8.5 \times 10^{-4}\%$.

D.4.3 Plane Layered Earth Model

It is well known that the subsurface of the earth is not a homogeneous medium. As a crude approximation, the outer crust of the earth can be considered to consist of horizontal plane layers. For such model, the Pocklington's integral equation can not any longer be used to model the current signal propagating along the well. Instead one has to resort to the Sommerfeld's integral equation.

For evaluation purposes, we will consider a simple three layered earth model for which the interfaces are located at $d_1 = 300\,\mathrm{m}$ and $d_2 = 500\,\mathrm{m}$. The conductivities of the various media are $\sigma_1 = 1\,\mathrm{S/m}$, $\sigma_2 = 4\,\mathrm{S/m}$, and $\sigma_3 = 1\,\mathrm{S/m}$, respectively. In this layered model, we assume that a vertical well of length $\ell = 1\,000\,\mathrm{m}$ and radius $a = 0.1\,\mathrm{m}$. The conductivity of the well casing is assumed to be $\sigma_a = 1 \times 10^6\mathrm{S/m}$. The electromagnetic source is located at depth $z_s = 900\,\mathrm{m}$ and the top of the well is located at $z = 0\,\mathrm{m}$.

By the method introduced above, we numerically solved the Sommerfeld's integral equation for the model, and Figure D.6 presents the current distribution along the length of the well. In performing these calculations, we had to substitute, as mentioned previously, the factor $\exp(\mathrm{i}k_z|z - z'|)$ appearing in Eq. (D.3.8) with a function, $F(z, z')$. The explicit mathematical form of $F(z, z')$ can be found in the Appendix 3.11.

From the simulation results presented in Figure D.6, it is observed that close to the source, the current distribution along the well follows closely the corresponding current distribution for a homogeneous $1\,\mathrm{S/m}$ medium. However, as for depths corresponding to the high conductive layer (medium 2), a steeper current gradient is readily observed. Near to the interface of medium 1 and medium 2, a reflection effect can be observed.

In order to be able to compare the quality of the numerical results based on the Sommerfeld's integral equation, Figure D.6 also presents results obtained by using the transmission line matrix method [25]. The predictions obtained by both methods compare favorably, which verifies the quality of our numerical results. However, the latter method is less general than the former, and can, for instance, not handle a geometry where the well is not perpendicular to the interfaces of the layers. When the well is tilted with respect to the plane layers (with an angle different from 90^o), the Sommer-

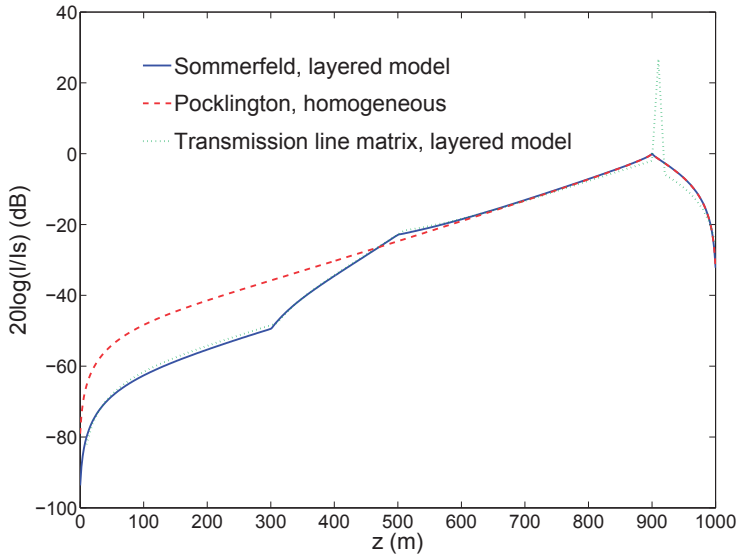

Figure D.6: Numerical result of $I(z')$ along the well relative to the source $I(z'_s)$ in dB when the integral step $|z - z'| = 2\,\mathrm{m}$. The length of the well is $\ell = 1\,000\,\mathrm{m}$ and the radius is $a = 0.1\,\mathrm{m}$. The source is located $100\,\mathrm{m}$ from the lower end of the well. The conductivity of the well is assumed to be $\sigma_a = 1 \times 10^6$ S/m and the conductivities of the layered media are assumed to be $\sigma_m = [1, 4, 1]\,\mathrm{S/m}$. The system operates at $f = 5\mathrm{Hz}$. The result is compared to the results for a homogeneous medium and the results computed by the transimission line matrix method.

feld's integral equation method is one of the few semi-analytic methods that can be used to obtain the current distribution along the well.

D.4.4 Experiment

In 2011, an experiment was carried out by Wins and Sintef on testing signal transmission along a metal well casing. Thanks for the kindness of Wins and Sintef, the experiment data can be applied to test the numerical results given by the method presented in this paper.

A sketch of the experiment is presented in Fig.D.7. Two equipments, named tool 1 and tool 2, was installed in the well and communicated with each other with single frequency signals. Tool 2 was installed at a depth of 2500m and tool 1 was first installed at 10m and then installed at 1500m. In order to correct the big calculation error near the end of the well, a 50m cable was connected to the top of the well.

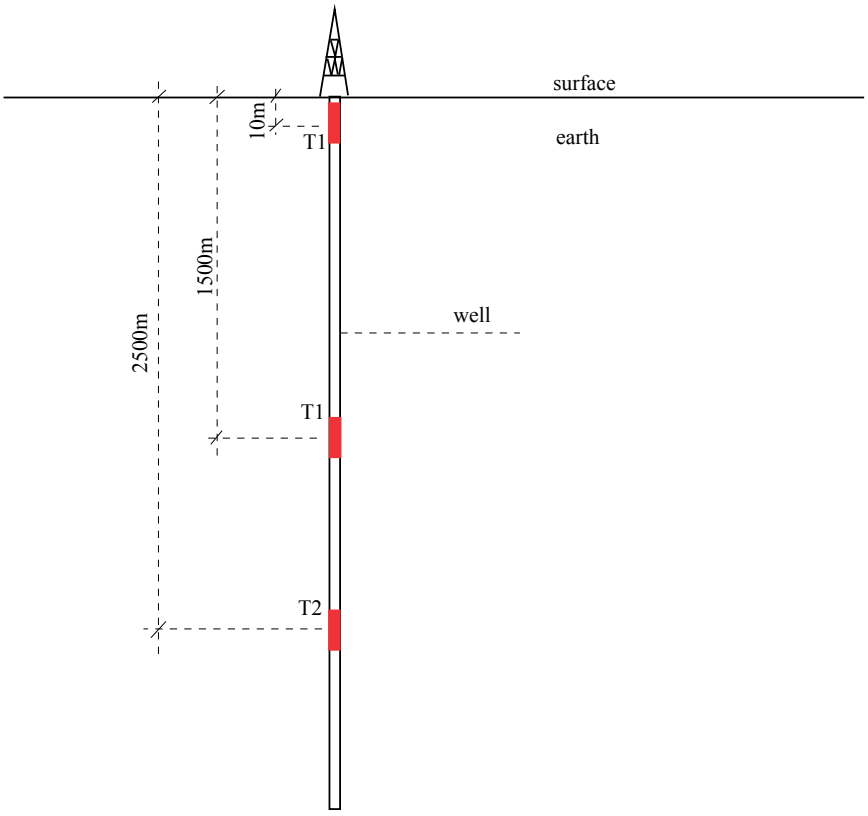

Figure D.7: A sketch of the experiment

To compare the experiment data to the numerical results, the signal received by the same tool with different distance to the source are compared. For tool 1 worked as a receiver, the difference between the signal received by it at 1500m and 10m are presented in Table.D.1 and the corresponding numerical results are presented in Fig.D.8. For tool 2 worked as a receiver, the difference between the signal transmitted by tool 1 when it was at 1500m and 10m are presented in Table.D.2 and the corresponding numerical results are presented in Fig.Fig.D.9.

Table D.1: Compare the experiment data received by tool 1 to the numerical results

	0.66 Hz	1 Hz	2 Hz	4 Hz
difference in experiment for tool 1 at 1500m and 10m	59.09dB	60.55dB	64.14dB	64.9dB
numerical results for tool 1 at 10m	−112.3dB	−113.3dB	−118.4dB	−132.6dB
numerical results for tool 1 at 1500m	−52.11dB	−52.66dB	−55.22dB	−62.19dB
difference in numerical model between 1500m and 10m	60.19dB	60.64dB	63.18dB	70.4dB
error between numerical model and experiment	1.1dB	0.09dB	−0.96dB	5.5dB

Table D.2: Compare the experiment data received by tool 2 to the numerical results

	0.66 Hz	1 Hz	2 Hz	4 Hz
difference in experiment for tool 1 at 1500m and 10m	59.68dB	61.64dB	66.06dB	66.68dB
numerical results for tool 1 at 10m	−110.3dB	−111.5dB	−117.2dB	−132.5dB
numerical results for tool 1 at 1500m	−48.22dB	−48.75dB	−51.26dB	−58.12dB
difference in numerical model between 1500m and 10m	62.08dB	62.75dB	65.94dB	74.38dB
error between numerical model and experiment	2.4dB	1.11dB	−0.12dB	7.7dB

Comparing the numerical results to the experiment results in Table.D.1 and Table.D.2, we can see that the results given by the numerical method

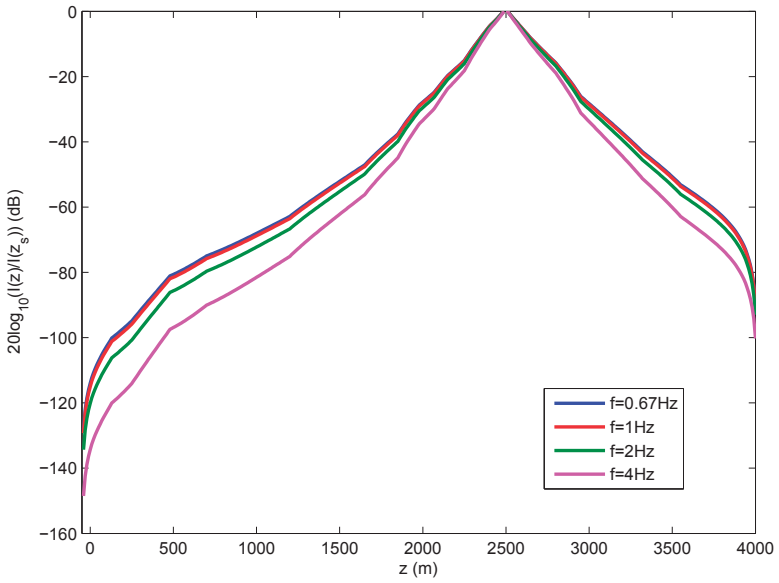

Figure D.8: Numerical results for the source at 2500m

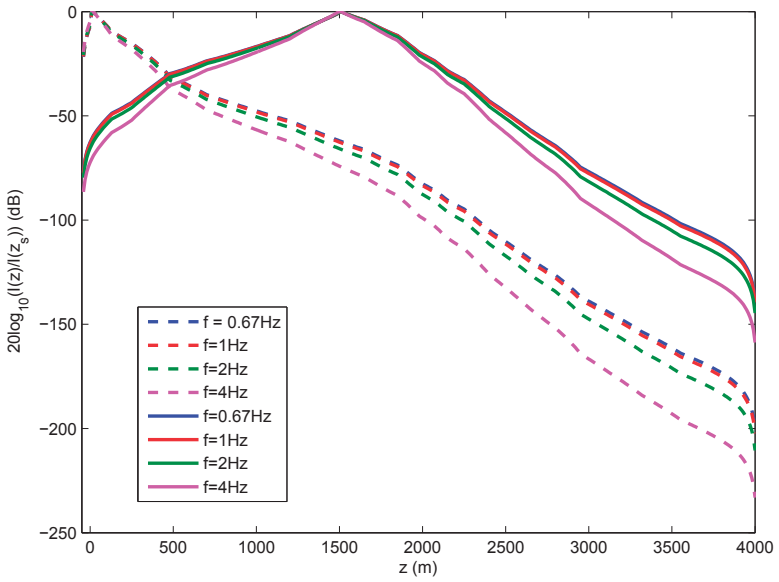

Figure D.9: Numerical results for the source at 10m and 1500m

are agree to the experiment results quite well except when $f = 4$Hz. There is no exact explanation for this and noise effect for weak signal can be one of the reason. For the sake of commercial confidence, no more detail of the experiment could be presented here.

D.5 Conclusion

In geophysics, the earth is often considered as a horizontally layered medium, where each layer is characterized by a conductivity. When an electric dipole source is placed over the earth or embedded in it, the electromagnetic wave radiated from it will be reflected and transmitted from the various layer boundaries. To calculate the electromagnetic field anywhere in the structure, the well developed plane wave theory for a horizontally layered medium can be applied. This amounts to expanding the source in plane waves, an expansion that introduces the so-called Sommerfeld integrals. However, such integrals are challenging to evaluate accurately due to the oscillating behavior and/or slow decay of the the integrand. In this paper, we present an efficient and accurate numerical method for evaluating such integrals in the low frequency limit, *i.e.* when $\mathrm{Im}(\varepsilon(\omega)) \gg \mathrm{Re}(\varepsilon(\omega))$ ($\sigma/\omega \gg \mathrm{Re}(\varepsilon)$). The method relies on adding and subtracting to the Sommerfeld integrand a functional form that has the same asymptotic form as the Sommerfeld integrand, but which can be evaluated analytically. The remaining integrand can accurately be integrated numerically since it is better behaved (in the large argument limit). By adding the two former integrals evaluated analytically and numerically, an accurate estimate for the original Sommerfeld integral is obtained. Our method is evaluated by presenting numerical results for the wave propagation from a source placed in a vertical well surrounded by either a homogeneous or horizontally layered medium. We find that the current along the well calculated with the method introduced in this paper compares favorably with what can be obtained by alternative methods. It is found that the proposed method produces results which are (for similar computational complexity) 50 times more accurate, at least for the examples studied in this paper. The application of the results presented in this work points towards obtaining more accurate computation of the strongly attenuated electromagnetic (or other) field in geophysical systems.

Bibliography

[1] B. Ursin. Review of elastic and electromagnetic wave propagation in horizontally layered media. *Geophysics*, 48(8):1063–1081, Aug. 1983.

[2] Weng Cho Chew. *Waves and Fields in Inhomogeneous Media*. IEEE Press, 1st edition, 1995.

[3] James R. Wait and David A. Hill. Theory of transmission of electromagnetic waves along a drill rod in conducting rock. *IEEE Transactions on Geoscience Electronics*, GE-17(2):21–24, Apr. 1979.

[4] J. Acharya, G. Sreechakra, J. C. Goswami, and D. Helioit. Hierarchical zonation technique to extract common boundaries of a layered earth model. *IEEE Antennas and Propagation Society International Symposium*, pages 1817–1820, Jun. 2007.

[5] A. D. Chave and C. S. Cox. Controlled electromagnetic sources for measuring electrical conductivity beneath the oceans 1. forward problem and model study. *J. Geophys. Res.*, 87(B7):5327–5338, Jul. 1982.

[6] S. Ellingsrud, T. Eidesmo, M. C. Shinha, L. M. MacGregor, and S. C. Constable. Remote sensing of hydrocarbon layers by seabed logging(sbl): Results from a cruise offshore angola. *The Leading Edge*, 21(10), Oct. 2002.

[7] Michael Wilt and David Alumbaugh. Oil field reservoir characterization and monitoring using electromagnetic geophysical techniques. *J. Petrol. Sci. ENG.*, 39:85–97, Aug. 2003.

[8] A. Sommerfeld. Uber die ausbreitung der wellen in der drahtlosen telegraphie. *Ann. Phys.*, 333:665, 1909.

[9] A. Hochman and Y. Leviatan. A numerical methodology for efficient evaluation of 2d sommerfeld integrals in the dielectric half-space problem. *Antennas and Propagation, IEEE Transactions on*, 58(2):413–431, Feb. 2010.

[10] J. D. Jackson. *Classical Electrodynamics*. New York, Wiley, 3rd edition, 1998.

[11] Constantine A. Balanis. *Antenna Theory*. John Wiley & Sons, Inc., 2nd edition, 1997.

[12] Constantine A. Balanis. *Advanced Engineering Electromagnetics*. John Wiley & Sons, Inc., 1st edition, 1989.

[13] P. DeGauque and R. Grudzinski. Propagation of electromagnetic waves along a drillstring of finit conductivity. *SPE Drilling Engineering*, pages 127–134, Jun. 1987.

[14] R. F. Harrington. *Field Computation by Moment Methods*. IEEE Press, 2nd edition, 1993.

[15] Milton Abramowitz and Irene A. Stegun. *Handbook of Mathematical Functions with Formulas, Graphs, and Mathematical Tables*. Dover Publications, 10th edition, 1972.

[16] Wei Yang, Carlos Torres-Verdin, Junsheng Hou, and Zhiyi Zhang. 1d subsurface electromagnetic fields excited by energized steel casing. *Geophysics*, 74(4):E159–E180, July 2009.

[17] P. J. Davis and P. Rabinowitz. *Methods of Numerical Integration*. Academic Press. Inc. Orlando, 2nd edition, 1984.

[18] J. N. Lyness. Integrating some infinite oscillating tails. *J. Comput. Appl. Math.*, 12-13:109–117, May 1985.

[19] P. Wynn. On a device for computing the $e_m(s_n)$ transformation. *MTAC*, 10:91–96, 1956.

[20] A. Sidi. The numerical evaluation of very oscillatory infinite integrals by extrapolation. *Math. Comput.*, 38(158):517–529, Apr. 1982.

[21] A. Sidi. Extrapolation methods for divergent oscillatory infinite integrals that are defined in the sense of summability. *J. Comput. Appl. Math.*, 17:105–114, Feb. 1987.

[22] S. K. Lucas and H. A. Stone. Evaluating infinite integrals involving bessel functions of arbitrary order. *J. Comput. Appl. Math.*, 64:217–231, Dec. 1995.

[23] Krzysztof A. Michalski. Extrapolation methods for sommerfeld integral tails. *IEEE Trans on Antennas and Propagation*, 46:1405–1418, Oct. 1998.

[24] Carl M. Bender and Steven A. Orszag. *Advanced Mathematical Methods for Scientists and Engineers*. Springer. Inc., 1st edition, 1999.

[25] Matthew N. O. Sadiku. *Numerical Techniques in Electromagnetics*. CRC, 2nd edition, 2000.

Part III

Appendix

Appendix

3.1 Maxwell equations and Constitutive relations

In vector notation and SI units, Maxwell's equations can be written in differential representations:

$$\nabla \cdot \mathbf{D}(\mathbf{r}, t) = \rho(\mathbf{r}, t), \tag{3.1.1a}$$
$$\nabla \cdot \mathbf{B}(\mathbf{r}, t) = 0, \tag{3.1.1b}$$
$$\nabla \times \mathbf{E}(\mathbf{r}, t) = -\frac{\partial}{\partial t}\mathbf{B}(\mathbf{r}, t), \tag{3.1.1c}$$
$$\nabla \times \mathbf{H}(\mathbf{r}, t) = \mathbf{J}(\mathbf{r}, t) + \frac{\partial}{\partial t}\mathbf{D}(\mathbf{r}, t), \tag{3.1.1d}$$

where $\mathbf{D}$ is the electric flux in $\mathrm{C/m^2}$, $\mathbf{B}$ is the magnetic flux in $\mathrm{Wb/m^2}$, $\mathbf{E}$ is the electric field in V/m and $\mathbf{H}$ is the magnetic field in A/m. $\mathbf{J}$ is the current density in $\mathrm{A/m^2}$ and ρ is the charge density in $\mathrm{C/m^2}$ [1, P.1].

If we assume the fields are time harmoic, Eq.3.1.1c and Eq.3.1.1d can be simplified as

$$\nabla \times \mathbf{E}(\mathbf{r}, t) = i\omega\mathbf{B}(\mathbf{r}, t), \tag{3.1.2a}$$
$$\nabla \times \mathbf{H}(\mathbf{r}, t) = \mathbf{J}(\mathbf{r}, t) - i\omega\mathbf{D}(\mathbf{r}, t), \tag{3.1.2b}$$

where ω is the angular frequency in rad/S.

In the differential equations above, the nabla operator ∇ has different forms in different coordinates. In Cartesian coordinate,

$$\nabla = \hat{x}\frac{\partial}{\partial x} + \hat{y}\frac{\partial}{\partial y} + \hat{z}\frac{\partial}{\partial z}. \tag{3.1.3}$$

In cylindrical coordinate,

$$\nabla = \hat{\rho}\frac{\partial}{\partial \rho} + \hat{\theta}\frac{1}{\rho}\frac{\partial}{\partial \theta} + \frac{\partial}{\partial z}\hat{z}. \tag{3.1.4}$$

In spherical coordinate,

$$\nabla = \hat{r}\frac{\partial}{\partial r} + \hat{\theta}\frac{1}{r}\frac{\partial}{\partial \theta} + \hat{\phi}\frac{1}{r\sin\theta}\frac{\partial}{\partial \phi}. \tag{3.1.5}$$

Although Maxwell's equations are extremely compact, the applications and solutions of Maxwell's equations turn out to be extremely comprehensive because in practical problems, the constitutive relations are specific to materials and substances:

$$\mathbf{D}(\mathbf{r},\omega) = \bar{\epsilon}(\mathbf{r},\omega)\cdot\mathbf{E}(\mathbf{r},\omega) + \bar{\xi}(\mathbf{r},\omega)\cdot\mathbf{H}(\mathbf{r},\omega) \tag{3.1.6a}$$

$$\mathbf{B}(\mathbf{r},\omega) = \bar{\zeta}(\mathbf{r},\omega)\cdot\mathbf{E}(\mathbf{r},\omega) + \bar{\mu}(\mathbf{r},\omega)\cdot\mathbf{H}(\mathbf{r},\omega) \tag{3.1.6b}$$

where $\bar{\epsilon}$, $\bar{\xi}$, $\bar{\zeta}$ and $\bar{\mu}$ are 3×3 tensors [1, P.5]. If the medium is assumed to be isotropic and homogeneous, ϵ and μ are constants

$$\mathbf{D} = \epsilon\mathbf{E} = \epsilon_r\epsilon_0\mathbf{E} \tag{3.1.7a}$$

$$\mathbf{B} = \mu\mathbf{H} = \mu_r\mu_0\mathbf{H} \tag{3.1.7b}$$

where $\epsilon_0 = 8.85\times 10^{-12}$F/m and $\mu_0 = 4\pi\times 10^{-7}$H/m, the permittivity and permeability in vacuum. ϵ_r and μ_r are respectively the dielectric constant and the relative permeability of the medium. If the medium is conductive for a conductivity σ, the permittivity is complex. From Eq.(3.1.2b) and Ohm's law $\mathbf{J} = \sigma\mathbf{E}$, we could obtain

$$\nabla\times\mathbf{H} = \mathbf{J} - i\omega\mathbf{D} = -i\omega\tilde{\epsilon}\mathbf{E}, \tag{3.1.8}$$

where the generalized permittivity $\tilde{\epsilon}$ equals

$$\tilde{\epsilon} = \epsilon + i\frac{\sigma}{\omega}. \tag{3.1.9}$$

3.2 Potentials and Lorenz gauge

For the convenience of calculation, vector and scalar potentials are defined from the Maxwell's equation. Since $\nabla\cdot\mathbf{B} = 0$, vector magnetic potential $\mathbf{A}$ can be defined by

$$\mathbf{B} \;=\; \nabla\times\mathbf{A}. \tag{3.2.1}$$

Put Eq.(3.2.1) into Eq.(3.1.2a), we can define the scalar potential Φ by

$$\mathbf{E} \;=\; -\nabla\Phi - \frac{\partial\mathbf{A}}{\partial t}. \tag{3.2.2}$$

The potentials defined in Eq.(3.2.1) and (3.2.2) are not unique. All the couples that fulfills the field will be a pair of solution. For example, $\mathbf{A}'$ and Φ' defined by the equations

$$\mathbf{A}' = \mathbf{A} + \nabla\Lambda, \tag{3.2.3a}$$

$$\Phi' = \Phi - \frac{\partial\Lambda}{\partial t}, \tag{3.2.3b}$$

will have the same fields derived from $\mathbf{A}$ and Φ. All the sets of $(\mathbf{A}, \Phi)$ which satisfies the relation

$$\nabla \cdot \mathbf{A} = -\mu\epsilon \frac{\partial \Phi}{\partial t} \tag{3.2.4}$$

belong to the Lorenz gauge.

Insert potential (3.2.1) and (3.2.2) into the inhomogeneous Maxwell equations Eq.(3.1.1a) and (3.1.2b), together with constitutive relations and Lorenz gauge, we can obtain the following Helmholtz equations:

$$(\nabla^2 + k^2)\Phi(\mathbf{r}) = -\frac{\rho(\mathbf{r}')}{\epsilon}, \tag{3.2.5a}$$

$$(\nabla^2 + k^2)\mathbf{A}(\mathbf{r}) = -\mu\mathbf{J}(\mathbf{r}'), \tag{3.2.5b}$$

in which the wavenumber $k = \omega\sqrt{\mu\epsilon}$, $\mathbf{r}'$ represents the source position.These two equations represent the electromagnetic wave induced by charge source $\rho(\mathbf{r}')$ and current source $\mathbf{J}(\mathbf{r}')$. In a conductive medium, k is complex and equals

$$k = \omega\sqrt{\mu\tilde{\epsilon}} = \omega \left[\sqrt{\mu(\frac{\sqrt{\epsilon^2 + (\frac{\sigma}{\omega})^2} + \epsilon}{2})} + i\sqrt{\mu(\frac{\sqrt{\epsilon^2 + (\frac{\sigma}{\omega})^2} + \epsilon}{2})} \right]. \tag{3.2.6}$$

If $\sigma/\omega >> \epsilon$, the wave number can be approximated by

$$k \approx \sqrt{\frac{\omega\mu\sigma}{2}}(1 + i). \tag{3.2.7}$$

3.3 Electromagnetic fileds induced by a current element in a homogeneous medium

To solve an inhomogeneous Helmholtz equation such as

$$(\nabla^2 + k^2)\mathcal{L}(\mathbf{r}) = s(\mathbf{r}'), \tag{3.3.1}$$

we need to study the case of a point source first,

$$(\nabla^2 + k^2)G(\mathbf{r}) = -\delta(\mathbf{r} - \mathbf{r}'), \tag{3.3.2}$$

where the solution $G(\mathbf{r})$ to this equation is called the scalar Green's function. In frequency domain, it equals

$$G(\mathbf{r}, \mathbf{r}') = \frac{e^{ikR}}{4\pi R}, \tag{3.3.3}$$

where $R = |\mathbf{r} - \mathbf{r}'|$. Then, for a given source $s(\mathbf{r}')$, the Holmheltz equation (3.3.1) can be solved by applying convolution theory

$$\mathcal{L}(\mathbf{r}) = \int d\mathbf{r}' G(\mathbf{r}, \mathbf{r}') s(\mathbf{r}'). \tag{3.3.4}$$

When the source $s(\mathbf{r}')$ is a current source, we first devided it into small elements, each of which can be considered as an electric dipole $I(\mathbf{r}')dl\hat{l}$. Next, we study the field induced by each of electric dipole and finally we can find the total field by summing up the fields from all of the dipoles. The vector potential $\mathbf{A}(\mathbf{r})$ induced by an electric dipole is equal to

$$\mathbf{A}(\mathbf{r}) = \frac{\mu I(\mathbf{r}')dl\hat{l}e^{ikR}}{4\pi R}. \tag{3.3.5}$$

By applying the definition of potential (3.2.2) and Lorenz gauge (3.2.4), we can get electric field $\mathbf{E}$ due to an electric dipole:

$$\mathbf{E}(\mathbf{r}) = i\omega\Big[\frac{\nabla\nabla}{\omega^2\mu\epsilon} + \bar{\mathbf{I}}\Big] \cdot \mathbf{A} = i\omega\mu\Big[\frac{\nabla\nabla}{\omega^2\mu\epsilon} + \bar{\mathbf{I}}\Big] \cdot \frac{e^{ikR}I(\mathbf{r}')dl\hat{l}}{4\pi R}. \tag{3.3.6}$$

We define

$$\bar{\mathbf{G}}(\mathbf{r}, \mathbf{r}') = \Big[\frac{\nabla\nabla}{\omega^2\mu\epsilon} + \bar{\mathbf{I}}\Big] \cdot \frac{e^{ikR}}{4\pi R}, \tag{3.3.7}$$

as the dyadic Green's function. In the equations above, $\bar{\mathbf{I}}$ denotes the unit dyad

$$\bar{\mathbf{I}} = \begin{bmatrix} 1 & 0 & 0 \\ 0 & 1 & 0 \\ 0 & 0 & 1 \end{bmatrix}. \tag{3.3.8}$$

By using the definition of the nabla operator (3.1.3), (3.1.4), (3.1.5), the tensor $\nabla\nabla$ can be calculated as following. In Cartesian coordiante,

$$\nabla\nabla = \begin{bmatrix} \partial_x \\ \partial_y \\ \partial_z \end{bmatrix} \begin{bmatrix} \partial_x & \partial_y & \partial_z \end{bmatrix} = \begin{bmatrix} \partial_{xx} & \partial_{xy} & \partial_{xz} \\ \partial_{yx} & \partial_{yy} & \partial_{yz} \\ \partial_{zx} & \partial_{zy} & \partial_{zz} \end{bmatrix}. \tag{3.3.9}$$

In cylindrical coordinate,

$$\nabla\nabla = \begin{bmatrix} \partial_\rho \\ \frac{1}{\rho}\partial_\theta \\ \partial_z \end{bmatrix} \begin{bmatrix} \partial_\rho & \frac{1}{\rho}\partial_\theta & \partial_z \end{bmatrix} = \begin{bmatrix} \partial_{\rho\rho} & \frac{1}{\rho}\partial_{\rho\theta} & \partial_{\rho z} \\ \frac{1}{\rho}\partial_{\theta\rho} & \frac{1}{\rho^2}\partial_{\theta\theta} & \frac{1}{\rho}\partial_{\theta z} \\ \partial_{z\rho} & \frac{1}{\rho}\partial_{z\theta} & \partial_{zz} \end{bmatrix}. \tag{3.3.10}$$

In spherical coordinate,

$$\begin{aligned}\nabla\nabla &= \begin{bmatrix} \partial_r \\ \frac{1}{r}\partial_\theta \\ \frac{1}{r\sin\theta}\partial_\phi \end{bmatrix} \begin{bmatrix} \partial_r & \frac{1}{r}\partial_\theta & \frac{1}{r\sin\theta}\partial_\phi \end{bmatrix} \\ &= \begin{bmatrix} \partial_{rr} & \frac{1}{r}\partial_{r\theta} & \frac{1}{r\sin\theta}\partial_{r\phi} \\ \frac{1}{r}\partial_{\theta r} & \frac{1}{r^2}\partial_{\theta\theta} & \frac{1}{r^2\sin\theta}\partial_{\theta\phi} \\ \frac{1}{r\sin\theta}\partial_{\phi r} & \frac{1}{r^2\sin\theta}\partial_{\phi\theta} & \frac{1}{r^2\sin^2\theta}\partial_{\phi\phi} \end{bmatrix}. \end{aligned} \tag{3.3.11}$$

We take an vertical electic dipole (VED) source for an example. Put a current element at the origin along z-axis of a cylindrical coordinate, which can be illustrated by $Idz\hat{z}$. The field components induced by this VED can be calculated by (3.3.6). E_z is equal to

$$E_z = \frac{i\omega\mu Idz}{4\pi k^2}(k^2 + \partial_{zz})\frac{e^{ikR}}{R}. \tag{3.3.12}$$

By using chain rule of derivative, we get

$$E_z = \frac{i\omega\mu Idz}{4\pi k^2}\frac{e^{ikR}}{R^5}\left[(1-ikR)(2R^2-3\rho^2) + (k\rho R)^2\right], \tag{3.3.13}$$

which is the integrand of the Pocklington's integral. E_ρ is equal to

$$E_\rho = \frac{i\omega\mu Idz}{4\pi k^2}\partial_{\rho z}\frac{e^{ikR}}{R} \tag{3.3.14}$$

$$= \frac{i\omega\mu Idz}{4\pi k^2}\frac{e^{ikR}}{R^5}\Big[\rho z(-k^2R^2 - 3ikR + 3)\Big] \tag{3.3.15}$$

E_z and E_ρ from a VED are illustrated in Fig.3.10 and 3.11.

The magnetic field $\mathbf{H}$ can be calculated from $\mathbf{A}$ by

$$\mathbf{H} = \frac{1}{\mu}\nabla\times\mathbf{A}. \tag{3.3.16}$$

3.4 Decomposition of electromagnetic fields

In a source free space, wave equations of fields E and H can be achieved from the Maxwell's equations:

$$(\nabla^2 + k^2)\mathbf{E} = 0, \tag{3.4.1a}$$

$$(\nabla^2 + k^2)\mathbf{H} = 0, \tag{3.4.1b}$$

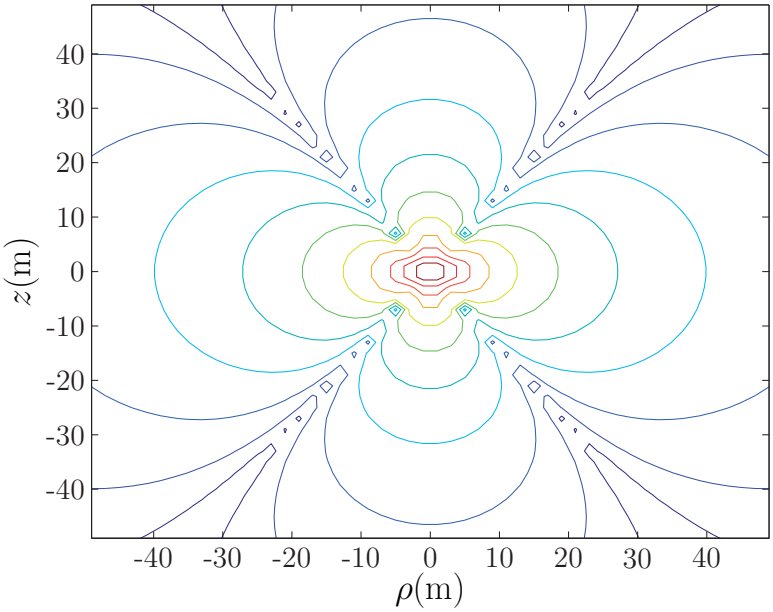

Figure 3.10: The electric field components $|E_{\mathrm{VED},z}|$ in ρz-plane, the field is valued in dB

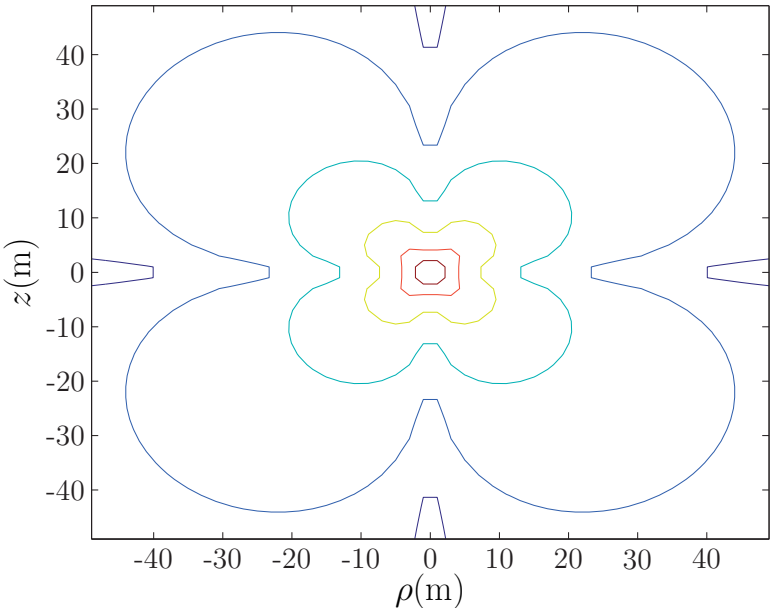

Figure 3.11: The electric field components $|E_{\mathrm{VED},x}|$ in ρz-plane, the field is valued in dB

which indicate that they will propagate in plane waves in a homogeneous medium:

$$\mathbf{E} = Ee^{i\mathbf{k}\cdot\mathbf{r}-i\omega t}, \tag{3.4.2a}$$

$$\mathbf{H} = He^{i\mathbf{k}\cdot\mathbf{r}-i\omega t}, \tag{3.4.2b}$$

where $\mathbf{k} = k\hat{k}$ and $\hat{k}$ is the propagating direction. Since the fields $\mathbf{E}$ and $\mathbf{H}$ are transverse to the propagating direction in this case, they propagate in TEM mode. Before studying the electromagnetic wave propagation in inhomogeneous medium, we need to study the decomposition of the fields first. We will consider the electric field $\mathbf{E}$ and the magnetic field $\mathbf{H}$ could be studied in a similar way.

Given an arbitrary direction which can be represented by a direction unit $\hat{u}$, the field $\mathbf{E}$ can then be decomposed into a component E_u which is in the direction of $\hat{u}$ and a component E_t which is transverse to $\hat{u}$ and lies in $\mathbf{E} - \hat{u}$ plane, as shown in Fig.3.12. By applying vector calculus theory, we can get $E_u = \mathbf{E} \cdot \hat{u}$ and $\mathbf{E}_t = \mathbf{E} - E_u\hat{u}$.

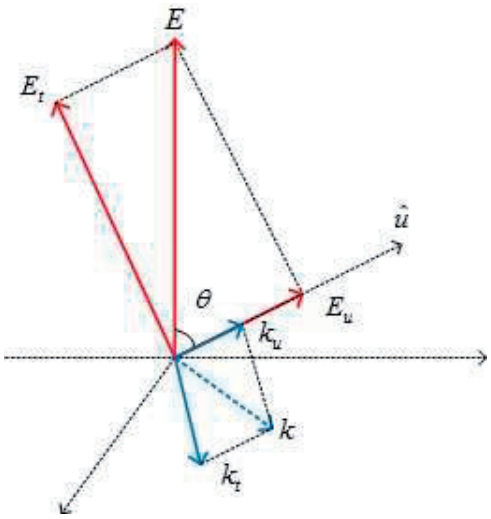

Figure 3.12: The longitudinal-transverse decomposition of E field

In the wave equations (3.4.1a), wave number $\mathbf{k}$ and nabla operator ∇ are also vectors and can be decomposed in the way of $\mathbf{E}$. The wave number $\mathbf{k}$ is decomposed into a longitudinal component k_u in $\hat{u}$ direction and a transverse component $k_t = \sqrt{k^2 - k_u^2}$ which is transverse to $\hat{u}$ and lies in $\mathbf{k} - \hat{u}$ plane. The nabla symbol ∇ is decomposed into $\frac{\partial}{\partial u}\hat{u}$ and $\nabla_t = \nabla - \frac{\partial}{\partial u}\hat{u}$. Put them back into Maxwell equations and together with vector calculus theory,

we can get the Maxwell equations in terms of transverse and longitudinal components [2, Ch.8.2] [3, Ch.5.3][4, Ch.9.5]

$$\nabla_t \cdot \mathbf{E}_t = -\frac{\partial E_u}{\partial u}, \tag{3.4.3a}$$

$$\nabla_t \cdot \mathbf{H}_t = -\frac{\partial H_u}{\partial u}, \tag{3.4.3b}$$

$$\hat{u} \cdot \nabla_t \times \mathbf{E}_t = i\omega\mu H_u, \tag{3.4.3c}$$

$$\frac{\partial \mathbf{E}_t}{\partial z} - \nabla_t E_z = -i\omega\mu\hat{u} \times \mathbf{H}_t, \tag{3.4.3d}$$

$$\hat{u} \cdot \nabla_t \times H_t\hat{t} = -i\omega\epsilon E_u, \tag{3.4.3e}$$

$$\frac{\partial \mathbf{H}_t}{\partial z} - \nabla_t B_z = i\omega\epsilon\hat{u} \times \mathbf{E}_t. \tag{3.4.3f}$$

Equations (3.4.3d) and (3.4.3f) can be used to get solutions for $\mathbf{E}_t$ and $\mathbf{H}_t$ in the longitudinal components E_u and H_u:

$$\mathbf{E}_t = \frac{i}{k^2 - k_u^2}[k_u \nabla_t E_u - \omega\mu\hat{u} \times \nabla_t H_u], \tag{3.4.4a}$$

$$\mathbf{H}_t = \frac{i}{k^2 - k_u^2}[k_u \nabla_t H_u + \omega\epsilon\hat{u} \times \nabla_t E_u]. \tag{3.4.4b}$$

Since in each of the equations (3.4.3a) and (3.4.3b), there are two forcing terms on the right hand side, E_u and H_u, we can take them independently and then use superposition method to get the total results.

$$\mathbf{E} = \mathbf{E}_1 + \mathbf{E}_2, \tag{3.4.5a}$$

$$\mathbf{H} = \mathbf{H}_1 + \mathbf{H}_2. \tag{3.4.5b}$$

For $H_u = 0$, $\mathbf{E}_2$ and $\mathbf{H}_2$ are equal to:

$$\mathbf{E}_2 = \mathbf{E}_{2t} + E_{2u}\hat{u}, \tag{3.4.6a}$$

$$\mathbf{H}_2 = \mathbf{H}_{2t}, \tag{3.4.6b}$$

in which

$$\mathbf{E}_{2t} = \frac{i}{k^2 - k_u^2}[k_u \nabla_t E_u], \tag{3.4.7a}$$

$$\mathbf{H}_{2t} = \frac{i}{k^2 - k_u^2}[\omega\epsilon\hat{u} \times \nabla_t E_u]. \tag{3.4.7b}$$

Since $H_u = 0$, it is a TM mode.

For $E_u = 0$, $\mathbf{E}_1$ and $\mathbf{H}_1$ are equal to:

$$\mathbf{E}_1 = \mathbf{E}_{1t}, \tag{3.4.8a}$$
$$\mathbf{H}_1 = \mathbf{H}_{1t} + H_{1u}\hat{u}, \tag{3.4.8b}$$

in which

$$\mathbf{E}_{1t} = \frac{i}{k^2 - k_u^2}[-\omega\epsilon\hat{u} \times \nabla_t H_u], \tag{3.4.9a}$$
$$\mathbf{H}_{1t} = \frac{i}{k^2 - k_u^2}[k_u \nabla_t H_u]. \tag{3.4.9b}$$

Since $E_u = 0$, it is a TE mode. In a homogeneous and isotropic medium, the TE and TM decomposition are shown in the Fig.3.13:

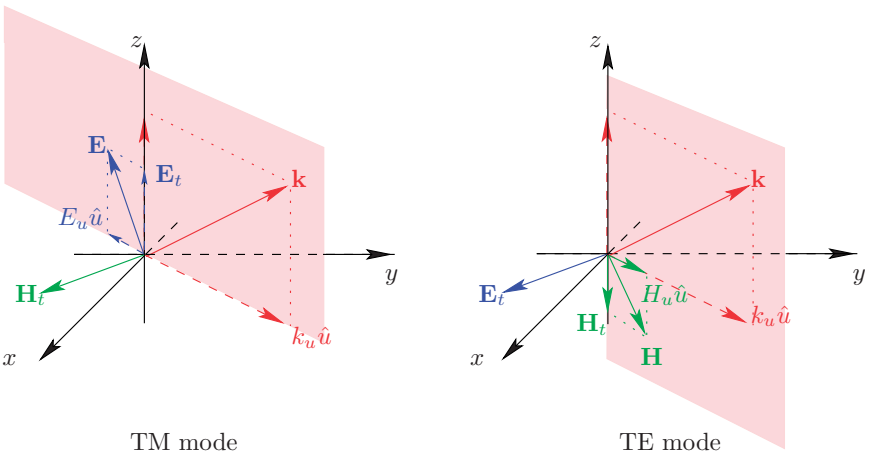

Figure 3.13: The components of the fields in TM mode and TE mode

From the analysis above, we can prove that the electromagnetic field can be completely characterized by the two longitudinal field components E_u and H_u [1, Ch.2.1][3, Ch.5.4]. For example, in a source free space, the field equations are equal to

$$(\nabla^2 + k^2)E_u = 0, \tag{3.4.10a}$$
$$(\nabla^2 + k^2)H_u = 0, \tag{3.4.10b}$$

3.5 Field components from an electric dipole

Equation (3.3.6) presented how to compute electric field induced by an electric dipole in a homogeneous medium. But when an electric dipole is embeded

in a layered medium, we need to decompose the field first by using Wyel's identity or Sommerfeld integral in order to apply the propagation theory of plane waves [1, Eq.2.2.27, 2.2.30],

$$\frac{e^{ikR}}{R} = \frac{i}{2\pi}\int_{-\infty}^{\infty}\int_{-\infty}^{\infty} dk_x dk_y \frac{e^{ik_x(x-x')+ik_y(y-y')+ik_z|z-z'|}}{k_z}, \tag{3.5.1a}$$

$$\frac{e^{ikR}}{R} = i\int_0^{\infty} dk_\rho \frac{k_\rho}{k_z} J_0(k_\rho(\rho-\rho'))e^{ik_z|z-z'|}. \tag{3.5.1b}$$

where $k_z = \sqrt{k^2 - k_\rho^2}$. In the following, we will study the field components induced by a VED source and a HED source respectively. The study will be done in a Cartesian coordinate.

For a VED source placed at the origin and along z-axis, there is no H_z component induced by it, which can be proved by (3.3.5) and (3.3.16). The electromagnetic wave induced by VED is in TM mode in z-direction. Since the model is symmetry in xy-plane, we only study the field components in xz-plane. By putting the Sommerfeld integral (3.5.1b) into equation (3.3.12), we can compute $E^{\mathrm{TM}}_{z,VED}$

$$\begin{aligned} E^{\mathrm{TM}}_{z,VED} &= \frac{-\omega\mu I dz}{4\pi}\int_0^{\infty} dk_x (k^2 + \frac{\partial^2}{\partial z^2})\frac{k_x}{k_z k^2} J_0(k_x x)e^{ik_z|z|} \\ &= \frac{-\omega\mu I dz}{4\pi}\int_0^{\infty} dk_x \frac{k_x^3}{k_z k^2} J_0(k_x x)e^{ik_z|z|}, \end{aligned} \tag{3.5.2}$$

where $k_x = \sqrt{k^2 - k_z^2}$. Similarly, the field component $E^{\mathrm{TM}}_{x,VED}$ is equal to

$$\begin{aligned} E^{\mathrm{TM}}_{x,VED} &= \frac{-\omega\mu I dz}{4\pi}\int_0^{\infty} dk_x (\frac{\partial^2}{\partial x \partial z})\frac{k_x}{k_z k^2} J_0(k_x x)e^{ik_z|z|} \\ &= \frac{i\omega\mu I dz}{4\pi}\frac{z}{|z|}\int_0^{\infty} dk_x \frac{k_x^2}{k^2} J_1(k_x x)e^{ik_z|z|}, \end{aligned} \tag{3.5.3}$$

An example is given in Fig.3.14 and Fig.3.15, which are the same as Fig.3.10 and Fig.3.11 and prove that both methods will present the same results in a homogeneous medium.

If the electric dipole at the origin is placed along x-axis, then it is a horizontal electric dipole (HED) for wave propagating in z-direction. Since HED will induce H_z component which inturn will induce E_x, it will be in TE mode. The H_z induced by a HED is equal to

$$H_{z,HED} = \hat{z}\cdot\left[\nabla \times \frac{I dx \hat{x} e^{ikR}}{4\pi R}\right] = -ik_y I dx \frac{e^{ikR}}{4\pi R}. \tag{3.5.4}$$

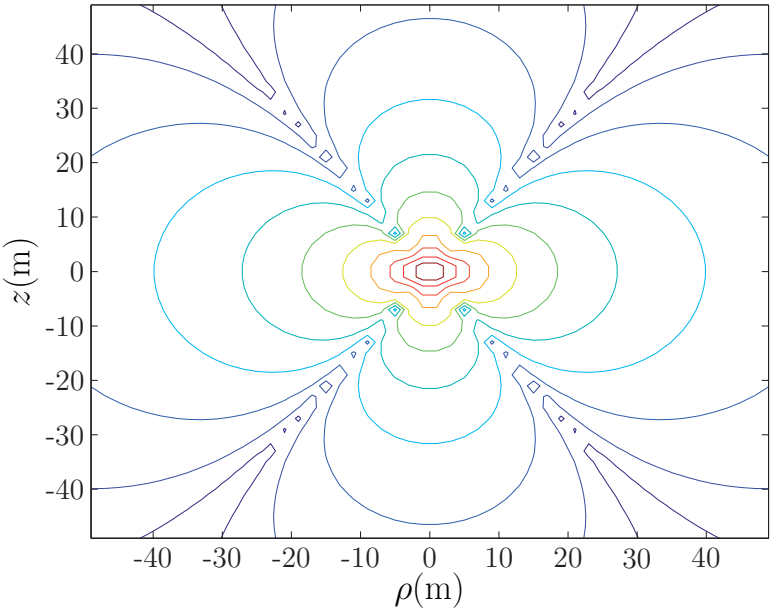

Figure 3.14: The electric field components $|E^{\mathrm{TM}}_{\mathrm{VED},z}|$ in xz-plane, the field is valued in dB

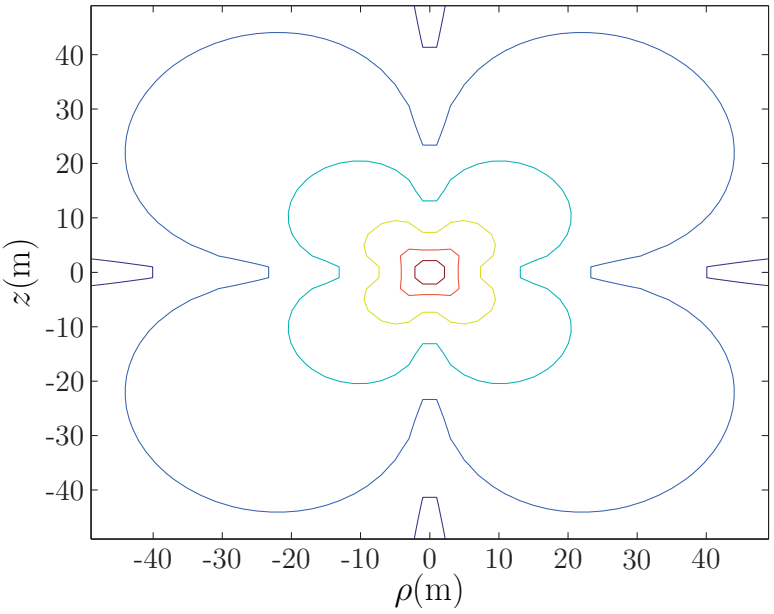

Figure 3.15: The electric field components $|E^{\mathrm{TM}}_{\mathrm{VED},x}|$ in xz-plane, the field is valued in dB

By using (3.4.9a), the $E_{x,HED}$ component induced by $H_{z,HED}$ is equal to

$$E_{x,HED}^{\mathrm{TE}} = \frac{i}{k^2 - k_x^2}[-\omega\epsilon\hat{z} \times \nabla_t H_z] = \frac{i\omega\mu}{k^2 - k_z^2}\frac{\partial H_z}{\partial y}. \tag{3.5.5}$$

Put (3.5.4) into (3.5.5) and applying Weyl identity (3.5.1a), $E_{x,HED}^{\mathrm{TE}}$ is equal to

$$E_{x,HED}^{\mathrm{TE}} = \frac{-\omega\mu I dx}{4\pi}\frac{1}{2\pi}\int_{-\infty}^{\infty}\int_{-\infty}^{\infty} dk_x dk_y (\frac{k_y^2}{k_x^2 + k_y^2})\frac{e^{ik_x x + ik_y y + ik_z|z|}}{k_z}. \tag{3.5.6}$$

The reason that we need to apply Weyl identity instead of Sommerfeld integral is that it is not symmetry in xy-plane anymore. In k domain, we have

$$k_\rho = \sqrt{k_x^2 + k_y^2}, \tag{3.5.7}$$

where $k_x = k_\rho \cos\alpha$, $k_y = k_\rho \sin\alpha$. In space domain,

$$\rho = \sqrt{x^2 + y^2}, \tag{3.5.8}$$

where $x = \rho\cos\beta$ and $y = \rho\sin\beta$. Therefore

$$e^{ik_x x + ik_y y} = e^{ik_\rho\rho(\cos\alpha\cos\beta + \sin\alpha\sin\beta)} = e^{ik_\rho\rho\sin\xi}, \tag{3.5.9}$$

in which $\xi = \alpha - \beta + \pi/2$. This can be expressed by a series of Bessel functions [5, 8.511]:

$$e^{ik_\rho\rho\sin\xi} = \sum_{-\infty}^{\infty} J_n(k_\rho\rho)e^{in\xi} \tag{3.5.10}$$

where $J_{-n}(k_\rho\rho) = (-1)^n J_n(k_\rho\rho)$. From this, one obtains [5, 8.411]:

$$J_0(k_\rho\rho) = \frac{1}{2\pi}\int_0^{2\pi} d\xi e^{ik_\rho\rho\sin\xi} \tag{3.5.11a}$$

$$J_1(k_\rho\rho) = \frac{1}{2\pi i}\int_0^{2\pi} d\xi \sin\xi e^{ik_\rho\rho\sin\xi} \tag{3.5.11b}$$

$$J_2(k_\rho\rho) = \frac{1}{2\pi}\int_0^{2\pi} d\xi \cos 2\xi e^{ik_\rho\rho\sin\xi} \tag{3.5.11c}$$

and the relationship between J_0, J_1 and J_2:

$$J_0(k_\rho\rho) + J_2(k_\rho\rho) = \frac{2}{k_\rho\rho}J_1(k_\rho\rho) \tag{3.5.12}$$

Equation (3.5.6) can be transformed into

$$E_{x,HED}^{\mathrm{TE}} = \frac{-\omega\mu I dx}{4\pi}\frac{1}{2\pi}\int_0^\infty dk_\rho k_\rho e^{ik_z|z|}\int_0^{2\pi} d\xi \frac{\sin^2\alpha}{k_z} e^{ik_\rho \rho \sin\xi}. \tag{3.5.13}$$

$$\sin^2\alpha = \cos^2(\xi+\beta) = \frac{1}{2} + \frac{1}{2}(\cos 2\xi\cos 2\beta - \sin 2\xi \sin 2\beta), \tag{3.5.14}$$

therefore,

$$E_{x,HED}^{\mathrm{TE}} = \frac{-\omega\mu I dx}{4\pi}\frac{1}{2\pi}\int_0^\infty dk_\rho \frac{k_\rho}{k_z} e^{ik_z|z|}\int_0^{2\pi} d\xi (\frac{1}{2} + \frac{\cos 2\xi\cos 2\beta}{2}) e^{ik_\rho\rho\sin\xi}, \tag{3.5.15}$$

which is equal to

$$E_{x,HED}^{\mathrm{TE}} = \frac{-\omega\mu I dx}{4\pi}\int_0^\infty dk_\rho \frac{k_\rho}{k_z}\Big[\sin^2\beta J_0(k_\rho\rho) + \frac{\cos 2\beta}{k_\rho\rho}J_1(k_\rho\rho)\Big] e^{ik_z|z|}. \tag{3.5.16}$$

In xz-plane, $\beta = 0$, the equation can be simplified as

$$E_{x,HED}^{\mathrm{TE}} = \frac{-\omega\mu I dx}{4\pi}\int_0^\infty dk_x \frac{1}{k_z x} J_1(k_x x) e^{ik_z|z|}. \tag{3.5.17}$$

An example of $E_{x,HED}^{\mathrm{TE}}$ is shown in Fig.3.16.

From (3.3.6), the total E_x induced by a HED is equal to

$$E_{x,HED}^{\mathrm{TM+TE}} = \frac{i\omega\mu I dx}{4\pi k^2}(k^2 + \partial_{xx})\frac{e^{ikR}}{R}. \tag{3.5.18}$$

By using Wyel identity, it is equal to

$$E_{x,HED}^{\mathrm{TM+TE}} = \frac{i\omega\mu I dx}{4\pi k^2}\frac{1}{2\pi}\int_{-\infty}^\infty\int_{-\infty}^\infty dk_x dk_y \frac{k^2 - k_x^2}{k^2}\frac{e^{ik_x x + ik_y y + ik_z|z|}}{k_z}. \tag{3.5.19}$$

The $E_{x,HED}^{\mathrm{TM}}$ will equal to $E_{x,HED}^{\mathrm{TM+TE}} - E_{x,HED}^{\mathrm{TE}}$, which is equal to

$$E_{x,HED}^{\mathrm{TM}} = \frac{i\omega\mu I dx}{4\pi k^2}\frac{1}{2\pi}\int_{-\infty}^\infty\int_{-\infty}^\infty dk_x dk_y \frac{k_x^2 k_z}{k^2(k_x^2+k_y^2)} e^{ik_x x + ik_y y + ik_z|z|}. \tag{3.5.20}$$

Apllying the properties of the Bessel function introduced above, we can get

$$E_{x,HED}^{\mathrm{TM}} = \frac{-\omega\mu I dx}{4\pi}\int_0^\infty dk_\rho \frac{k_\rho k_z}{k^2}\left[\cos^2\beta J_0(k_\rho\rho) - \frac{\cos 2\beta}{k_\rho\rho}J_1(k_\rho\rho\right] e^{ik_z|z|}. \tag{3.5.21}$$

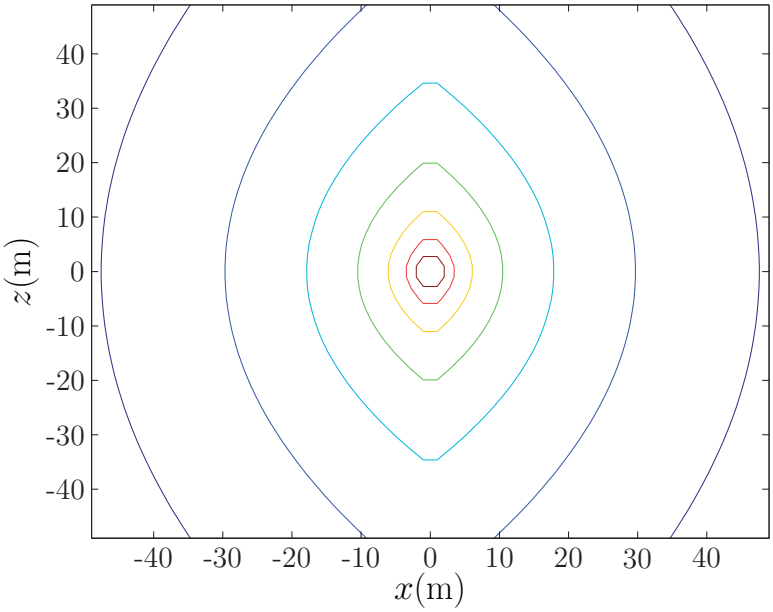

Figure 3.16: The electric field components $|E^{\mathrm{TE}}_{\mathrm{HED},x}|$ in xz-plane, the field is valued in dB

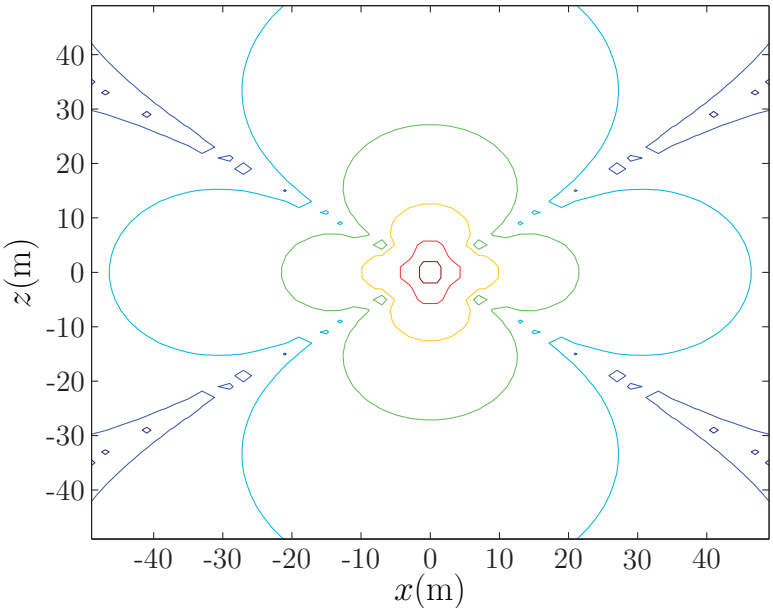

Figure 3.17: The electric field components $|E^{\mathrm{TM}}_{\mathrm{HED},x}|$ in xz-plane, the field is valued in dB

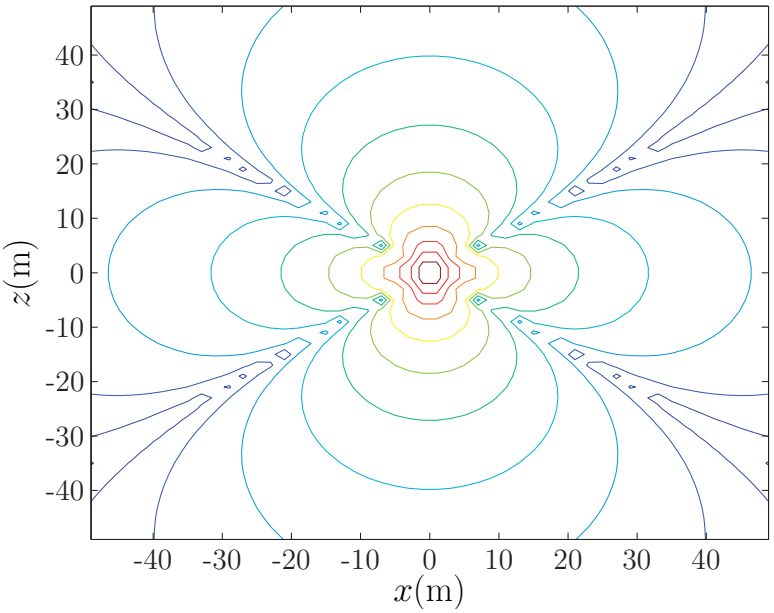

Figure 3.18: The electric field components $|E^{\mathrm{TE+TM}}_{\mathrm{HED},x}|$ in xz-plane, the field is valued in dB

in xz-plane, it is equal to

$$E^{\mathrm{TM}}_{x,HED} = \frac{-\omega\mu I dx}{4\pi}\int_0^\infty dk_\rho \frac{k_x k_z}{k^2}\left[J_0(k_x x) - \frac{1}{k_x x}J_1(k_x x)\right]e^{ik_z|z|}. \quad (3.5.22)$$

Fig.3.17 shows an example of $E^{\mathrm{TM}}_{x,HED}$. The total $E_{x,HED}$ is shown in Fig.3.18, which is equal to $E_{z,VED}$.

Finally, E_z component induced by a HED will be always in TM mode in z-direction and it can be calculated from (3.3.6) directly

$$E^{\mathrm{TM}}_{z,HED} = \frac{i\omega\mu dz}{4\pi}\frac{z}{|z|}\int_0^\infty dk_x \frac{k_x^2}{k^2}J_1(k_x x)e^{ik_z|z|} = E^{\mathrm{TM}}_{x,VED}. \quad (3.5.23)$$

This is shown in Fig.3.19

To sum up, the electric field components in xz-plane, which are induced

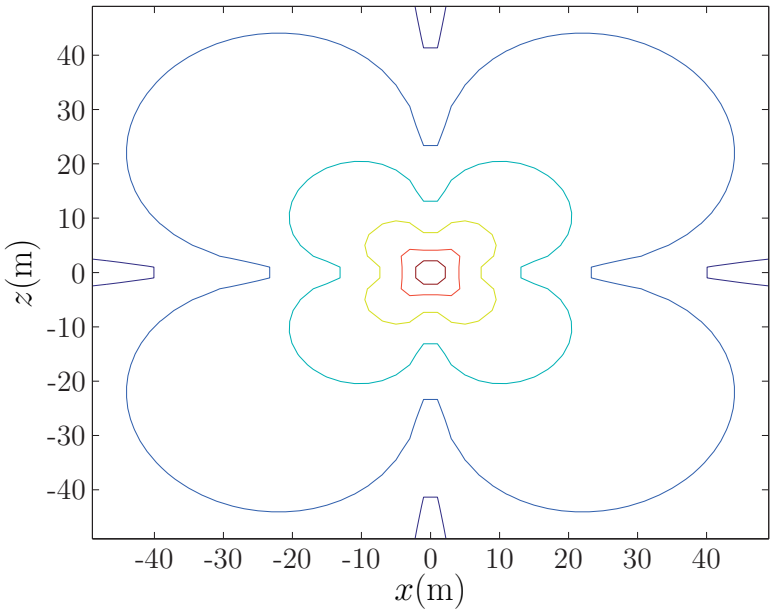

Figure 3.19: The electric field components $|E^{\mathrm{TM}}_{\mathrm{HED},z}|$ in xz-plane, the field is valued in dB

by a VED and a HED placed at the origin, are listed below:

$$E^{\mathrm{TM}}_{z,VED} = \frac{-\omega\mu I dz}{4\pi}\int_0^\infty dk_x \frac{k_x^3}{k_z k^2} J_0(k_x x) e^{ik_z|z|}, \tag{3.5.24a}$$

$$E^{\mathrm{TM}}_{x,VED} = \frac{i\omega\mu I dz}{4\pi}\frac{z}{|z|}\int_0^\infty dk_x \frac{k_x^2}{k^2} J_1(k_x x) e^{ik_z|z|}, \tag{3.5.24b}$$

$$E^{\mathrm{TM}}_{z,HED} = \frac{i\omega\mu dz}{4\pi}\frac{z}{|z|}\int_0^\infty dk_x \frac{k_x^2}{k^2} J_1(k_x x) e^{ik_z|z|}, \tag{3.5.24c}$$

$$E^{\mathrm{TM}}_{x,HED} = \frac{-\omega\mu I dx}{4\pi}\int_0^\infty dk_x \frac{k_x k_z}{k^2}\left[J_0(k_x x) - \frac{1}{k_x x} J_1(k_x x)\right] e^{ik_z|z|}, \tag{3.5.24d}$$

$$E^{\mathrm{TE}}_{x,HED} = \frac{-\omega\mu I dx}{4\pi}\int_0^\infty dk_x \frac{1}{k_z x} J_1(k_x x) e^{ik_z|z|}. \tag{3.5.24e}$$

3.6 E field from a dipole source (small current) embeded in earth

Assuming a small current source, a VED is embeded in earth, which is a conductive medium, the fields induced by the source have already been

studied before, which can be obtained by using dyadic Green's function. In a cylindrical coordinate, E^z and E^ρ are equal to

$$E^{z,TM}_{VED} = \frac{i\omega\mu I\ell}{4\pi}[1+\frac{\partial^2_{z,z}}{k^2}]\frac{e^{ikr}}{r} \tag{3.6.1}$$

$$E^{\rho,TM}_{VED} = \frac{i\omega\mu I\ell}{4\pi}[\frac{\partial^2_{\rho,z}}{k^2}]\frac{e^{ikr}}{r} \tag{3.6.2}$$

which gives

$$\begin{aligned} E^{z,TM}_{VED} &= \frac{i\omega\mu I\ell}{4\pi k^2}[k^2+\frac{\partial^2}{\partial z^2}]\frac{e^{ikr}}{r} \\ &= \frac{i\omega\mu I\ell}{4\pi k^2}\frac{e^{ikr}}{r^5}\Big[(kr\rho)^2+(2r^2-3\rho^2)(1-ikr)\Big] \qquad (3.6.3) \\ E^{\rho,TM}_{VED} &= \frac{i\omega\mu I\ell}{4\pi k^2}[\frac{\partial^2}{\partial\rho\partial z}]\frac{e^{ikr}}{r} \\ &= \frac{i\omega\mu I\ell}{4\pi k^2}\frac{e^{ikr}\rho z}{r^5}\Big[-k^2r^2-3ikr+3\Big] \qquad (3.6.4) \end{aligned}$$

in which $\rho = r\sin\theta$ and $z = r\cos\theta$, $k = \omega\sqrt{\mu\tilde{\epsilon}}$ is the wavenumber. From E^z and E^ρ, we can found E^r and E^θ components in a corresponding spherical cooridnate, which are equal to

$$E^r_{VED} = E^z\cos\theta + E^\rho\sin\theta \tag{3.6.5}$$

$$E^\theta_{VED} = -E^z\sin\theta + E^\rho\cos\theta \tag{3.6.6}$$

which is given in the text book as

$$\begin{aligned} E^r_{VED} &= \frac{Z_0 I\ell\cos\theta e^{ikr}}{2\pi}\left[\frac{1}{r^2}-\frac{1}{ikr^3}\right] \\ &= \frac{i\omega\mu I\ell\cos\theta e^{ikr}}{4\pi k^2}\left[\frac{2k}{ir^2}+\frac{2}{r^3}\right] \qquad (3.6.7) \\ E^\theta_{VED} &= -\frac{ikZ_0 I\ell\sin\theta e^{ikr}}{4\pi}\left[\frac{1}{r}-\frac{1}{ikr^2}-\frac{1}{k^2r^3}\right] \\ &= -\frac{i\omega\mu I\ell\sin\theta e^{ikr}}{4\pi k^2}\left[\frac{k^2}{r}-\frac{k}{ir^2}-\frac{1}{r^3}\right] \qquad (3.6.8) \end{aligned}$$

The common constant is defined as

$$\mathcal{K} = \frac{i\omega\mu I\ell}{4\pi k^2} \tag{3.6.9}$$

by which we can simplify the equations above

$$E_{VED}^{z,TM} = \mathcal{K}e^{ikr}\Big[\frac{k^2\sin^2\theta}{r} - \frac{2ik - 3ik\sin^2\theta}{r^2} + \frac{2-3\sin^2\theta}{r^3}\Big] \quad (3.6.10)$$

$$E_{VED}^{\rho,TM} = \mathcal{K}e^{ikr}\Big[\frac{-k^2\sin\theta\cos\theta}{r} - \frac{3ik\sin\theta\cos\theta}{r^2} + \frac{3\sin\theta\cos\theta}{r^3}\Big] \quad (3.6.11)$$

$$E_{VED}^{r} = \mathcal{K}e^{ikr}\left[\frac{-i2k}{r^2} + \frac{2}{r^3}\right]\cos\theta \quad (3.6.12)$$

$$E_{VED}^{\theta} = \mathcal{K}e^{ikr}\left[\frac{k^2}{r} + \frac{ik}{r^2} - \frac{1}{r^3}\right]\sin\theta \quad (3.6.13)$$

which shows that at far zone, E^z, E^ρ and E^θ attenuates with e^{ikr}/r, while E^r doesn't have far zone element. At far zone, the power propagate in $\hat{r}$ direction since the Poynting vector $\mathbf{S} = \mathbf{E} \times \mathbf{H} = E^\theta\hat{\theta} \times H^\phi\hat{\phi}$. In Fig.3.20, the E_z field estimated by using (3.6.10) and the far zone equation (3.6.14) are compared with each other for $\theta = \pi/2$.

$$E_{VED}^{z,TM} = \mathcal{K}e^{ikr}\frac{k^2\sin^2\theta}{r} \quad (3.6.14)$$

when $\theta = \pi/2$, the equations (3.6.10) and (3.6.14) are equal to

$$E_{VED}^{z,TM} = \mathcal{K}e^{ikr}\Big[\frac{k^2}{r} + \frac{ik}{r^2} - \frac{1}{r^3}\Big] \quad (3.6.15)$$

$$E_{VED}^{z,TM} = \mathcal{K}e^{ikr}\frac{k^2}{r} \quad (3.6.16)$$

In Fig.3.20, the model is assumed that the operating frequency is 1Hz and the conductivity of the medium is 1S/m. Under such a condition, there is a big difference between the results from the two methods.

Comparing E_z field for $\theta = 0$ and $\theta = \pi/2$, we can see that for the far field, $\theta = \pi/2$ will be higher, which are shown in Fig.3.21 and Fig.3.22

If the medium is not conductive, the comparison between them will be

$$E_{VED}^{z,TM} = \Big[\frac{k^2}{r} + \frac{ik}{r^2} - \frac{1}{r^3}\Big] \quad (3.6.17)$$

$$E_{VED}^{z,TM} = \frac{k^2}{r} \quad (3.6.18)$$

This indicates that we could not use the far zone equation to calculate the field when the medium is lossy.

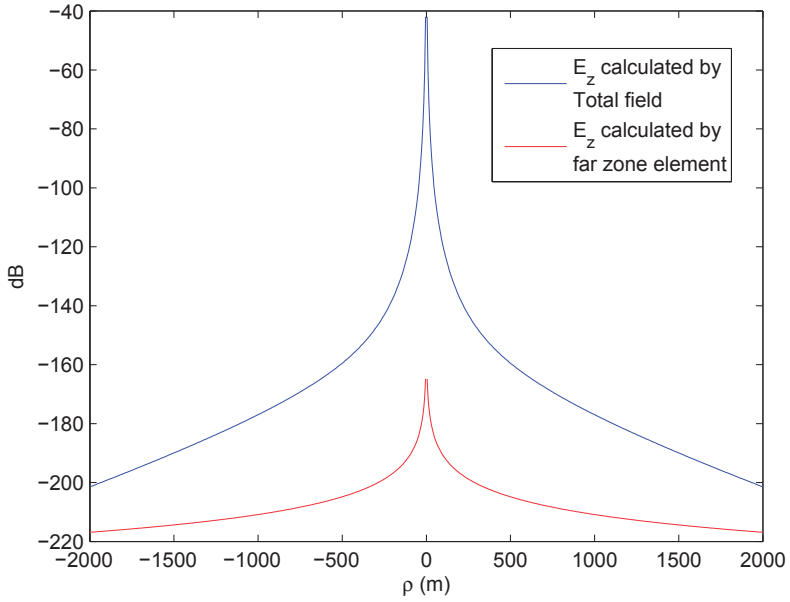

Figure 3.20: Comparison of E_z field calculated by using total equation and only far zone element, when the medium is lossy

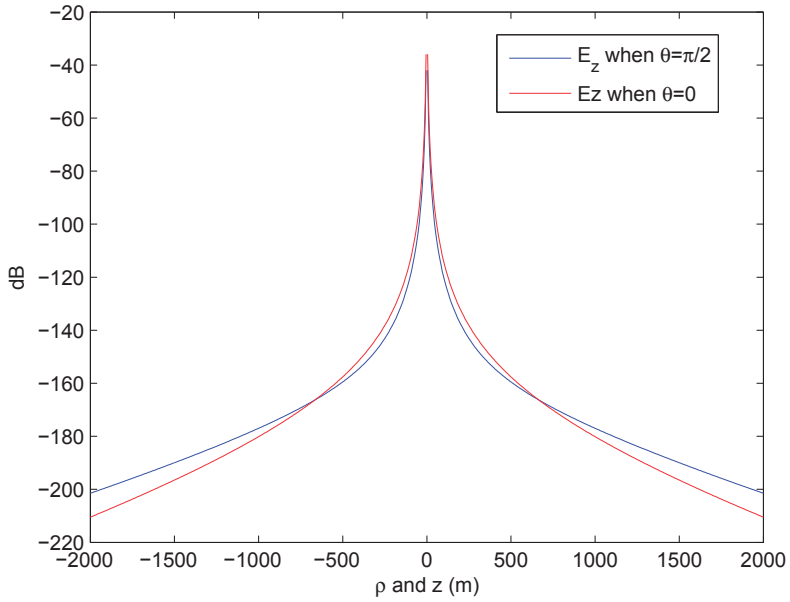

Figure 3.21: Comparison of E_z field for $\theta = 0$ and $\theta = \pi/2$

3.7 Comparison of the field with a metal casing and without a metal casing

A question is when there is a metal casing, what is the difference of the field to the case that the metal casing does not exists. In the following, this problem is studied. It is assumed in the model that the conductivity of the metal casing is 1×10^6S/m and the conductivity of the earth is 1S/m. The operating frequency is 1Hz. The results are shown in Fig.3.24-3.27.

According to the simulation results, it shows that the field is stronger when a metal casing exists in all directions. By comparing Fig.3.24 and Fig.3.25, it is possible to communicate signal along casing or in a vertical direction. The way to transmit signal along a metal casing is the best way in them.

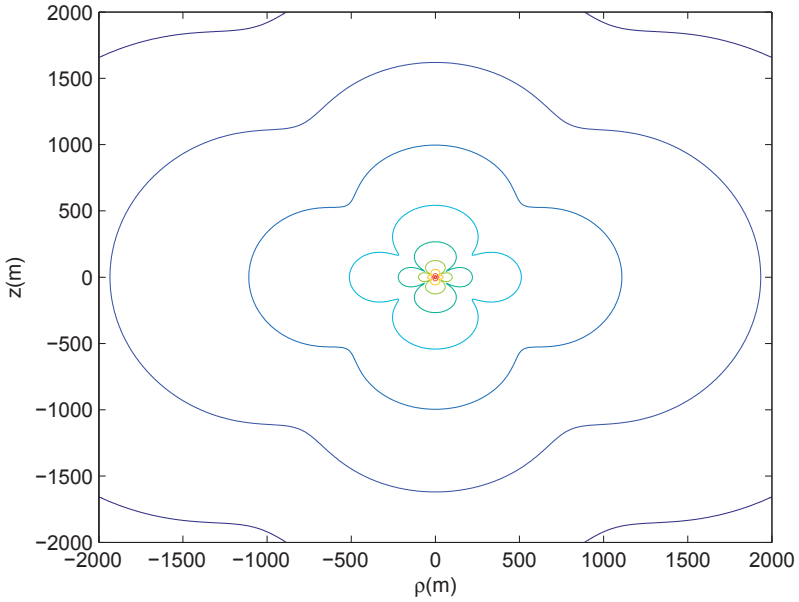

Figure 3.22: Contour of E_z in ρz plane

3.8 Asymptotic equations for Sommerfeld integrals

As studied above, the electric field components induced by a VED and a HED can be expressed as

$$E(r,r') = \frac{i\omega\mu Idl}{4\pi k^2}\int_0^\infty dk_x \Phi(k_x,z,z'), \tag{3.8.1}$$

where

$$\Phi(k_x) = \begin{cases} \Phi^{\mathrm{TM}}_{z,\mathrm{VED}} = \frac{ik_x^3}{k_z} J_0(k_x x) e^{ik_z|z-z'|} \\ \Phi^{\mathrm{TM}}_{x,\mathrm{VED}} = \frac{z-z'}{|z-z'|} k_x^2 J_1(k_x x) e^{ik_z|z-z'|} \\ \Phi^{\mathrm{TM}}_{z,\mathrm{HED}} = \frac{z-z'}{|z-z'|} k_x^2 J_1(k_x x) e^{ik_z|z-z'|} \\ \Phi^{\mathrm{TM}}_{x,\mathrm{HED}} = \frac{ik_x k_z}{2}[J_0(k_x x) - J_2(k_x x)] e^{ik_z|z-z'|} \\ \Phi^{\mathrm{TE}}_{x,\mathrm{HED}} = \frac{ik_x k^2}{2k_z}[J_0(k_x x) + J_2(k_x x)] e^{ik_z|z-z'|} \end{cases}, \tag{3.8.2}$$

$k_x = \sqrt{k^2 - k_z^2}$, and $J_0()$ and $J_1()$ are Bessel functions of the first kind. The integral can be transformed into

$$\int_0^\infty dk_x \Phi(k_x) = \int_0^{k_{x,m}} dk_x \Phi(k_x) + \int_{k_{x,m}}^\infty dk_x \Phi(k_x), \tag{3.8.3}$$

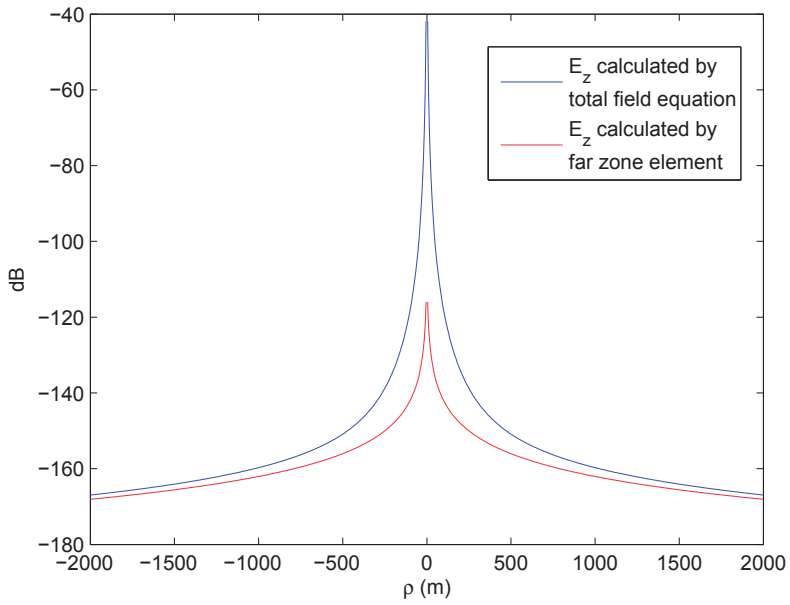

Figure 3.23: Comparison of E_z field calculated by using total equation and only far zone element, when the medium is lossless

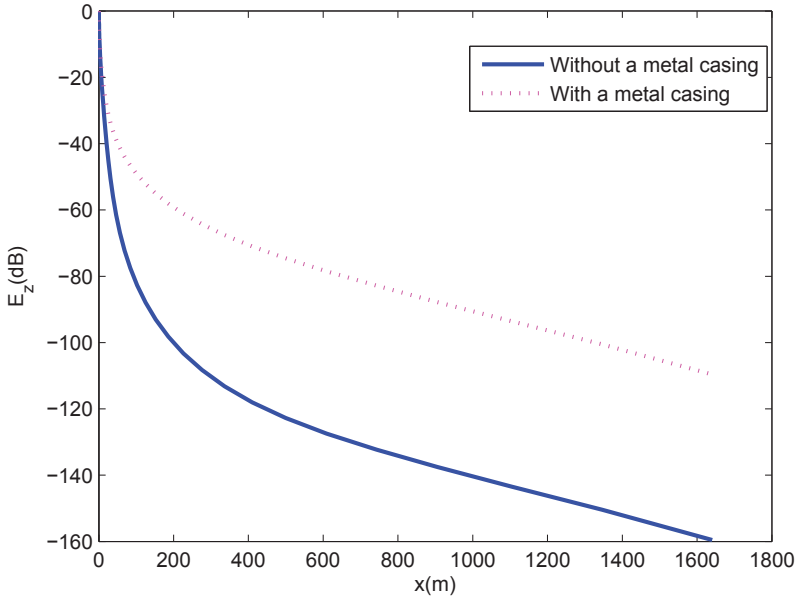

Figure 3.24: Comparison field E_z when $\theta = \pi/2$ for the cases with a metal casing and without a metal casing

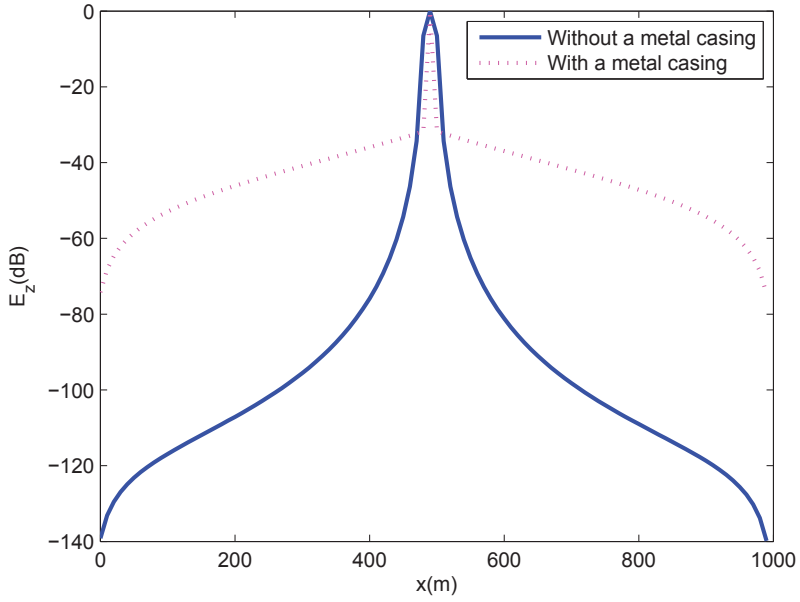

Figure 3.25: Comparison field E_z along $\rho = 0.1$ for the cases with a metal casing and without a metal casing

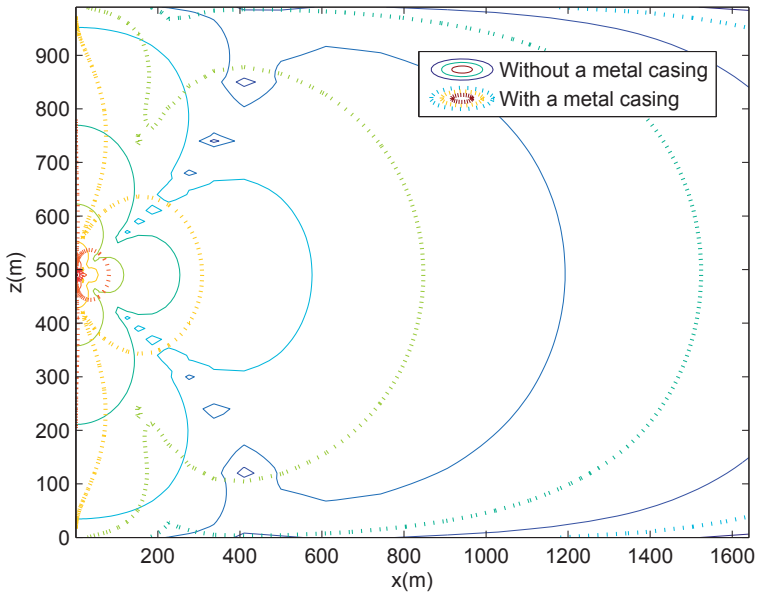

Figure 3.26: Comparison field E_z in a contour figure for the cases with a metal casing and without a metal casing

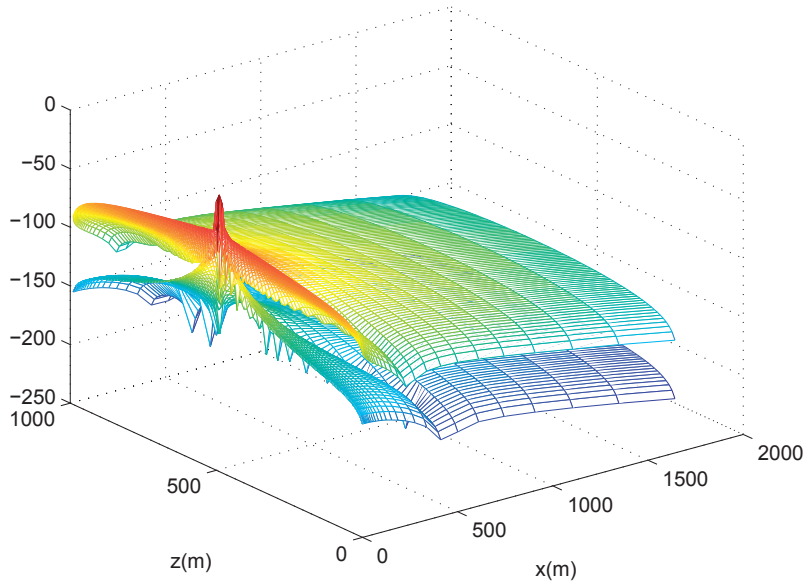

Figure 3.27: Comparison field E_z in a surf figure for the cases with a metal casing and without a metal casing

in which the first element could be calculated numerically and the second element which is the tail could be estimated asymptotically.

3.8.1 $\Phi^{\mathrm{TM}}_{z,\mathrm{VED}}$

For the integrand

$$\Phi^{\mathrm{TM}}_{z,\mathrm{VED}} = \frac{ik_x^3}{k_z} J_0(k_x x) e^{ik_z|z-z'|}, \tag{3.8.4}$$

when $k_z \to ik_x$, it asymptotically equals

$$\Psi^{\mathrm{TM}}_{z,\mathrm{VED}} = \sqrt{\frac{2}{\pi x}} k_x^{\frac{3}{2}} \cos(k_x x - \frac{\pi}{4}) e^{-k_x|z-z'|}. \tag{3.8.5}$$

The tail can be estimated by

$$T^{\mathrm{TM}}_{z,\mathrm{VED}} \approx \int_{k_{x,m}}^{\infty} dk_x \Psi^{\mathrm{TM}}_{z,\mathrm{VED}} = \int_0^{\infty} dk_x \Psi^{\mathrm{TM}}_{z,\mathrm{VED}} - \int_0^{k_{x,m}} dk_x \Psi^{\mathrm{TM}}_{z,\mathrm{VED}}, \tag{3.8.6}$$

where the second term of RHS could be calculated numerically and the first term could be calculated by the Laplace transform:

$$\int_0^{\infty} dk_x \Psi^{\mathrm{TM}}_{z,\mathrm{VED}} = \frac{3}{4}\sqrt{\frac{1}{2x}} \Big[e^{-i\frac{\pi}{4}} s^{-\frac{5}{2}}|_{s=|z-z'|-ix} + e^{i\frac{\pi}{4}} s^{-\frac{5}{2}}|_{s=|z-z'|+ix} \Big]. \tag{3.8.7}$$

3.8.2 $\Phi^{\mathrm{TM}}_{x,\mathrm{VED}}$

For the equation

$$\Phi^{\mathrm{TM}}_{x,\mathrm{VED}} = k_x^2 J_1(k_x x) e^{ik_z|z-z'|}, \tag{3.8.8}$$

when $k_z \to ik_x$, it approximately equals

$$\Psi^{\mathrm{TM}}_{x,\mathrm{VED}} = \sqrt{\frac{2}{\pi x}} k_x^{\frac{3}{2}} \cos(k_x x - \frac{3\pi}{4}) e^{-k_x|z-z'|} \tag{3.8.9}$$

The tail can be estimated by

$$T^{\mathrm{TM}}_{x,\mathrm{VED}} \approx \int_{k_{x,m}}^{\infty} dk_x \Psi^{\mathrm{TM}}_{x,\mathrm{VED}} = \int_0^{\infty} dk_x \Psi^{\mathrm{TM}}_{x,\mathrm{VED}} - \int_0^{k_{x,m}} dk_x \Psi^{\mathrm{TM}}_{x,\mathrm{VED}}, \tag{3.8.10}$$

where

$$\int_0^{\infty} dk_x \Psi^{\mathrm{TM}}_{x,\mathrm{VED}} = \frac{3}{4}\sqrt{\frac{1}{2x}} \Big[e^{-i\frac{3\pi}{4}} s^{-\frac{5}{2}}|_{s=|z-z'|-ix} + e^{i\frac{3\pi}{4}} s^{-\frac{5}{2}}|_{s=|z-z'|+ix} \Big]. \tag{3.8.11}$$

3.8.3 $\Phi^{\mathrm{TM}}_{z,\mathrm{HED}}$

Third, Since $\Phi^{\mathrm{TM}}_{z,\mathrm{HED}} = \Phi^{\mathrm{TM}}_{x,\mathrm{VED}}$, it is the same as above.

3.8.4 $\Phi^{\mathrm{TM}}_{x,\mathrm{HED}}$

For the equation

$$\Phi^{\mathrm{TM}}_{x,\mathrm{HED}} = \frac{ik_\rho k_z}{2}[J_0(k_x x) - J_2(k_x x)]e^{ik_z|z-z'|}, \tag{3.8.12}$$

when $k_z \to ik_x$, it approximately equals

$$\begin{aligned}
\Psi^{\mathrm{TM}}_{x,\mathrm{HED}} &= -\frac{1}{2}\sqrt{\frac{2}{\pi x}}k_x^{\frac{3}{2}}\Big[\cos(k_x x - \frac{\pi}{4}) - \cos(k_x x - \frac{5\pi}{4})\Big]e^{-k_x|z-z'|} \\
&= \sqrt{\frac{2}{\pi x}}k_x^{\frac{3}{2}}\sin(k_x x - \frac{3\pi}{4})e^{-k_x|z-z'|} \\
&= -\sqrt{\frac{2}{\pi x}}k_x^{\frac{3}{2}}\cos(k_x x - \frac{\pi}{4})e^{-k_x|z-z'|} \\
&= -\Phi^{\mathrm{TM}}_{z,\mathrm{VED}}
\end{aligned} \tag{3.8.13}$$

The tail can be estimated by

$$T^{\mathrm{TM}}_{x,\mathrm{HED}} \approx \int_{k_{x,m}}^{\infty} dk_x \Psi^{\mathrm{TM}}_{x,\mathrm{HED}} = \int_0^{\infty} dk_x \Psi^{\mathrm{TM}}_{x,\mathrm{HED}} - \int_0^{k_{x,m}} dk_x \Psi^{\mathrm{TM}}_{x,\mathrm{HED}}, \tag{3.8.14}$$

where

$$\int_0^{\infty} dk_x \Psi^{\mathrm{TM}}_{x,\mathrm{HED}} = -\frac{3}{4}\sqrt{\frac{1}{2x}}\Big[e^{-i\frac{\pi}{4}}s^{-\frac{5}{2}}|_{s=|z-z'|-ix} + e^{i\frac{\pi}{4}}s^{-\frac{5}{2}}|_{s=|z-z'|+ix}\Big] \tag{3.8.15}$$

3.8.5 $\Phi^{\mathrm{TE}}_{x,\mathrm{HED}}$

For equation

$$\Phi^{\mathrm{TE}}_{x,\mathrm{HED}} = \frac{ik^2 k_x}{2k_z}[J_0(k_x x) + J_2(k_x x)]e^{ik_z|z-z'|}, \tag{3.8.16}$$

when $k_z \to ik_x$, it approximately equals

$$\begin{aligned}
\Psi^{\mathrm{TM}}_{x,\mathrm{HED}} &= \frac{k^2}{2}\sqrt{\frac{2}{\pi x}}k_x^{-\frac{1}{2}}\Big[\cos(k_x x - \frac{\pi}{4}) + \cos(k_x x - \frac{5\pi}{4})\Big]e^{-k_x|z-z'|} \\
&= k^2\sqrt{\frac{2}{\pi x}}k_x^{-\frac{1}{2}}\cos(k_x x - \frac{3\pi}{4})\cos(\frac{\pi}{2})e^{-k_x|z-z'|} \\
&= 0
\end{aligned} \tag{3.8.17}$$

3.8.6 Laplace transform and Bessel function

In the above, we need to apply the properties of Laplace transform:

$$\mathcal{L}(f(t)) = \int_0^\infty dt f(t) e^{-st}, \tag{3.8.18a}$$

$$\mathcal{L}(t^{-\frac{1}{2}}) = \sqrt{\frac{\pi}{s}}, \tag{3.8.18b}$$

$$\mathcal{L}(t^n g(t)) = (-1)^n G^{(n)}(s), \tag{3.8.18c}$$

we can get

$$\mathcal{L}(t^{\frac{1}{2}}) = \mathcal{L}(tt^{-\frac{1}{2}}) = -\frac{d(\sqrt{\pi/s})}{ds} = \frac{\sqrt{\pi}}{2} s^{-\frac{3}{2}}, \tag{3.8.19a}$$

$$\mathcal{L}(t^{\frac{3}{2}}) = \mathcal{L}(t^2 t^{-\frac{1}{2}}) = \frac{d^2(\sqrt{\pi/s})}{ds^2} = \frac{3\sqrt{\pi}}{4} s^{-\frac{5}{2}}. \tag{3.8.19b}$$

For the Bessel function of the first kind, it has asymptotic equation

$$J_\alpha(x) = \sqrt{\frac{2}{\pi x}} \cos(x - \frac{\alpha\pi}{2} - \frac{\pi}{4}) \tag{3.8.20}$$

when $x \to \infty$ [6, 9.2.1].

3.9 Plane wave in a two layered source-free medium

The problem of waves propagating in inhomogeneous media is very complicated. A special case for an inhomogenous medium is a planarly multi-layered medium, where each layer is homogeneous and isotropic, that can be characterized by its independent parameters ϵ and μ. The simplest model is two layers with an interface plane, where wave reflection and transmission occur.

In a two layered medium case, we take the interface between the two layers to be xy-plane and we take its normal to be z-axis. The wave direction unit $\hat{k}$ and z-axis form the xz-plane. As we mentioned above, the field can be decomposed into TM and TE mode. In the given coordinate, H and E field will only have y-component H_y and E_y in TM and TE mode respectively as illustrated in Fig.3.28.

The propagation of electromagnetic wave in a homogeneous medium were given in (3.4.2a) and (3.4.2b). In our case, we are more interested in the electric field propagation. Assuming that electromagnetic wave propagates

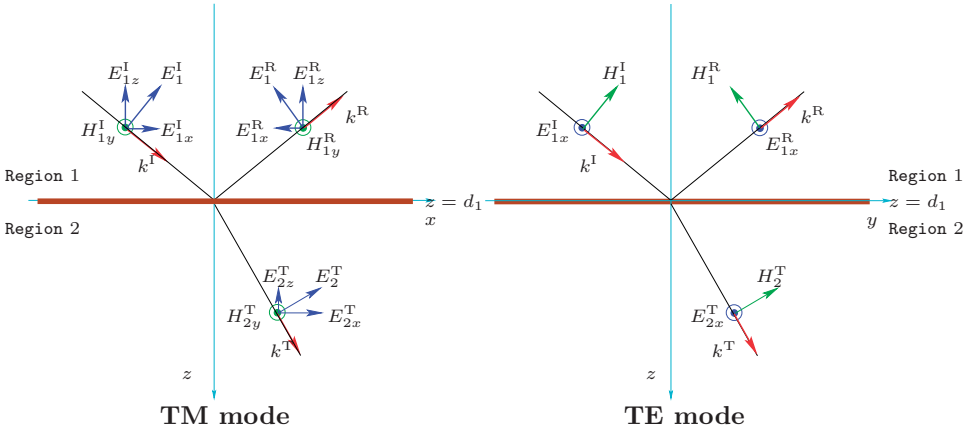

Figure 3.28: Reflection and transmission of plane wave at the interface of two piecewise constant regions

from layer 1 to layer 2, the E-field components in layer 1 are equal to

$$E_{1z} = A_{z0}[e^{ik_{1z}z} + R_{E_z}^{\mathrm{TM}} e^{2ik_{1z}d_1 - ik_{1z}z}], \tag{3.9.1a}$$
$$E_{1x} = A_{x0}[e^{ik_{1z}z} + R_{E_x}^{\mathrm{TM}} e^{2ik_{1z}d_1 - ik_{1z}z}], \tag{3.9.1b}$$
$$E_{1y} = A_{y0}[e^{ik_{1z}z} + R_{E_y}^{\mathrm{TE}} e^{2ik_{1z}d_1 - ik_{1z}z}], \tag{3.9.1c}$$

in which, A_0 are the amplitudes of the incident wave components. R are reflection coefficients. In layer 2, the field components are equal to

$$E_{2z} = A_{z0} T_{E_z}^{\mathrm{TM}} e^{2ik_{1z}d_1 - ik_{1z}z}, \tag{3.9.2a}$$
$$E_{2x} = A_{x0} T_{E_x}^{\mathrm{TM}} e^{2ik_{1z}d_1 - ik_{1z}z}, \tag{3.9.2b}$$
$$E_{2y} = A_{y0} T_{H_y}^{\mathrm{TE}} e^{2ik_{1z}d_1 - ik_{1z}z}, \tag{3.9.2c}$$

where T are the transmission coefficients. For TM mode, the reflection coefficient is equal to

$$R_{12}^{\mathrm{TM}} = \frac{H_{1y}^{\mathrm{R}}}{H_{1y}^{\mathrm{I}}} = \frac{\frac{k_{1z}}{\tilde{\epsilon}_1} - \frac{k_{2z}}{\tilde{\epsilon}_2}}{\frac{k_{1z}}{\tilde{\epsilon}_1} + \frac{k_{2z}}{\tilde{\epsilon}_2}}. \tag{3.9.3}$$

By applying the boundary condition,

$$H_{1y}^{\mathrm{I}} + H_{1y}^{\mathrm{R}} = H_{2y}^{\mathrm{T}}, \tag{3.9.4}$$

we can get the transmission coefficient

$$T_{12}^{\mathrm{TM}} = 1 + R_{12}^{\mathrm{TM}}. \tag{3.9.5}$$

The reflection and transmission coefficients of the electric field can be calculated then. In source free space,

$$i\mathbf{k}\times\mathbf{H}=-i\omega\tilde{\epsilon}\mathbf{E}, \tag{3.9.6}$$

which indicates the electric field components are equal to

$$\omega\tilde{\epsilon}E_x=k_zH_y, \tag{3.9.7a}$$
$$\omega\tilde{\epsilon}E_z=-k_xH_y. \tag{3.9.7b}$$

In the two halfspaces, assume $\mu_1=\mu_2$, we have the following equations in wavenumber

$$k_{1x}^{\mathrm{R}}=k_{1x}^{\mathrm{I}}, \tag{3.9.8a}$$
$$k_{2x}^{\mathrm{T}}=k_{1x}^{\mathrm{I}}, \tag{3.9.8b}$$
$$k_{1z}^{\mathrm{R}}=-k_{1z}^{\mathrm{I}}, \tag{3.9.8c}$$
$$(\frac{k_1}{k_2})^2=\frac{\tilde{\epsilon_1}}{\tilde{\epsilon_2}}. \tag{3.9.8d}$$

Then the reflection and transmission coefficients of the electric components E_z and E_x in TM mode are equal to

$$\frac{\tilde{\epsilon}_1E_{1z}^{\mathrm{R}}}{\tilde{\epsilon}_1E_{1z}^{\mathrm{I}}}=\frac{k_{1x}^{\mathrm{R}}H_{1y}^{\mathrm{R}}}{k_{1x}^{\mathrm{I}}H_{1y}^{\mathrm{I}}}=R_{12}^{\mathrm{TM}}\quad\Rightarrow\quad\frac{E_{1z}^{\mathrm{R}}}{E_{1z}^{\mathrm{I}}}=R_{E_z}^{\mathrm{TM}}=R_{12}^{\mathrm{TM}}, \tag{3.9.9a}$$
$$\frac{\tilde{\epsilon}_2E_{2z}^{\mathrm{T}}}{\tilde{\epsilon}_1E_{1z}^{\mathrm{I}}}=\frac{k_{2x}^{\mathrm{T}}H_{2y}^{\mathrm{T}}}{k_{1x}^{\mathrm{I}}H_{1y}^{\mathrm{I}}}=T_{12}^{\mathrm{TM}}\quad\Rightarrow\quad\frac{E_{2z}^{\mathrm{T}}}{E_{1z}^{\mathrm{I}}}=T_{E_z}^{\mathrm{TM}}=(\frac{k_1}{k_2})^2T_{12}^{\mathrm{TM}}, \tag{3.9.9b}$$
$$\frac{\tilde{\epsilon}_1E_{1x}^{\mathrm{R}}}{\tilde{\epsilon}_1E_{1x}^{\mathrm{I}}}=\frac{k_{1z}^{\mathrm{R}}H_{1y}^{\mathrm{R}}}{k_{1z}^{\mathrm{I}}H_{1y}^{\mathrm{I}}}=-R_{12}^{\mathrm{TM}}\quad\Rightarrow\quad\frac{E_{1x}^{\mathrm{R}}}{E_{1x}^{\mathrm{I}}}=R_{E_x}^{\mathrm{TM}}=-R_{12}^{\mathrm{TM}}, \tag{3.9.9c}$$
$$\frac{\tilde{\epsilon}_2E_{2x}^{\mathrm{T}}}{\tilde{\epsilon}_1E_{1x}^{\mathrm{I}}}=\frac{k_{2z}^{\mathrm{T}}H_{2y}^{\mathrm{T}}}{k_{1z}^{\mathrm{I}}H_{1y}^{\mathrm{I}}}=\frac{k_{2z}^{\mathrm{T}}}{k_{1z}^{\mathrm{I}}}T_{12}^{\mathrm{TM}}\quad\Rightarrow\quad\frac{E_{2x}^{\mathrm{T}}}{E_{1x}^{\mathrm{I}}}=T_{E_x}^{\mathrm{TM}}=1-R_{12}^{\mathrm{TM}}. \tag{3.9.9d}$$

In TE mode, as shown in Fig.3.28, the reflection and transmission coefficients of the electric field can be directly calculated by the following equations

$$R_{12}^{\mathrm{TE}}=\frac{E_{1x}^{\mathrm{R}}}{E_{1x}^{\mathrm{I}}}=\frac{\frac{k_{1z}}{\mu_1}-\frac{k_{2z}}{\mu_2}}{\frac{k_{1z}}{\mu_1}+\frac{k_{2z}}{\mu_2}}, \tag{3.9.10a}$$
$$T_{12}^{\mathrm{TE}}=\frac{E_{2x}^{\mathrm{T}}}{E_{1x}^{\mathrm{I}}}=1+R_{12}^{\mathrm{TE}} \tag{3.9.10b}$$

3.10 Plane wave in a multi-layered source-free medium

If there are more than two layers, for example, a three layer model illustrated in Fig.3.29, a series of multiple reflections will occur at the interfaces.

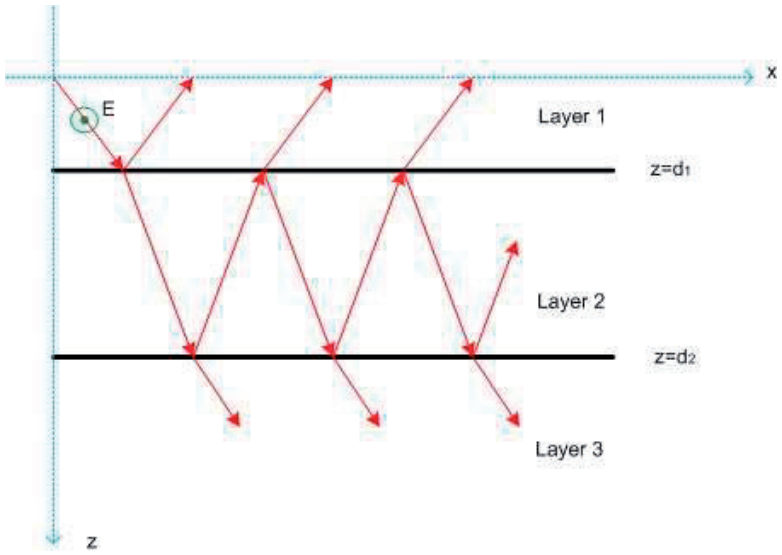

Figure 3.29: Multiple reflections of a TE wave at interfaces in a multilayer medium

In this case, take TE mode for example, the electric field in the three regions are respectively equal to:

$$E_{1y}^{\mathrm{TE}} = A_1[e^{ik_{1z}z} + \tilde{R}_{12}^{\mathrm{TE}} e^{2ik_{1z}d_1 - ik_{1z}z}], \tag{3.10.1a}$$

$$E_{2y}^{\mathrm{TE}} = A_2[e^{ik_{2z}z} + R_{23}^{\mathrm{TE}} e^{2ik_{1z}d_1 - ik_{2z}z}], \tag{3.10.1b}$$

$$E_{3y}^{\mathrm{TE}} = A_3 e^{ik_{3z}z}, \tag{3.10.1c}$$

in which A_1 is the amplitude in the first layer and the amplitudes in the second and third layer A_2 and A_3 can be calculated by the boundary conditions, which are equal to:

$$A_2 = \frac{T_{12}^{\mathrm{TE}} A_1 e^{i(k_{1z} - k_{2z})d_1}}{1 - R_{21}^{\mathrm{TE}} R_{23}^{\mathrm{TE}} e^{2ik_{2z}(d_2 - d_1)}}, \tag{3.10.2a}$$

$$A_3 = (1 + R_{23}^{\mathrm{TE}}) A_2 e^{i(k_{2z} - k_{3z})d_2}. \tag{3.10.2b}$$

$\tilde{R}_{12}^{\mathrm{TE}}$ in (3.10.1a) is the generalized reflection coefficient between layer 1 and layer 2 at interface $z = d_1$, which is equal to

$$\tilde{R}_{12}^{\mathrm{TE}} = R_{12}^{\mathrm{TE}} + \frac{T_{12}^{\mathrm{TE}} R_{23}^{\mathrm{TE}} T_{21}^{\mathrm{TE}} e^{2ik_{2z}(d_2-d_1)}}{1 - R_{21}^{\mathrm{TE}} R_{23}^{\mathrm{TE}} e^{2ik_{2z}(d_2-d_1)}}. \tag{3.10.3}$$

If more layeres are added below layer 3 and the interfaces are denoted by d_i, the generalized reflection coefficient for each layer can be calculated recursively, [1, Eq.2.1.23]

$$\tilde{R}_{i,i+1} = R_{i,i+1} + \frac{T_{i,i+1}\tilde{R}_{i+1,i+2}T_{i+1,i}e^{2ik_{i+1,z}(d_{i+1}-d_i)}}{1 - R_{i+1,i}\tilde{R}_{i+1,i+2}e^{2ik_{i+1,z}(d_{i+1}-d_i)}}. \tag{3.10.4}$$

where $R_{i,i+1}$ and $T_{i,i+1}$ are the reflection and transmission coeffients for a wave from layer i to layer $i+1$. k_i is the wavenumber of layer i.

3.11 A point source embeded in a layered medium

As given in (3.3.3), in homogeneous space, a point source will induce spherical wave. When a point source is embeded in a layered medium, as shown in Fig.3.30, we can first expand the spherical wave into an integral summation of plane waves and then apply the propagation theory of plane waves in a layered medium.

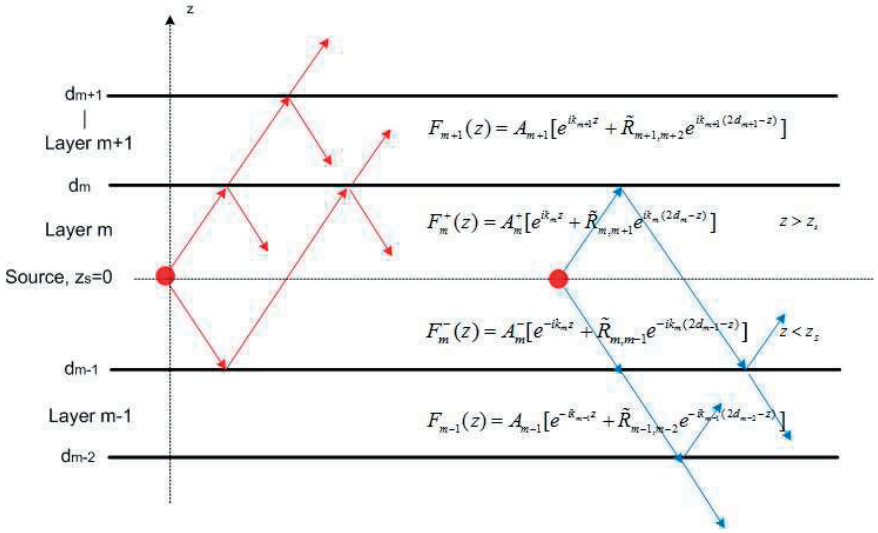

Figure 3.30: A point source in a multilayer medium

The expansion of a spherical wave can be achieved by using Weyl identity (3.5.1a) or Sommerfeld identity (3.5.1b). In Fig.3.30, a coordinate system is established which let $x-y$ plane parallel to the interfaces and z-axis parallel to the normal and pointing upwards. The point source is assumed to be embeded at $z=z'$ in layer m. Since the positive z-axis in this case points upwards, layer m is mathematically constrained to be within the limits $d_{m-1}<z'<d_m$. The z-variation of an upgoing and downgoing wave can be expressed as $F(z,z')$. The field inside layer m due to a source in layer m can be divided into two parts, representing an upgoing wave (F^+) and a downgoing wave (F^-), which can be expressed as

$$F_m^+(z,z') = A_m^+[e^{ik_{m,z}(z-z')} + \tilde{R}_{m,m+1}e^{ik_{m,z}(2d_m-(z-z'))}], \tag{3.11.1a}$$

$$F_m^-(z,z') = A_m^-[e^{-ik_{m,z}(z-z')} + \tilde{R}_{m,m-1}e^{-ik_{m,z}(2d_m-(z-z'))}], \tag{3.11.1b}$$

where $\tilde{R}_{m,m+1}$ and $\tilde{R}_{m,m-1}$ represent generalized reflection coefficients for waves emanating from layer m into layer $m+1$ and $m-1$, which can be calculated by (3.10.4). d_m denotes the z-coordinate of the interface separating medium m and $m+1$, and $k_{m,z}$ is used to indicate the z-component of the wave vector k_m of layer m. The amplitudes in (3.11.1a) and (3.11.1b) are equal to

$$A_m^+ = \frac{1+\tilde{R}_{m,m-1}e^{-2ik_{m,z}(d_{m-1}-z')}}{1-\tilde{R}_{m,m+1}\tilde{R}_{m,m-1}e^{2ik_{m,z}(d_m-d_{m-1})}}, \tag{3.11.2a}$$

$$A_m^- = \frac{1+\tilde{R}_{m,m+1}e^{2ik_{m,z}(d_m-z')}}{1-\tilde{R}_{m,m+1}\tilde{R}_{m,m-1}e^{2ik_{m,z}(d_m-d_{m-1})}}. \tag{3.11.2b}$$

In a similar fashion, the field variation in layer $m+1$ and $m-1$ can be written as

$$F_{m+1}(z,z') = A_{m+1}^+[e^{ik_{m+1,z}(z-d_m)} + \tilde{R}_{m+1,m+2}e^{ik_{m+1,z}(2d_{m+1}-(z-d_m))}], \tag{3.11.3a}$$

$$F_{m-1}(z,z') = A_{m-1}^-[e^{-ik_{m-1,z}(z-d_{m-1})} + \tilde{R}_{m-1,m-2}e^{-ik_{m-1,z}(2d_{m-2}-(z-d_{m-1}))}], \tag{3.11.3b}$$

where

$$A_{m+1}^+ = \frac{T_{m,m+1}A_m^+e^{ik_{m,z}(d_m-z')}}{1-R_{m+1,m}\tilde{R}_{m+1,m+2}e^{2ik_{m+1,z}(d_{m+1}-d_m)}}, \tag{3.11.4a}$$

$$A_{m-1}^- = \frac{T_{m,m-1}A_m^-e^{-ik_{m,z}(d_{m-1}-z')}}{1-R_{m-1,m}\tilde{R}_{m-1,m-2}e^{2ik_{m-1,z}(d_{m-1}-d_{m-2})}}. \tag{3.11.4b}$$

The expressions $T_{m,m+1}$ and $R_{m+1,m}$ as well as $T_{m,m-1}$ and $R_{m-1,m}$ represent transmission and reflection coefficients between layer m and the adjacent layers $m+1$ and $m-1$. The field variations within the layers above $m+1$ or below $m-1$ are obtained through a recursive approach.

3.12 Current distribution along metal casing tilted in a layered medium

In chapter 3, the tilt model is studied but the results are not stable because of the error in the evaluation of the Sommerfeld integral. Now the new method introduced in Chapter 4 is applied to the model and the results are presented in Fig.3.31, Fig. 3.32 and Fig.3.33. Numerical results shows that under geophysics condition, which the operating frequency is very low and the surrounding medium is highly conductive, the tilt angle doesn't have much effect on the current distribution, which allows us to use a corresponding vertical model to estimate the results.

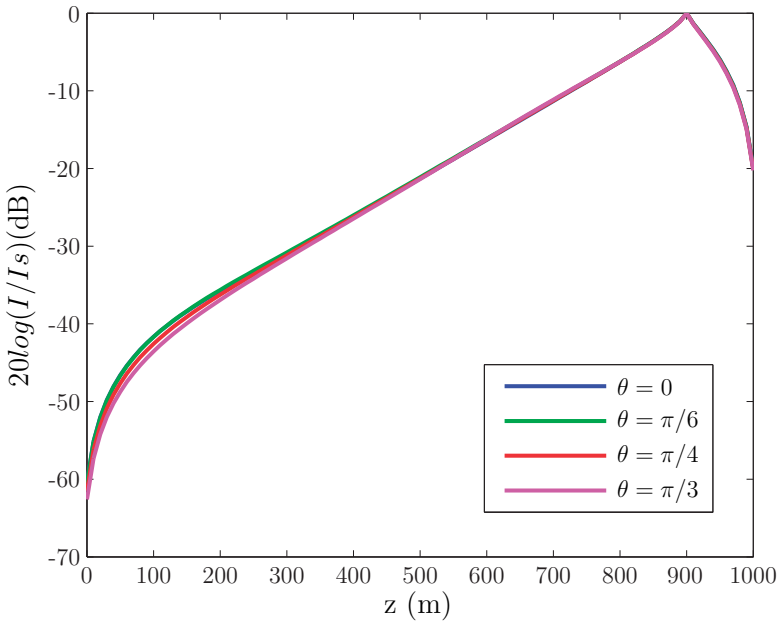

Figure 3.31: Numerical results for a homogeneous model where the conductivities of the medium and the well are assumed to be $\sigma_m = 1$S/m and $\sigma_c = 1 \times 10^6$ S/m respectively. The relative permeability of the metal casing is assumed to be $\mu_r = 100$. The radius of the well is assumed to be 0.1 m and the operating frequency is assumed to be 5Hz. The source is located at 100m from the lower end. The tilt angle is assumed to be 0, $\pi/6$, $\pi/4$ and $\pi/3$ respectively.

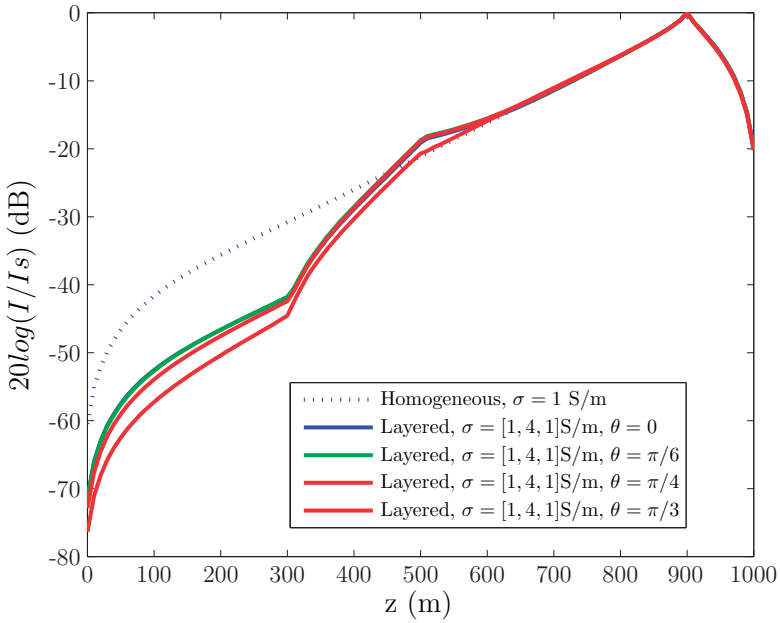

Figure 3.32: Numerical results for the same model in Fig.3.31 for the second 3-layer model with the interface $d = [300, 500] \cos\theta$ m, the conductivities for the 3 layers are assumed to be $\sigma_m = [1, 4, 1]$ S/m.

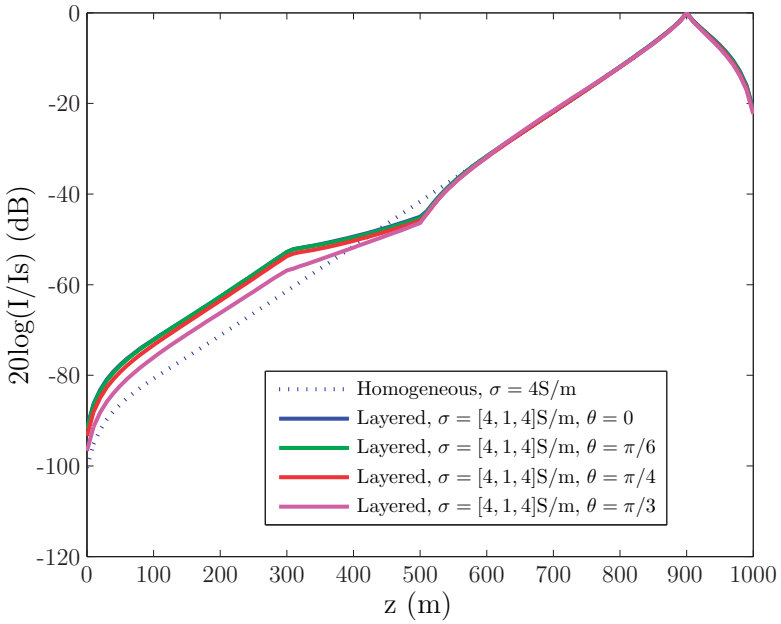

Figure 3.33: Numerical results for the same model in Fig.3.31 for the second 3-layer model with the interface $d = [300, 500] \cos\theta$ m, the conductivities for the 3 layers are assumed to be $\sigma_m = [4, 1, 4]$ S/m.

Bibliography

[1] Weng Cho Chew. *Waves and Fields in Inhomogeneous Media*. IEEE Press, 1st edition, 1995.

[2] J. D. Jackson. *Classical Electrodynamics*. New York, Wiley, 3rd edition, 1998.

[3] E. J. Rothwell and M. J. Cloud. *Electromagnetics*. CRC, 1st edition, 2001.

[4] David Griffiths. *Introduction to Electrodynamics*. Englewood Cliffs, N.J. Prentice Hall, 3rd edition, 1999.

[5] I. S. Gradshteyn and I. M. Ryzhik. *Table of Integrals, Series, and Products*. Academic Press, 7th edition, 2007.

[6] Milton Abramowitz and Irene A. Stegun. *Handbook of Mathematical Functions with Formulas, Graphs, and Mathematical Tables*. Dover Publications, 10th edition, 1972.